

**Universität für Bodenkultur Wien**

University of Natural Resources and Life Sciences, Vienna

Department of Water - Atmosphere - Environment (WAU)  
Institute of Hydrology and Water Management (HyWa)



**ANALYSING CANOPY TEMPERATURE IN A MAIZE FIELD DURING HEAT  
STRESS DAYS WITH A THERMAL CAMERA MOUNTED ON AN UAV**

**Master thesis**

**In partial fulfillment of the requirements**

**for the degree of**

**Master of Science**

Submitted by:

**LÖCKER, VALENTIN PETER**

Supervisor: Univ. Prof. Dipl. Geoökol. Dr. rer. nat. Karsten Schulz

Co-Supervisor: Univ.Ass. Bano Mehdi, MSc., Ph.D.

Co-Supervisor: DI Claire Brenner

Student number: 01041051

## **Acknowledgements**

First of all, I want to thank **Claire Brenner** for her continuous support during preparation, field measurements and analysis of this thesis. Thank you for letting me use your preprocessing Python code, introducing and strongly assisting me in Python coding. Thank you for doing all the work during the field measurements, while I was comfortable sitting in your camping chair.

I want to thank **Prof. Karten Schulz** and **Bano Mehdi** for giving me great support during the writing process of the thesis. Your input and impulses really helped me to complete this work.

I gratefully want to thank my great friends **Steffi, Bene** and **Hannes** for the countless times you had to proofread my work and correct my bad English. Thank you also for hearing me and being very understanding every time I talked and complained about this thesis!

## **Affirmation**

I certify, that the master thesis was written by me, not using sources and tools other than quoted and without use of any other illegitimate support.

Furthermore, I confirm that I have not submitted this master thesis either nationally or internationally in any form.

A handwritten signature in blue ink, appearing to be 'V. Löcker', written in a cursive style.

Klagenfurt, 25.08.2019

Löcker Valentin

## Table of contents

<b>1</b>	<b>Introduction and Objectives</b>	<b>1</b>
<b>2</b>	<b>Literature Review</b>	<b>4</b>
2.1	<i>Overview of the definition of drought</i>	4
2.2	<i>Crop water use</i>	5
2.2.1	Overview of water stress in plants	5
2.2.2	Drought indices	7
2.3	<i>Energy balance approach</i>	10
2.4	<i>Overview of the term land surface temperature (LST)</i>	11
2.5	<i>Relationship of LST and ET</i>	12
2.6	<i>Characteristics of remote sensed TIR-imagery</i>	13
2.6.1	Measuring LST at small scales	13
2.7	<i>Benefits of the impact of crop cultivation on soil water budget</i>	14
2.7.1	Mulch	15
<b>3</b>	<b>Materials and Methods</b>	<b>16</b>
3.1	<i>The Field Site</i>	16
3.2	<i>UAV carrier unit</i>	18
3.2.1	UAV	19
3.2.2	RGB Camera	20
3.2.3	TIR Camera	21
3.3	<i>EcoBot</i>	21
3.4	<i>Handheld Infrared Thermometer</i>	23
3.5	<i>Data collection</i>	24
3.6	<i>Data Preprocessing</i>	26
3.6.1	TIR images	26
3.6.2	Flir data	27
3.7	<i>Separation of soil and canopy pixels</i>	28
3.7.1	Statistical method	28
3.7.2	Method derived from Otsu (1979)	28
3.7.3	Sensitivity of thresholding	30
3.8	<i>Estimating crop water stress using the CWSI</i>	31
<b>4</b>	<b>Results and discussion</b>	<b>35</b>
4.1	<i>TIR Camera validation</i>	35
4.1.1	TIR data acquisition	35
4.1.2	Temperature Drift of TIR camera	35
4.1.3	Temperature Drift of IRT camera	36
4.1.4	Comparison of TIR and IRT	37
4.2	<i>Separation of Canopy pixels</i>	39
4.2.1	Statistical Method of pixel separation	40
4.2.2	OTSU method	42
4.2.3	Comparison of the two approaches	44
4.3	<i>Temperature difference as the foundation of CWSI</i>	48
4.4	<i>Applying the CWSI</i>	49
4.4.1	Statistical Method	49
4.4.2	Empirical Method	51
4.4.3	Comparison SUS vs CON	56
4.5	<i>Mean Temperature Distribution</i>	58

<b>5</b>	<b>Conclusion and outlook</b>	<b>61</b>
<b>6</b>	<b>References</b>	<b>63</b>
<b>7</b>	<b>Appendix</b>	<b>69</b>
7.1	<i>Checklist UAV Flight</i>	69
7.2	<i>Flight Log book</i>	70
7.3	<i>SUSI Layout 2016 / 2017</i>	81

## List of Figures

Figure 1 Drought duration and impacts for drought types (NDMC 2019).....	4
Figure 2 Physiological, biochemical and molecular basis of drought stress tolerance in plants (Shao et al. (2008)).....	6
Figure 3 Conceptual LST - NDVI triangle (Sandholt, Rasmussen, and Andersen 2002) .....	8
Figure 4 Transformation of energy (Bonan (2008)).....	10
Figure 5 Relationship between leaf temperature and stomatal opening (Jones and Vaughan 2010).....	13
Figure 6 Overview of SUSI field site representing the area under study. Yellow rectangles show 'conventional' (CON) scheme plots, red rectangles indicate plots being cropped according to 'sustainable' (SUS) scheme (see also Table 1). Blue dots indicate the starting points of unmanned aerial vehicles (source: Valentin Löcker).....	17
Figure 7 Precipitation and temperature data for the SUSI project in 2017. Red line (Left ordinate) indicates the maximum temperature per day (°Celsius), blue columns (right ordinate) shows precipitation per day (mm). Red dotted lines show heat stress days, grey lines indicate reference days as defined in Sethmacher (2018). .....	18
Figure 8 used UAV (source: Claire Brenner) .....	19
Figure 9 RC unit from Graupner (Graupner/SJ GmbH) .....	20
Figure 10 Sony Alpha 6000 RGB camera (Sony Corporation).....	20
Figure 11 Optris Pi Lightweight TIR camera with on-board computer (Optris GmbH) .....	21
Figure 12 Sketch of EcoBot (Wohlfahrt (2014)).....	22
Figure 13 FLIR e50bx IRT (Flir Systems, Inc.) .....	23
Figure 14 a) sample RGB image b) TIR image of the maize plots .....	23
Figure 15 Flight routes. Left Image 20m routes, where orange is the north route and blue is the south route. Right image 25m routes, where green is the north route and violet is the south route (source: Valentin Löcker). .....	24
Figure 16 RGB picture taken from 20m altitude of Black & White pads for validation purposes (source: Valentin Löcker) .....	25
Figure 17 GPS reference points (left image), chosen images from flights (right image) (source: Valentin Löcker).....	26
Figure 18 TIR image of a 35m altitude flight. Red lines mark the cropping line (source: Valentin Löcker).27	
Figure 19 Example for an empirical CWSI calculation with lower and upper baselines (Lola Suárez and Berni 2012).....	32
Figure 20 Temperature Drift TIR Camera (source: Valentin Löcker) .....	36
Figure 21 Temperature Drift Flir IRT. (source: Valentin Löcker).....	37
Figure 22 Comparison TIR Camera and Flir IRT camera. Start_b=temperature of the black pad at the beginning of the flight ; start_w = temperature of the white pad at the beginning of the flight ; stop_b= temperature of the black pad at the end of the flight ; stop_w= temperature of the white pad at the end of the flight (source: Valentin Löcker).....	38
Figure 23 Sample TIR image plotted of the NorthMaize20m-flight 03.08.2017 (source: Valentin Löcker).39	
Figure 24 Matching RGB image (corresponding Figure 23) of the NorthMaize20m-flight 03.08.2017 (source: Valentin Löcker).....	40
Figure 25 Canopy Related pixels (Assumption A) Statistical Method, NorthMaize20m 03.08.2017 (source: Valentin Löcker) .....	40
Figure 26 Canopy Pixels Statistical Method 20m, NorthMaize20m 03.08.2017 (source: Valentin Löcker) 41	
Figure 27 Separation of canopy pixels statistical method 35m, NorthMaize35m 03.08.2017 (source: Valentin Löcker) .....	41
Figure 28 Separation of canopy pixels OTSU method 20m, NorthMaize20m 03.08.2017 (source: Valentin Löcker).....	42
Figure 29 Separation of canopy pixels OTSU method 35m, NorthMaize35m 03.08.2017 (source: Valentin Löcker).....	43
Figure 30 OTSU performance on a day with lower incoming radiation, 20m NorthMaize 05.08.2017 (source: Valentin Löcker).....	44
Figure 31 Temperature Distribution histogram of the NorthMaize20m-flight 03.08.2017 (source: Valentin Löcker).....	45

Figure 32 Temperature Distribution histogram of the NorthMaize35m-flight 03.08.2017 (source: Valentin Löcker).....	46
Figure 33 Temperature Distribution histogram of the NorthMaize20m-flight 05.08.2017 (source: Valentin Löcker).....	47
Figure 34 Temperature Distribution histogram of the NorthMaize35m-flight 05.08.2017 (source: Valentin Löcker).....	47
Figure 35 Boxplot of all delta T values from all flights; Tc= canopy temperature ; Ta= atmospheric temperature, VPD= vapour pressure deficit(source: Valentin Löcker).....	48
Figure 36 Delta T spatial distribution of the 03.08.2019 North 20m flight (source: Valentin Löcker) .....	49
Figure 37 CWSI CWSI estimated according to the statistical method and statistical threshold proposed by (Alchanitis et. al. (2010)). Ta= atmospheric temperature . (source: Valentin Löcker).....	50
Figure 38 CWSI calculated according to the statistical method proposed by (Alchanitis et. al. (2010)) in comparison with the CWSI computed with OTSU threshold (Otsu 1979). Ta= atmospheric temperature (source: Valentin Löcker) .....	50
Figure 39 Lower Baseline Tulln VPD= vapor pressure deficit (source: Valentin Löcker).....	51
Figure 40 Lower Baselines found in literature (source: Valentin Löcker).....	52
Figure 41 Climate diagram from Tulln, Austria (time range of data: 1982-2012) (source: de.climate-data.org).....	53
Figure 42 Climate diagram from Oakes, North Dakota, USA (time range of data: 1982-2012) (source: de.climate-data.org).....	53
Figure 43 Calculated CWSI with Lower Baseline Tulln (source: Valentin Löcker) .....	55
Figure 44 Calculated CWSI with Lower Baseline Oakes (source: Valentin Löcker).....	55
Figure 45 Spatial distribution of the CWSI values from the 03.08.2017 North 20m flight (source: Valentin Löcker).....	56
Figure 46 CWSI comparison of all flights. For each flight two pictures were compared. SUS = sustainable ; CON = conventional ; (source: Valentin Löcker).....	57
Figure 47 Mean temperature distribution of all north route 35m altitude flights on heat stress days. Graphs show the variation of mean temperature during the flight from west to east on every flight (source: Valentin Löcker).....	58
Figure 48 Mean temperature distribution of south 35m altitude flight on August 3 <sup>rd</sup> at 13:30 (source: Valentin Löcker) .....	59
Figure 49 Flight tracks from Figure 36. green circle= start / picture 1 ; red circle = stop / last picture ; red line = temperature drop (source: Valentin Löcker) .....	60

## List of Tables

Table 1 Crop rotations in the SUSI project. CC= catch crop ; NC = nurse crop (source: Valentin Löcker)....	16
Table 2 Protocol of successfully carried out flights. The colors indicate the four different routes as a result of different flight heights and routes, e.g. NorthMaize20 indicates that the flight covered the northern route at an altitude of 20m above ground (source: Valentin Löcker). .....	25
Table 3 Methods to determine wet and dry baselines for the CWSI (Cohen et al. 2017) .....	31

## Abbreviations

ABA	Abscisic Acid
ASTER	Advanced Spaceborn Thermal Emission and Reflection Radiometer
CC	Catch Crop
BOKU	University of Natural Resources and Life Sciences Vienna
CON	Conventional
CWSI	Crop Water Stress Index
ET	Evapotranspiration
FAO	Food and Agriculture Organization of the United Nations
GPS	Global Positioning System
IRT	(handheld) Infrared Thermometer
LST	Land Surface Temperature
Meteosat	Meteorological Satellite
MODIS	Moderate-resolution Imaging Spectroradiometer
NC	Nurse Crop
NDVI	Normalized Difference Vegetation Index
NDMC	National Drought Mitigation Center
nws	Non-water stressed
PA	Precision Agriculture
RC	Remote Control
RGB	Red-Green-Blue
RMSE	Root mean square error
SMC	Soil Moisture Content
SUS	Sustainable
TIR	Thermal Infrared
UAV	Unmanned Aerial Vehicle
VPD	Vapor Pressure Deficit
WP	Waypoint

## Abstract

Due to climate change, global agriculture is facing the challenge of hotter summers combined with a decline of rainfall. This may result in a higher probability of heat and water stress for crops.

Land surface temperature (LST) is a key factor to serve as a proxy for crop water budget parameters. In this thesis, the difference between conventionally (market-oriented crop rotation, standard tillage and fertilization practices, CON) and sustainable managed (8-year-crop rotation with several winter catch crops, undersown crop rotation and special tillage technique, SUS) plots of *Zea mays* was examined in terms of LST distribution. Data was collected between 25<sup>th</sup> of July and 7<sup>th</sup> of August 2017 near Tulln, Lower Austria, using an unmanned aerial vehicle (UAV) carrier unit equipped with RGB and TIR cameras. Auxiliary environmental data was collected using a mobile measurement device called Ecobot. This approach focuses on data acquisition, with a high temporal and spatial resolution, processing and analyzing of the data. Because the pure LST data lacks regional and crop specific information, two different approaches of the Crop Water Stress Index (CWSI) were established. The CWSI is a water stress index basing on calculations of the gradient between the plant surface temperature and the atmospheric temperature. When analyzing the CWSI in the CON vs the SUS plot, even though the atmospheric temperature was above 30°C and there was no precipitation during the field campaign, the maize crops in both treatments did not appear to suffer severe water stress. One possible reason for that could be the high resistance of maize crops to water scarce and hot conditions.

# 1 Introduction and Objectives

A decline of rainfall in combination with a rise of temperatures in summer months poses new challenges for the global agricultural industry (Eitzinger 2007). Due to climate change and global warming, Central Europe gets more and more exposed to extreme weather conditions often in the form of water deficit (droughts) (Trnka et al. 2016; Lisar et al. 2012; Eitzinger 2007). With about 80% of total freshwater used, the agricultural industry is by far the biggest consumer of freshwater resources in the world (Anderson et al. 2012). Therefore, different crop management practices combined with precise drought monitoring become more and more important for agricultural production, especially crop production (Gerhards et al. 2019; Rud et al. 2014).

Crops need water for growth and cooling purposes. The water is absorbed by the roots out of the soil and transported into the stomata cells where it transpires. The water use of crops is dependent on weather, soil, water availability and crop species (Al-Kaisi and Broner 2014). The process of evaporation on the crop's surface needs a severe amount of energy and therefore causes a cooling effect on the crop's surface (Monteith and Unsworth 2013). Water stressed crops close their stomata in order to reduce water and energy loss through transpiration (Gerhards et al. 2019). In this case, as plants are lacking the possibility to transpire, plant surface temperature increases. Therefore, temperature measurements of the plants surface, in case of crop plants the canopy, provides information on the plants' water status (Jones and Vaughan 2010).

Historically, canopy temperature measurements were taken ground based, mostly using handheld thermal infrared measurement systems (IRT). Ground based measurements require a relatively high amount of human workforce and are limited in their spatial expansion and temporal resolution (Li and Duan 2018). With the rise of remote sensing technologies such as satellites, airplanes or balloons, land surface temperature<sup>1</sup> (LST) can be obtained for larger regions without the need of manpower surveying the area (Anderson et al. 2012). However, high costs, high operational complexity, low spatial resolution and/or poor revisiting times have prevented this technology from being applied outside of scientific projects (Zhang and Kovacs 2012). Nevertheless, studies show that LST data derived from satellites can be used for drought monitoring (Cammalleri and Vogt 2015).

Working towards these shortcomings, civil unmanned aerial vehicles (UAV) emerged as a viable option for small and medium scale remote sensing measurements. The development of UAV provides new possibilities to acquire remote sensing data with high temporal and spatial resolution at relatively low costs (Berni et al. 2009). UAV systems have the potential to provide high-resolution data on small and medium scales making it a highly useful tool to fill the gap between low resolution satellite images and micro scale in situ measurements (Gerhards et al. 2019).

---

<sup>1</sup> land surface temperature (LST) and canopy temperature are NOT the same. LST is the temperature derived from remote sensing measurements. LST contains pixels from all points of the earth's surface such as e.g. soil, water, rock or vegetation. Canopy temperature is the surface temperature of plants only.

Temperature of plant surface alone provides limited information on plant water use (Zargar et al. 2011). To combine information on influencing variables, indices are often used in order to express water stress levels in plants. Therefore, over 150 drought indices to quantify different drought types and stages were established by scientists (Zargar et al. 2011). The crop water stress index (CWSI) is an index based on calculations of the gradient between the plant surface temperature, the atmospheric temperature and the vapor pressure deficit (Jackson and Idso 1981). In a recent review, Gerhards et.al. (2019) stated that the CWSI is very accurate in hot, dry climate regions, where also most of the research about drought and crop water stress is done. However, the outcome of research done in these climate conditions is not transferable to colder climate regions (Ihuoma and Madramootoo 2017). So far only a few scientific publications of the application of the CWSI in the Central European region exist. Therefore, one focus of this thesis is the application of the CWSI in this climatic region.

As mentioned, Central Europe gets more and more exposed to extreme weather conditions. Timespan and extend of extraordinary temperatures combined with decreasing precipitation, result in water deficit for crops (Lisar et al. 2012). In order to develop strategies coping with water stress, e.g. via irrigation, information on levels of water stress in plants is inevitable (Zargar et al. 2011). Another approach is via plant cultivation management, e.g. to implement crop rotation or tillage schemes that help to improve water storage capacity or availability in soil (Walker et al. 2016; Wall 2007).

To account for the above-mentioned future challenges, the University of Natural Resources and Life Sciences Vienna (BOKU) launched a long-time trial where two different crop management practices of different crop species are compared to each other. The project called SUSI, short for 'sustainable intensification', consists of field plots which are managed either sustainable (SUS) or conventional (CON). The management practices differ especially in crop rotation and soil cultivation. In the context of SUSI project, various measurements are taken to examine the differences in the two management practices.

The framework of this thesis focuses on evaluating the impact of different field management practices in a maize (*Zea mays*) crop grown in Tulln, Lower Austria. Data collection was carried out by a UAV carrier unit equipped with TIR and RGB cameras. The obtained TIR imagery data provides key LST data, which builds the foundation for further evaluations of this study. The focus of this thesis is the implementation of a UAV-based TIR system to acquire remote sensing data of respective maize plots on a small scale. Furthermore, the data is used to create a statement for the accuracy of TIR data. For monitoring the crops' water stress level two different approaches of the crop water stress index were applied.

The one central question that arises during the project's analyses is:

- Do sustainable managed maize crops tend to show less water stress during hot drought periods than conventional managed maize crops?

The thesis is structured in six main parts. The first part presents the literature available and provides a theoretical foundation and the fundamentals for further research. The following section focuses on the actual field study carried out in Tulln, Lower Austria, Austria and makes a transition towards the data preparation phase. This part highlights the path from raw data to fully processed and applicable datasets. The next section shows and interprets the results of the acquired data following the objectives of the thesis. The thesis finishes with a final discussion of the results, a conclusion and an outlook for further studies.

The work on this thesis started in February 2017, including a field study in July/August 2017 and was finished in August 2019. The field study included ground measurements and survey flights, which were carried out over the SUSI plots.

## 2 Literature Review

### 2.1 Overview of the definition of drought

Drought is often considered as a period of time with lower than average rainfall for a region (Graham 2000; Wilhite and Glantz 1985). However, using average rainfall as the only indicator to detect droughts is insufficient because more often than not meteorologists summarize rainfall statistics on a yearly basis rather than focusing on the growing season. Therefore, definitions of drought need to be specified for certain areas and respective science fields (Wilhite and Glantz 1985). The National Drought Mitigation Center (NDMC) from the University of Nebraska, USA, categorized drought in five different types, meteorological, agricultural, hydrological, socioeconomic and ecological droughts. The first three mentioned approaches account for ways to measure drought as a physical occurrence and the latter two approaches address the effects of droughts for socioeconomic systems (NDMC 2019). Further on, droughts are characterized in three dimensions: severity, duration and spatial distribution (Zargar et al. 2011).

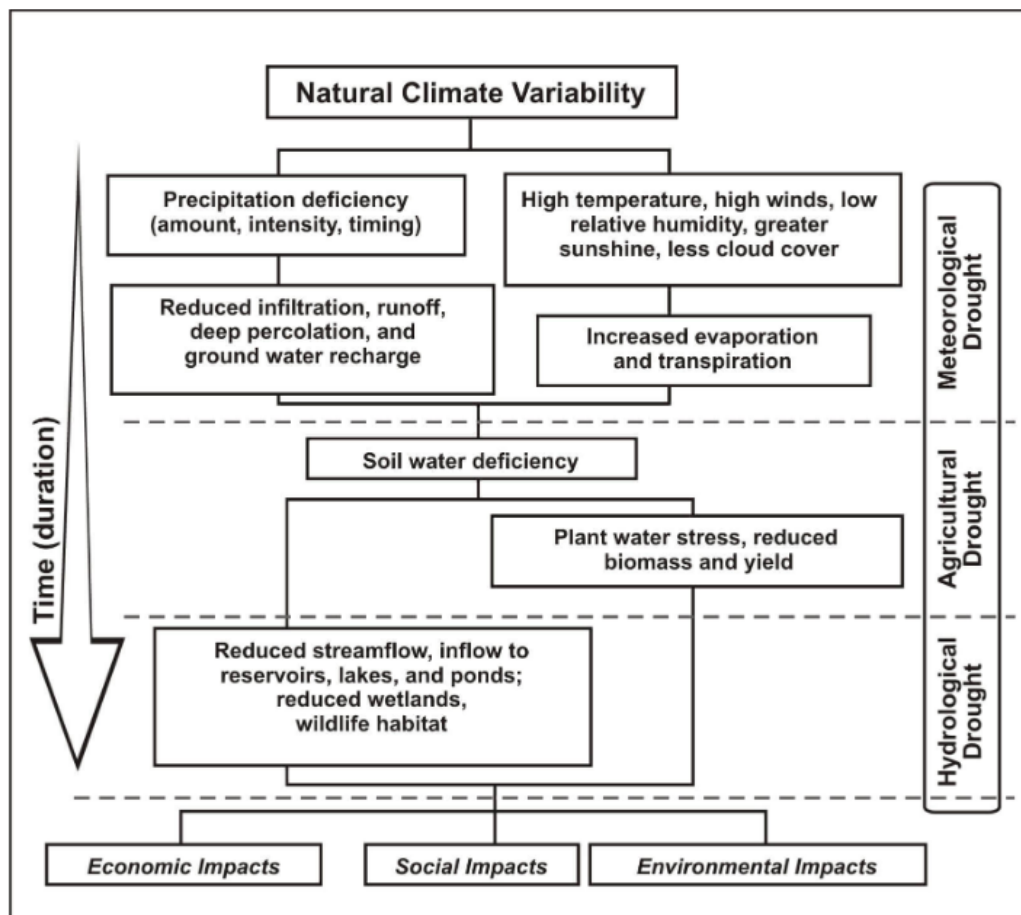


Figure 1 Drought duration and impacts for drought types (NDMC 2019)

Figure 1 shows the connection between duration of the drought and the different drought types. A drought event starts with the first day without precipitation (Wilhite and Glantz 1985). Various meteorological factors such as high temperatures, high wind speed and stronger radiation due to lower cloud cover increase evapotranspiration and therefore cause meteorological drought. However, as shown in Figure 1 also the timing of the meteorological drought event and local factors such as groundwater recharge determine if the meteorological drought affects the soil water content. If it affects the soil water content, the NDMC speaks from agricultural drought. Agricultural drought can result in plant water stress, reduced biomass and yield. If the drought event goes on beyond reduced soil water content and affects bigger hydrological processes, the NDMC speaks of hydrological drought. In the stage of hydrological drought, streamflow is reduced, standing waters suffer from lower inflow, wetlands and wildlife habitats are reduced. The spatial scale of hydrologic droughts is usually measured on a watershed or river basin scale. Many economic goods are directly connected with elements of the three above mentioned types of drought. For example, reduced yield, reduced populations of fish or a lower potential of hydroelectric power affect human beings on a socioeconomic scale. The last and also newest type described by the NDMC is the ecological drought (NDMC 2019). This type of drought is defined by a prolonged deficit of water that drives ecosystems to change through water scarcity (Crausbay et al. 2017).

This thesis focuses on agricultural drought especially on the effects of plant water stress.

## 2.2 Crop water use

Water is essential for crop growth and cooling purposes (Al-Kaisi and Broner 2014; Brouwer and Heibloem 1986; Pirson and Zimmermann 1982). Crop water use is also known as evapotranspiration (ET), where evaporation is water evaporating from the wet soil or plant surface and transpiration is water transpired to the atmosphere from the stomata. Water is absorbed from the soil by the roots. Most of this water is lost via transpiration as an unavoidable part of the photosynthetic process (Pirson and Zimmermann 1982). Crop water use is dependent on many factors such as weather conditions, growth stage, crop species and available water in the soil (Al-Kaisi and Broner 2014). The Food and Agriculture Organization of the United Nations (FAO) stated that maize needs between 500 – 800 mm of water column and growing period. As outlined before, the crop's growth stage is a major factor for water use or water need of plants. If crops do not have sufficient water at their disposal to fulfill their water need in their current growth stage, they are going to suffer water stress (Brouwer and Heibloem 1986).

### 2.2.1 Overview of water stress in plants

Water stress is one of the major abiotic stresses. It greatly affects crop growth and yield. In severe cases of prolonged drought, dehydration causes many plants to die (Lisar et al. 2012, Jaleel et al. 2009). Non-woody plants consist of 80-90% water. This makes water

the major molecule in all physiological processes. Water is the most important medium for transporting nutrients and metabolites within the plant. Therefore, water stress affects plants at various physiological processes. Water deficit affects all plants and all plants can tolerate water stress until a certain extent, but also plants respond differently. This varies from species to species (Lisar et al. 2012). Figure 1 offers a short graphical overview over the physiological, biochemical and molecular responses of plants to water or drought stress.

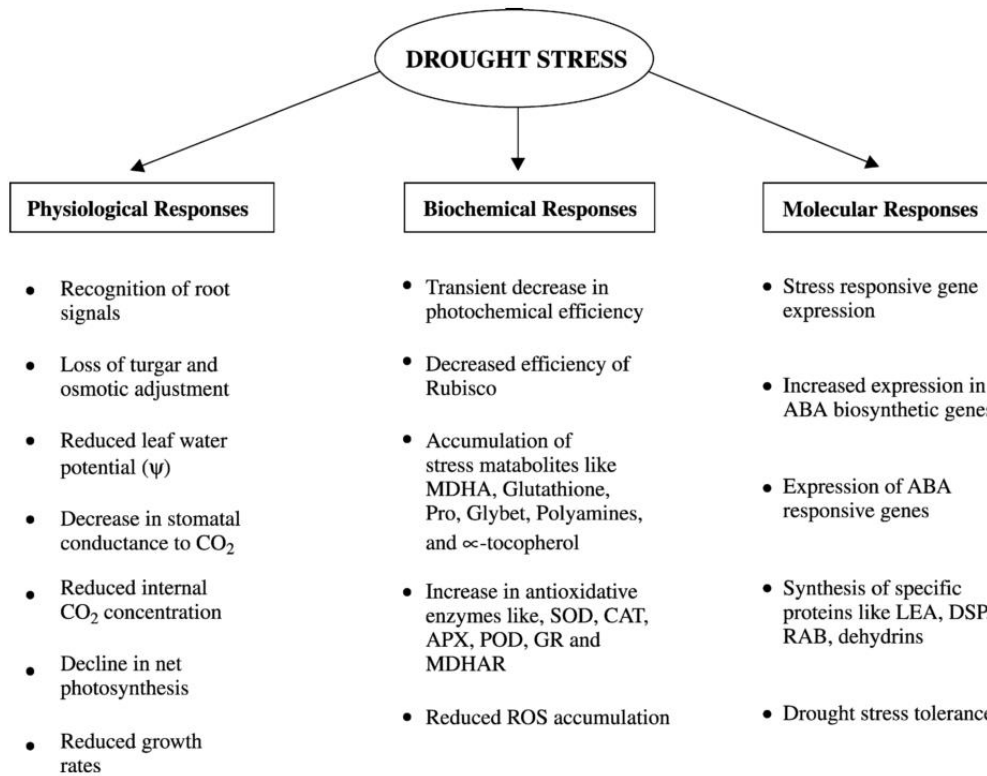


**Figure 2** Physiological, biochemical and molecular basis of drought stress tolerance in plants (Shao et al. (2008))

As mentioned before water stress affects many processes in plants. The most important processes for farmers and stakeholders are shortly explained in the latter:

### Morphological and anatomical changes

Water stress leads to changes in leaf anatomy and structure of plants. (Lisar et al. 2012) Lower water availability leads to lower cell turgor pressure, which results in lower cell enlargement and cell growth. This can be stated as one of the reasons for a reduced plant growth in general. Reduced plant growth results in a reduction of leaf size and stem growth and elongation, e.g. 25% lower plant height for some citrus species (Lisar et al. 2012; Jaleel et al. 2009; Shao et al. 2008). Although smaller leaf size (or leaf area) saves water for the plant, it also causes mayor losses in yield due to lower photosynthesis potential (Lisar et al. 2012).

### Photosynthesis changes

It is known that decrease of leaf water potential causes decrease of photosynthesis rate. The effects are mainly caused by stomatal closure and metabolic impairment. Scientists are divided which of the two mentioned factors has more impact on the photosynthesis rate of a plant suffering drought stress (Jaleel et al. 2009). Photosynthesis rate decreases in both  $C_3^2$  and  $C_4^3$  plants under drought conditions. Studies found that  $C_4$  plants respond better to water scarcity than  $C_3$  plants. That explains their predominance in hot, arid regions (Lisar et al. 2012; Crafts-Brandner and Salvucci 2002). The enzyme RuBisCo fixates  $CO_2$  in metabolic pathways of all plants. In dry conditions it also is responsible for the fixation of oxygen (photorespiration<sup>4</sup>), which can be (in high concentrations) toxic for plants (Gowik and Westhoff 2011).

There are various other factors such as protein synthesis, lipids, mineral nutrition and abscisic acid (ABA) accumulation, which influence the plants response to water stress (Lisar et al. 2012). These factors are not further described in this thesis.

The main scientific disciplines, which do research in the drought monitoring area, are Meteorology, Agriculture and Hydrology. Due to the different requirements in each of the respective scientific fields, different specific indices were established (Zargar et al. 2011). This thesis focuses on small-scale agricultural remote sensing indices.

In the following subchapter the most widely used indices for remote sensing are introduced shortly.

#### 2.2.2 Drought indices

Drought indices are able to quantify water stress levels by processing data from one or several indicators such as LST and precipitation into a single numerical value in order, e.g. to form the basis for irrigation management. Therefore, indices make the data more usable than raw indicator data. Drought characterizing data enables drought early warning and drought risk analysis, which furthermore improve the preparation and planning for drought events. Drought stress indices can display various climate anomalies based on their founding indicators (Zargar et al. 2011).

A selection of widely used indices for the quantification of drought stress are introduced shortly in the following.

---

<sup>2</sup>  $C_3$  plants are named after the  $C_3$  carbon fixation process, which is a metabolic pathway to operate photosynthesis.  $C_3$  plants convert carbon dioxide and ribulose bishophshate (RuBP or RuBisCo) into 3-phosphoglycerate in the first step of the Calvin-Benson cycle. This process works best in climate where sunlight intensity is moderate. (Gowik and Westhoff 2011) Approximately 95% of earth's biomass is represented through  $C_3$  plants. (Raven and Edwards 2001)

<sup>3</sup>  $C_4$  plants evolved the  $C_3$  photosynthetic cycle to perform better in high light, high temperature and dry conditions. Therefore they can use water more efficiently. (Gowik and Westhoff 2011)

<sup>4</sup> Photorespiration is performed simultaneously to photosynthesis. In photorespiration the enzyme RuBisCo uses  $O_2$  instead of  $CO_2$  as a substrate for the metabolic cycle.

### The normalized difference vegetation index (NDVI)

The NDVI uses the reflectance of red and near infrared wavelengths to detect the condition of observed vegetation (Rouse et al. 1974). The formula is given in Equation 1

Equation 1

$$NDVI = \frac{NIR - R}{NIR + R}$$

where *NIR* is near infrared spectral reflectance and *R* stands for visible red spectral reflectance. The NDVI uses the fact that healthy plants contain more chlorophyll, which absorbs light and therefore reflects less visible red light resulting in a higher NDVI value. Unhealthy plants reflect more visible red light resulting in a lower NDVI value. The NDVI is building the foundation for many remote sensing indices (Zargar et al. 2011).

### Temperature Vegetation Dryness Index (TVDI)

Sandholt et al. (2002) found that there is a clear positive correlation between LST and NDVI. Therefore, they suggested an index combining these two Parameters. The formula is given in Equation 2.

Equation 2

$$TVDI = \frac{LST - LST_{min}}{a + bNDVI - LST_{min}}$$

where LST stands for the observed land surface temperature at a given pixel,  $LST_{min}$  represents the wet edge and is displayed as the lower horizontal line of the triangle in Figure 3. NDVI is the observed normalized difference index, *a* and *b* are the intercept and slope of the dry edge modeled as a linear fit to data where  $T_{max}$  ( $T_{max} = a + bNDVI$ ) is the maximum land surface temperature for a given NDVI (J.-J. Bai, Yu, and Di 2016; Sandholt, Rasmussen, and Andersen 2002).

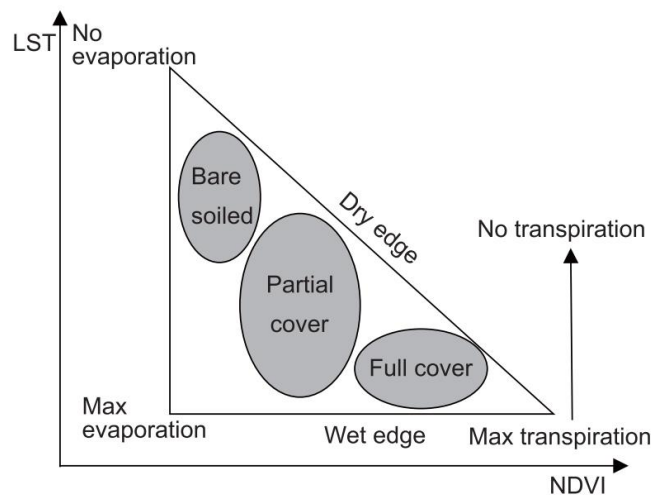


Figure 3 Conceptual LST - NDVI triangle (Sandholt, Rasmussen, and Andersen 2002)

Figure 3 shows the conceptual LST – NDVI triangle. Remote sensed data from an area containing of bare soiled, partial covered and full covered is simplified into a triangle. The dry edge of the triangle represents line where no transpiration is done by the plants. The wet edge represents a fully water saturated crop (or soil in case of bare soiled ground) (Sandholt, Rasmussen, and Andersen 2002). The big disadvantage of this index is that it requires all three types of vegetation cover in order to calculate the wet and dry edges (J. Bai, Yu, and Di 2016).

### Crop Water Stress Index (CWSI)

The CWSI (Jackson and Idso 1981) estimates plant water stress using the relationship between atmospheric temperature<sup>5</sup> and canopy temperature. The formula given is Equation 3

Equation 3

$$CWSI = \frac{(T_c - T_a) - (T_c - T_a)_{ul}}{(T_c - T_a)_{ul} - (T_c - T_a)_{ll}}$$

where  $(T_c - T_a)$  is the measured temperature difference between canopy temperature ( $T_c$ ) and atmospheric temperature ( $T_a$ ),  $ll$  stands for a full watered crop and  $ul$  for a fully stressed crop. More specific details on the CWSI are to be found in chapter 3.8.

### The degrees above non-stressed index (DANS)

A simplification of the CWSI the DANS index should provide better usability for farmers because only the actual canopy temperature needs to be measured and also the calculation process is simplified. As shown in Equation 4 the DANS index uses a simple subtraction of two temperature variables

Equation 4

$$DANS = T_S - T_{NS}$$

where  $T_S$  stands for the actual canopy temperature and  $T_{NS}$  represents the so called non-stressed canopy temperature which is derived from an empirical established lower baseline. Studies showed that the DANS index responds similar like the CWSI. (Taghvaeian et al. 2014)

This list of indices represents a selection of widely used indices to estimate drought stress in plants from small to large scales. The list should give an overview of the existing methods and is far from complete. Zargar et al. (2011) reviewed 74 important drought indices and categorized them according to the drought types established by the NDMC.

---

<sup>5</sup> Measured 2m above ground

### 2.3 Energy balance approach

Energy is provided by the sun in form of solar radiation. Solar radiation and atmospheric longwave radiation warm the earth surface and are responsible for weather and climate. (Bonan 2008). For objects there are five means to transform the incoming energy. As shown in Figure 4 every object (except of blackbodies) reflect a given part of the incoming energy. The remaining part is absorbed. Depending on temperature of the body, longwave radiation is emitted. Heat is transferred by movement of air (sensible heat) and by direct contact to another surface (conduction<sup>6</sup>). Most important for this study is latent heat exchange, which is defined as the part where heat is transformed through a change from water into gas (Bonan 2008; Monteith and Unsworth 2013). When water changes its physical state from liquid to vapor, energy is absorbed from the evaporating surface without a rise in surface temperature (Jones and Vaughan 2010).

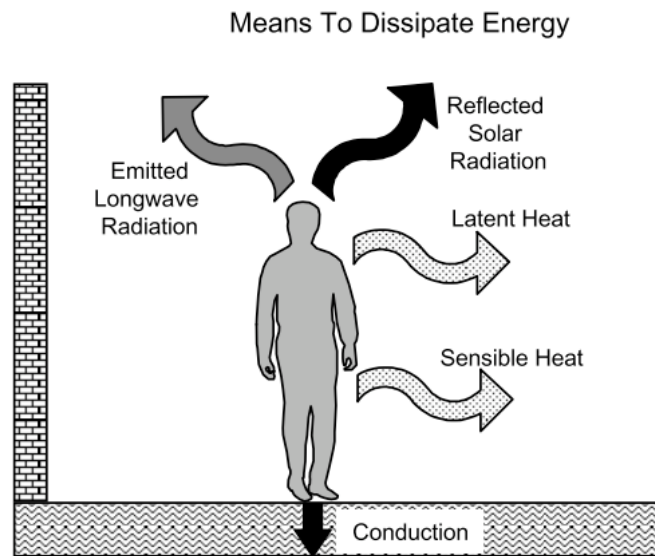


Figure 4 Transformation of energy (Bonan (2008))

The principle of energy conservation is displayed at Equation 5. It shows a balance between energy arriving at the earth surface and energy leaving the surface.

Equation 5

$$(1 - r)S \downarrow + L \downarrow = L \uparrow + H + \lambda E + G$$

where  $r$  is the albedo,  $S \downarrow$  is the incoming shortwave radiation,  $(1-r)S \downarrow$  is the sum of the absorbed solar radiation and  $L \downarrow$  stands for incoming longwave radiation, respectively.  $L$

<sup>6</sup> in the latter equations conduction is referred as 'G - ground flux'

$\uparrow$  is upwelling longwave radiation,  $H$  is sensible heat,  $\lambda E$  is latent heat and  $G$  is ground flux or conductive heat exchange. From Equation 6 we are able to derive the net radiation ( $R_n$ ).

Equation 6

$$R_n = (1 - r)S \downarrow + (L \downarrow - L \uparrow) = H + \lambda E + G$$

Equation 6 shows that net radiation is balanced by sensible, latent and conduction heat fluxes. Net radiation is the part of radiation, which arrives at the object and is absorbed. From Equation 6 we can easily derive the part of latent heat.

Equation 7

$$\lambda E = R_n - H - G$$

Estimate evaporation as a residual of the energy balance equation is the most commonly used approach for remote sensing although it can lead to severe errors when  $ET^7$  is small (Jones and Vaughan 2010). The approach depends on good estimations of the three measured or calculated terms. (Anderson et al. 2012; Jones and Vaughan 2010). A disadvantage of the energy balance approach is that only vertical fluxes are recognized and horizontal energy transport through advection is not considered in the calculations. This makes the approach very inaccurate in smaller areas, uneven sites and areas with distinct vegetation. Stored heat and released heat as well as energy needed for metabolic processes are also not being considered by this approach (Allen et al. 1998).

## 2.4 Overview of the term land surface temperature (LST)

Land surface temperature (LST) is considered as the driving force between long-wave radiation and turbulent heat fluxes at the surface-atmosphere interface. This makes LST one of the most important parameters in physical processes with regard to surface energy and water balance (Z. I. Li and Duan 2018; Coll et al. 2012; Dash et al. 2002). However, there is still uncertainty about the exact definition of LST because of the unclear meaning of the satellite derived temperature and the inhomogeneity of the earth's surface (Z. I. Li and Duan 2018), but it is described as the radiative skin temperature of the land surface (European Commission Joint Research Centre 2017). LST is derived from surface leaving radiation measured by sensors. Its calculation is based on Planck's law, which relates the radiative energy emitted by a black body, where the emissivity equals 1, to its temperature. An emissivity of 1 means that the object absorbs all radiation (Dash et al. 2002).

Equation 8 shows the radiometric temperature of a blackbody with the radiance,

---

<sup>7</sup>  $ET$  = Evapotranspiration. Is the sum of transpiration of water from plants and animals and evaporation of water and soil surfaces.

Equation 8

$$T_{sr} = B_{\lambda}^{-1} \left[ \frac{R_{\lambda} - (1 - \epsilon_{\lambda})R_{at \ \lambda\downarrow}}{\epsilon_{\lambda}} \right]$$

where  $T_{sr}$  is the radiometric temperature,  $B_{\lambda}(T)$  is the Planck function,  $R_{\lambda}$  is the spectral radiance measured by a radiometer pointed toward the surface,  $\lambda$  is the wavelength,  $\epsilon_{\lambda}$  is the spectral emissivity, and  $R_{at \ \lambda\downarrow}$  is the downwelling hemispheric spectral atmospheric radiance (Z. I. Li and Duan 2018).

Validation for satellite derived LST is done either temperature based, radiation based or cross validated (using other validated and well documented satellite data)(Z. I. Li and Duan 2018). In this thesis LST validation was done temperature based using ground measurements to verify the measured LST values. Black and white pads were installed to establish a homogenous surface following the approach of Berni et al. (2009).

### 2.5 Relationship of LST and ET

All terms of the energy balance equation (Equation 5) depend on LST (Kalma, McVicar, and McCabe 2008). Evaporation of water requires a severe amount of energy, e.g. for water at 20°C it's 2,454 MJ per kg which is almost three orders of magnitude higher than the amount of latent heat that is needed to raise water temperature by 1K (1,01kJ kg<sup>-1</sup>) (Jones and Vaughan 2010). Evaporation causes major cooling effects on wet surfaces. Therefore LST data can serve as a proxy for water budget components and ET (Cammalleri and Vogt 2015).

Plants need to open their stomata in order to perform photosynthesis. In condition of unlimited water supply, plants are able to open their stomata, transpire and therefore perform photosynthesis. Because of evaporation the leaf-temperature stays close to or even drops below air temperature (Monteith and Unsworth 2013). A schematic diagram showing this relationship is displayed in Figure 5. When plants suffer water scarcity, they close their stomata in order to reduce transpiration and therefore reduce water loss. This results in a significant rise of leaf temperature (Cammalleri and Vogt 2015).

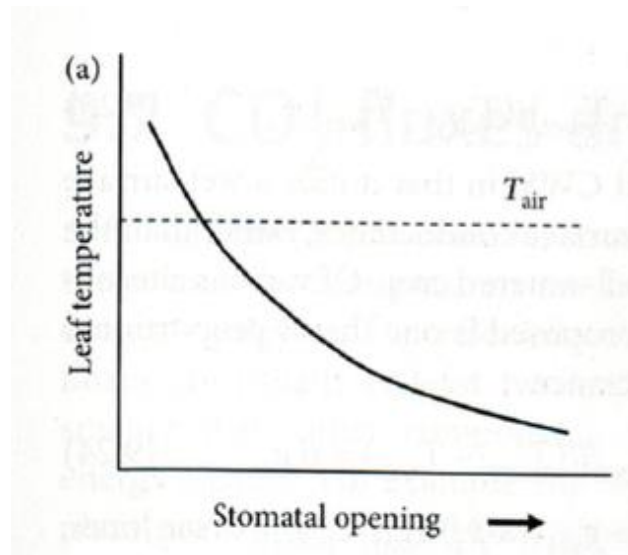


Figure 5 Relationship between leaf temperature and stomatal opening (Jones and Vaughan 2010)

As stated before, the relationship between LST and air temperature is often used as a proxy for ET or other water status parameters (Cammalleri and Vogt 2015). LST-based algorithms strongly correlate to important crop parameters such as yield, water use efficiency, irrigation rates, seasonal evapotranspiration and midday leaf water potential. This points out the importance of LST in ET processes (Ihuoma and Madramootoo 2017).

## 2.6 Characteristics of remote sensed TIR-imagery

Since TIR data acquisition doing ground surveys with IRTs is a time and cost intensive process, which needs a lot of manpower, remote sensing provides a viable option (Martínez et al., 2016). For larger scale surveys, data acquisition by hand gets impossible. Remote sensing provides the possibility of collecting data from small scales to larger scales (Berni et al. 2009). Larger scales are usually captured with satellites while there exist many different systems to acquire TIR data on a small to medium scale. (Anderson et al. 2012; Jones and Vaughan 2010). Remote sensed data represents a valuable source of information for the estimation of vegetation parameters such as ET, LAI and energy fluxes. This, however facilitates the derivation of conclusions about drought stress, SMC among other parameters (Zhang and Kovacs 2012). In order to set up a complete and viable data-base, the incorporation of ground based data such as air temperature, net radiation etc. to countercheck the remote sensing data, is necessary (Laliberte et al. 2011).

### 2.6.1 Measuring LST at small scales

Remote sensing is categorized in either large scale or small scale applications. Remote sensing on a large scale is done by satellites. Large scale remote sensing has disadvantages

compared to small scale applications in the forms of lower spatial and temporal resolution (Anderson et al. 2012; Berni et al. 2009).

Due to the above-mentioned technical and organizational shortcomings of satellites, other systems need to be applied for regional and local remote sensing surveys. Different systems like airplanes, helicopters, balloons, parachutes and unmanned aerial vehicles (UAV) may be applied in order to acquire data with high temporal and spatial resolution. Additionally small UAV give the operator flexibility in his applications, given the possibility to adjust flight altitude, flight speed, flight routes and timetable on his own terms (Zhang and Kovacs 2012). Small UAV are able to serve as the main system for PA mainly because of their low costs and easy applicability. Due to low flight altitudes images with a resolution in the centimeter range can be taken and utilized. Low flight altitudes do not interfere with cloud cover (Martinez et al. 2016). Although data acquisition through UAV appears to be a relatively easy and straightforward task, the system lacks a standardized process for image processing and mosaicking, which are prerequisites of application of UAV reasonable for farmers. Other concerns for the use of small UAV are the short flight duration, limited engine power and the difficulties to maintain stable flight conditions (flight altitude, maneuverability and stability) in windy and turbulent conditions. An additional restriction poses the limited payload weight, which is a major factor for flight duration (Zhang and Kovacs 2012). Nevertheless, the advantages of UAV are outweighing the concerns by far and with UAV technique evolving enormous in recent years, it appears reasonable to assume that this UAV systems will gain more importance in the field of drought monitoring (Berni et al. 2009).

### **2.7 Benefits of the impact of crop cultivation on soil water budget**

Crop cultivation can be done in various different ways and forms, from monocultures with intensive tillage to complex crop rotation principles with zero tillage. The impact of the different cultivation forms on water budget can be visible in short and longtime studies (Ward, Torquebiau, and Xie 2016). In Africa's drylands where droughts are relatively common disasters and irrigation is not standardly deployed in most regions, conservation agriculture (or in this project (see 3.1) called sustainable agriculture) is the dominant cultivation form (Wall 2007). "Conservation agriculture is based on three management principles: (1) minimizing displacement of the soil; (2) maintaining permanent ground cover, usually with crop residues; and (3) using crop rotations" (Walker et al. 2016).

Wall (2007) observed a higher and more sustainable production by means of conservation agriculture with following immediate and medium-term effects:

#### Immediate Effects

- Increased water infiltration into the soil due to the protection of surface structure by the residues.
- Reduced water run-off and soil erosion due to the increased infiltration and the ponding effect of the residues.

- Reduced evaporation of moisture from the soil surface as the residues protect the surface from solar radiation.
- Better crop water balance, less frequent and intense moisture stress because of the increased infiltration and reduced evaporation.
- Reduced traction and labor requirements for land preparation, and thus savings in fuel and labor costs

### Medium-Term Effects

- Increased soil organic matter resulting in better soil structure, higher cation exchange capacity and nutrient availability, and greater water-holding capacity.
- Increased and more stable crop yields.
- Reduced production costs.
- Increased biological activity in both the soil and the aerial environment leading to more biological control of pests.

#### 2.7.1 Mulch

Mulching is a management technique in conservation agriculture. Mulch is mostly described as loose organic material that covers the soil surface, but there are also forms of plastic mulch used in agriculture. It helps in the preservation of soil moisture by reducing evaporation from the soil, repression of weeds, reduction of peak temperatures, lessening of erosion, improving soil consistency and builds a better protection for insect pest assault (Zamir et al. 2013).

In terms of energy balance and ground heat fluxes, studies show that mulch does not change heat fluxes over a full growing period, but has a high impact in the daily heat fluxes as it reduces the temperature peaks in the upper layer of the soil by preventing solar radiation from entering directly into the soil and also reducing heat losses at night (Li et al. 2016). Studies also show that the impact of mulch on the energy balance is not constant over the growing period. The more canopy cover overcasts the bare soil or mulch, the less impact mulching has on the soil energy fluxes (Feng et al. 2017).

### 3 Materials and Methods

#### 3.1 The Field Site

The field site is located on the campus of the BOKU University in Tulln, Lower Austria. It consisted of a block layout with 2 blocks, each with 12 plots measuring 21 m by 150 m. This site is referred to as SUSI (Sustainable Intensification). The first plots were laid out in spring 2014, so the first harvest of the SUSI plots was in fall 2014. In SUSI, two different crop cultivation schemes are being investigated.

The first cultivation scheme is a reference system that is based on the “conventional” (CON) system typical of farming practices in Lower Austria and represents a typical crop rotation and tillage with fertilization practices. The conventional 4-year crop rotation consists of the three most cultivated plants in Lower Austria in a rotation of sugar beet-winter wheat- maize- winter wheat. The plots are cultivated with a chisel plough to a depth of 20-30 cm. There is only sown one winter catch crop in the winter wheat rows in August after the wheat is harvested.

The second cultivation scheme is based on a more “sustainable” (SUS) system in which an 8-year-crop rotation consisting of sugar beet-winter wheat- maize- soybean- winter barley- sunflower- fava bean- and winter wheat with several winter catch crops and an undersown crop (Table 1). The SUS plots are cultivated with a share cultivator (modification of the chisel plough) to a depth of 6-15cm. Some crops in the SUS rotation are designated to increase the humus content of soil organic matter and to fix atmospheric nitrogen, which lowers the need of fertilization, however the fertilizer amounts applied to the maize, sugar beet and winter wheat crops are the same as in the conventional plots. In the maize plots, an underseed of clover was foreseen, however due to the dry spring conditions, it did not germinate. Therefore, a straw mulch consisting of harvested winter wheat was laid out on the surface in each subplot at a rate of 200 g/m<sup>2</sup>.

The crops and crop rotations applied in the SUSI project are listed in Table 1.

Table 1 Crop rotations in the SUSI project. CC= catch crop ; NC = nurse crop (source: Valentin Löcker)

Year	Conventional (CON)		Sustainable (SUS)	
	Main Crop	CC -NC	Main Crop	CC - NC
1	Sugar beet		Sugar beet	
2	Winter wheat		Winter wheat -CC	Egyptian clover, chickling vetch, California bluebell, mustard
3	Maize		Maize (NC)	White clover (undersown)
4	Winter wheat - CC	Buckwheat, radish, mustard, lentil	Soybean	
5			Winter barley -CC	Buckwheat, mustard, Egyptian clover
6			Sunflower	
7			Fava bean -CC	Buckwheat, mustard, Egyptian clover
8			Winter wheat -CC	Buckwheat, radish, mustard, lentil

The detailed plot layout of 2016/2017 can be found in the Appendix 7.3 .

The study site was located close to the city Tulln, federal country of Lower Austria, in the Tullner Becken, which is a sub-catchment of the much larger Danube basin. The Pannonian climate prevails with an average annual precipitation of 593mm and an average annual temperature of 9.2°C. The Pannonian climate is characterized by cold snow scarce winters, dry, hot summers and steady windy conditions. The landscape of the Tullner Becken is characterized by fertile soils and therefore is used mainly for intensive agriculture. The soils of the field site were lime free humid black soils with very high clay shares of about 60% in the upper 70cm of the soil (Sethmacher 2018). Figure 6 shows an overview of the experimental site and the designed routes for the UAV. A dense hedge approximately 7m high is located on the west border of the study site to protect the plots from wind. Close to the northern end of the plots is a transformer station. In total 24 study plots were laid out in the SUSI project. Each plot is about 21m wide and 150m long.

In this thesis, the 4 maize plots were examined (year 3 of SUSI project see Table 1), which means 2 plots were in the CON treatment and 2 were in the SUS treatment. Each maize plot was further split into 2 subplots (to increase the replicates), in which all the measurements were taken. Because the undersown white clover in the SUS plots did not grow at all, straw was laid on the bare soil to simulate covered ground. During the study the maize plants had already reached heights over 2 meters.



Figure 6 Overview of SUSI field site representing the area under study. Yellow rectangles show 'conventional' (CON) scheme plots, red rectangles indicate plots being cropped according to 'sustainable' (SUS) scheme (see also Table 1). Blue dots indicate the starting points of unmanned aerial vehicles (source: Valentin Löcker).

Figure 7 shows the precipitation and temperature distribution from the 15.7. – 31.8.2017. The data was gathered by the BOKU weather measurement station in Tulln near the SUSI field site. The heat stress days were defined as days with an atmospheric temperature of more than 30°C. However, the reference days in Figure 7 refer to the reference days of the SUSI measurement campaign of the thesis from Vivian Sethmacher and do not refer to the reference day measurements of this thesis.

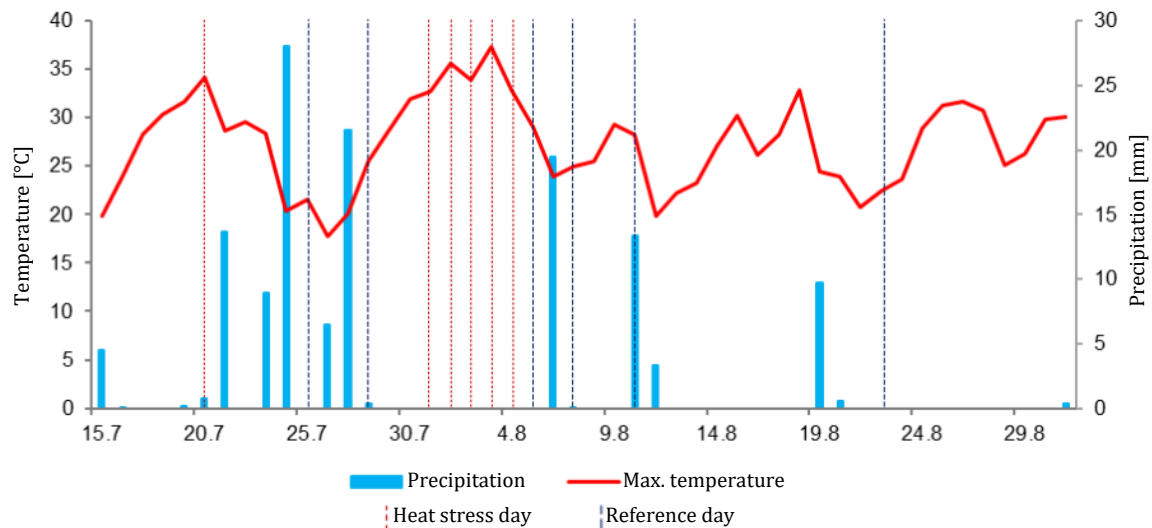


Figure 7 Precipitation and temperature data for the SUSI project in 2017. Red line (Left ordinate) indicates the maximum temperature per day (°Celsius), blue columns (right ordinate) shows precipitation per day (mm). Red dotted lines show heat stress days, grey lines indicate reference days as defined in Sethmacher (2018).

From July 15<sup>th</sup> 2017 till July 28<sup>th</sup> 2017 a total of 84,6mm precipitation was measured. With 28mm on July 24<sup>th</sup> 2017 the biggest precipitation event was recorded. During the heat stress measurements (31.7.2017 – 5.8.2017) the temperature maxima were always above 30°C with no precipitation in between. With 37,3°C the highest temperature was measured on August 3<sup>rd</sup> of 2017.

### 3.2 UAV carrier unit

The UAV carrier unit contained of the UAV itself with two cameras (RGB camera, TIR camera) mounted on a gimbal unit. The unit was built and first tested in 2015 at the University of Natural Resources and Life Sciences, Vienna (BOKU) by Claire Brenner and Florian Elsässer (see Figure 8). For more technical details about the UAV system and UAV flight regulation law in Austria see Elsässer (2015).

### 3.2.1 UAV

For this survey a UAV from HiSystems Mikrokopter MkOkto (MikroKopter OktoXL, HiSystems GmbH, Moormerland, Germany) was used. The UAV consists of eight high torque motors, a gimbal unit to stabilize the mounted cameras, a GPS unit and is powered by two LiPo 22,2V 3300mAh / 20C batteries. The remote-control panel (HiSystems MC-32 HoTT) is connected with the receiver unit (HiSystems GR-16 HoTT) and enables the pilot to fully control the UAV.



Figure 8 used UAV (source: Claire Brenner)

### Gimbal Unit

In order to gather images from a nadir angle<sup>8</sup>, a gimbal unit was mounted on the UAV. Due to movement induced angle changes the gimbal unit stabilizes the requested view angle. The gimbal unit corresponds with the mission planner software and adjusts the device to the in the mission planner software configured angle. In one of the test-flights prior to the field campaign the gimbal motor broke. Because there was no time to install a new motor, the gimbal unit was temporary fixed to a 90° angle using cable ties.

### Mission Planner Software

The mission planner software from Mikrokopter was used for waypoint (WP) navigation assistance and telemetry. The software provides many useful functions:

1. Planning routes using WPs
2. Set Flight height and speed
3. Set angle for gimbal unit
4. Display live flight information from the UAV
5. Transfer values from point 1-3 to the UAV

The software tool can communicate with the UAV via either Bluetooth, a special wireless device or a simple Ethernet cable.

---

<sup>8</sup> Nadir means pointing vertically downward from the observer.

### Remote Control Unit

The 'Graupner MC-32 HoTT' remote control (RC) unit consists of a RC panel and a RC receiver. The panel enables the pilot to fully control the UAV. The small display it also provides the pilot with viable live information about the flight, e.g. flight time, flight height, battery status etc. The RC unit communicates bidirectional via a 2.4 GHz transmission technology. Additionally, the RC panel includes a voice output of a few selected telemetry parameters. The 'Graupner GR-16 HoTT' receiver is directly mounted on the UAV and weights approximately 12g. It can receive up to 8 channels and communicates with the RC panel.



Figure 9 RC unit from Graupner (Graupner/SJ GmbH)

### 3.2.2 RGB Camera

RGB images were captured with a Sony Alpha 6000 (Sony Corporation, Tokyo, Japan) standard RGB system camera. The camera takes images with a resolution of 24,3 megapixel and weighs 344g (with battery and data storage unit). Pictures were taken every second using a continuous advance app from the Sony software.



Figure 10 Sony Alpha 6000 RGB camera (Sony Corporation)

### 3.2.3 TIR Camera

For this thesis the Optris PI Lightweight (Optris GmbH, Berlin, Germany) camera was used to acquire thermal infrared data. The camera can record a spectrum from 7.5-13  $\mu\text{m}$  and has a thermal sensitivity of 80 mK and accuracy of  $\pm 2^\circ\text{C}$ . The optical resolution is 382x288 pixels. In this study the emissivity was set to 0.98. However, a constant emissivity does not exist in nature, which further limits the accuracy of the camera (Gerhards et al. 2019).

The TIR camera is specially designed for remote sensing purposes. The camera needs an on-board computer with special software (Optris Pi Connect) to gather TIR data. Optris Pi Connect is later on also used to preprocess the TIR data into usable data sets on a personal computer. The TIR Kit weights just 380 grams, which is one of the most important properties for the use on UAV carrier units. The camera's focus was calibrated manually to 20m & 35m in order to get the best possible resolution. The resolution for the carried out flights were 36mm per pixel for 20m and 64mm for 35m.



Figure 11 Optris Pi Lightweight TIR camera with on-board computer (Optris GmbH)

### 3.3 EcoBot

The EcoBot is a mobile device to quantify the surface energy balance. It was built by scientists of the University of Innsbruck, Austria. The EcoBot consists of a four-component net-radiometer for quantification of net radiation, albedo and infrared surface temperature. These components are completed with sensors to measure air temperature, 3D- wind speed, soil temperature and soil water content and a battery powered data logger. The four-component net-radiometer unit is mounted on a 1.5m long pole, which is to be held parallel to the measured ground. The data logger and battery are mounted on a backpack. Attached on a vertical pole of said backpack are the thermometer, 3D-wind anemometer, hygrometer and a GPS unit. The sensors for soil temperature and soil water content are linked with cables directly to the data logger and need to be plugged into the

soil where the sensors can measure 5cm depth. See Figure 12 for a scheme of the EcoBot, for detailed description see (Wohlfahrt and Tasser 2014).

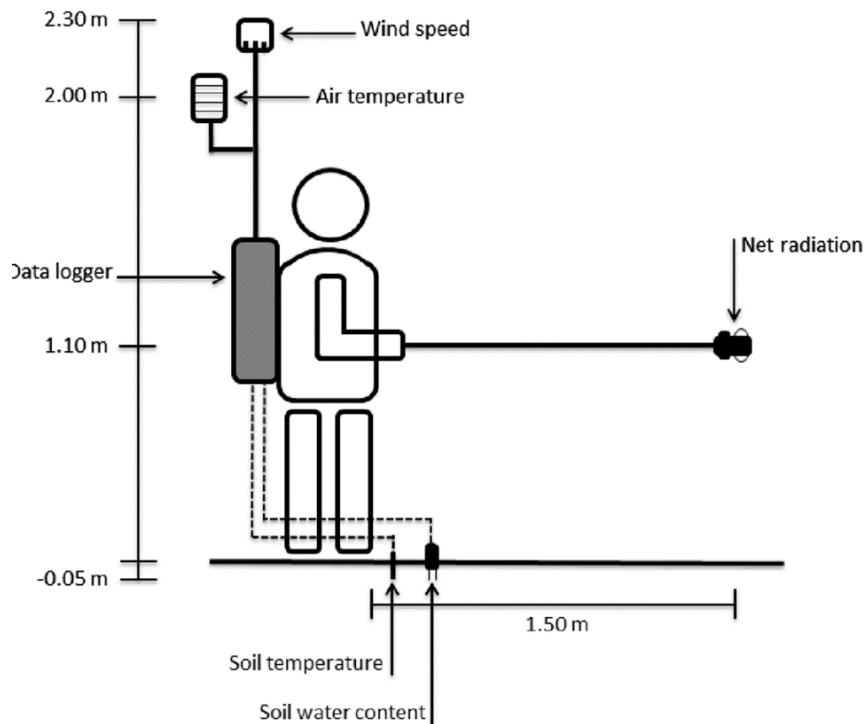


Figure 12 Sketch of EcoBot (Wohlfahrt (2014))

The EcoBot provides a tool for quantification of small-scale (few square meters) spatial variability in the surface energy balance. It is designed as a connective technology between remote sensed data and stationary tower-based measurements. It is best used for canopies not higher than one meter (Wohlfahrt and Tasser 2014). The measurement height of the EcoBot is limited to the height of the human being carrying it. In this study the canopy height was over 2m, which caused problems using the EcoBot's four-component-radiometer in the examined plots, therefore canopy measurements were taken with the help of a ladder. Measurements were also taken between the rows of plants. However, the data of these measurements are not analyzed in this thesis.

For this thesis measurements of air temperature and relative humidity were taken three times in between every flight. The average mean value of this measurements was taken for subsequent calculations of the VPD.

It was nearly impossible to plug soil moisture and soil temperature sensors into the dry clay soil. Additionally, these two sensors need a few minutes to get accustomed to the new environment. This also diminishes the potential of a better spatial depiction because of the relatively low temporal resolution.

### 3.4 Handheld Infrared Thermometer

A handheld infrared thermometer (IRT) was used for counterchecking of the measured remote sensed TIR data. In this study the FLIR e50bx IRT (Flir Systems, Wilsonville, Oregon, USA) was used. The IRT takes RGB and TIR images simultaneously. The TIR camera can record a spectrum from 7.5-13  $\mu\text{m}$  on 240x180 pixels with an accuracy of  $\pm 2^\circ\text{C}$ . The RGB camera records images with a resolution of 3.1 Megapixel. The emissivity was set to 0.98. The images need to be processed with the FLIR Tools<sup>9</sup> software, which provides many functions to extract thermal information of the TIR images. An example of the pictures taken by the IRT is given in Figure 14.



Figure 13 FLIR e50bx IRT (Flir Systems, Inc.)

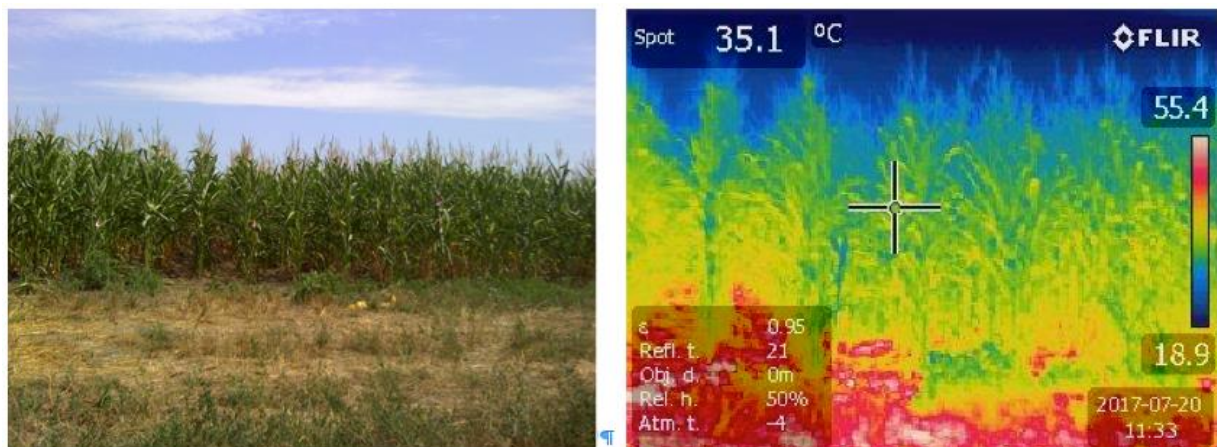


Figure 14 a) sample RGB image b) TIR image of the maize plots

---

<sup>9</sup> The FLIR Tools basic package is freeware. For more functions one needs to buy the pay version FLIR Tools pro

### 3.5 Data collection

The field campaign consisted of a period that lasted from the end of July until the beginning of August 2017. Before the main campaign (31.07.2017-05.08.2017) there was one precipitation event. During the main campaign, however, there was no precipitation and high air temperatures (daily maxima above 30°C) were prevailing. Reference flights were conducted after precipitation days (see Figure 7).

The flights were operated from 13:00h to 14:00h as the gradient between air temperature and canopy temperature is considered to be the highest at this time of the day. Images were taken from the four maize plots, 2 SUS and 2 CON, respectively. Due to the low flight endurance of the UAV, primarily caused by low endurance of batteries, two routes for every flight height were established (see: Figure 15). The routes are referred to as 'north' and 'south' route, respectively. Each route includes one sustainable and one conservative cultivated plot. At the 'north' route the two maize plots were side by side with no buffer in between. At the 'south' route the two maize plots were in distant of each other, which caused greater flight times. As the distance of the UAV was shorter and so a safe landing in case of damage or other errors was considered safer, the 'north' route was always the first one to be examined. The flight heights, as described, were 20m and 35m above ground. Each of the 60 operated flights was documented with a flight log book, which is attached in the appendix of this thesis (see: 7.2)

Altogether these different variants result in a total of four different routes and therefore four different flights per day. Additionally, a so-called 'Panorama' route was operated on some days with a flight height of 100 meters. This route intentioned to give an overview over the plots. The data acquired during these flights was not used in subsequent calculations or analysis because it was not possible to detect the examined subplots correctly.

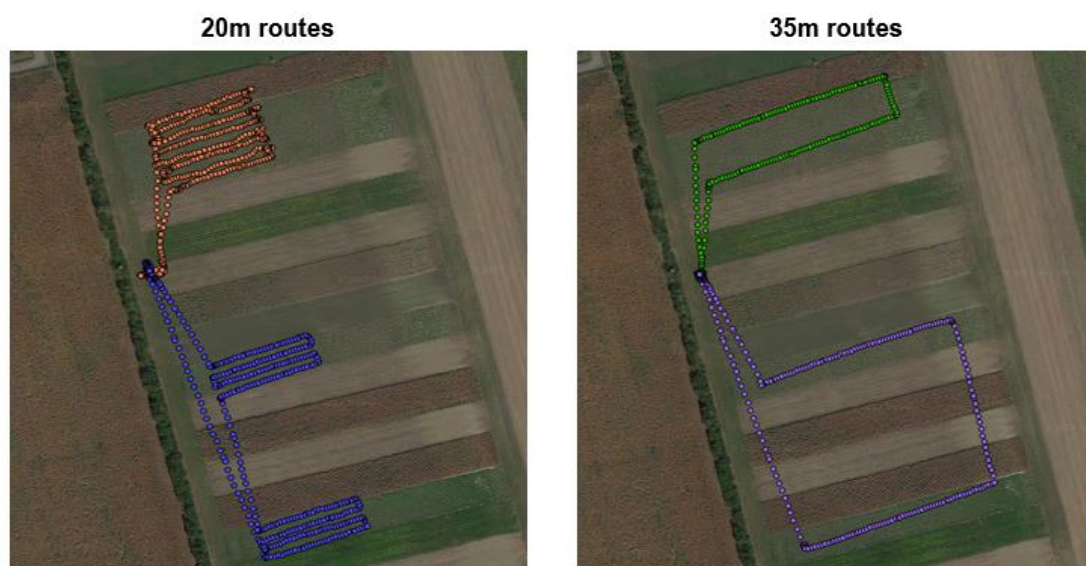


Figure 15 Flight routes. Left Image 20m routes, where orange is the north route and blue is the south route. Right image 25m routes, where green is the north route and violet is the south route (source: Valentin Löcker).

## Materials and Methods

Table 2 Protocol of successfully carried out flights. The colors indicate the four different routes as a result of different flight heights and routes, e.g. NorthMaize20 indicates that the flight covered the northern route at an altitude of 20m above ground (source: Valentin Löcker).

Successful carried out flights					
Date	Time (hh:mm)				
	13:00	13:15	13:30	13:45	14:00
20.07.2017				SouthMaize35	NorthMaize35
25.07.2017		NorthMaize20		SouthMaize20	
28.07.2017	NorthMaize20	SouthMaize20			
31.07.2017	NorthMaize20			NorthMaize35	SouthMaize35
01.08.2017	NorthMaize20	SouthMaize20		NorthMaize35	
02.08.2017			NorthMaize20	SouthMaize20	North & South Maize 35
03.08.2017	NorthMaize20	SouthMaize20	North & South Maize 35		
04.08.2017	NorthMaize20	SouthMaize20	North & South Maize 35		
05.08.2017	North & South Maize 35		NorthMaize20	SouthMaize20	
07.08.2017		NorthMaize20	SouthMaize20	North & South Maize 35	

NorthMaize20

SouthMaize20

NorthMaize35

SouthMaize35

North & South Maize 35

Both 20m flights from 01.08. did not have TIR coverage for the entire flight.

During each flight, three measurements with the EcoBot were taken concurrently in the plots to measure air temperature and relative humidity.

Every route started and ended with a flyover over black and white pads (See: Figure 16). These pads should simulate a plain, homogeneously surface to evaluate if the TIR camera drifted during the flight. Also surface temperature measurements with the IRT were taken before and after the UAV passed the pads. The IRT and TIR measurements were compared afterwards for validation purposes.

When analyzing in interpreting this thesis it needs to be considered that the IRT was not available on all days during the study (also see Table 2).



Figure 16 RGB picture taken from 20m altitude of Black & White pads for validation purposes (source: Valentin Löcker)

A checklist to standardize the procedure, which was used and ticked off before every flight can be found in the Appendix (7.1).

### 3.6 Data Preprocessing

#### 3.6.1 TIR images

The TIR camera provided TIR videos with the frequency of one Hertz. These videos were converted into .csv files using the Optris PiConnect software. The .csv files built the foundation of further LST calculations.

As mentioned before the maize plots were split into two subplots where further instruments were installed. In order to get TIR data from exactly these subplots, a GPS point in the middle of the subplot was defined as a positional reference. The TIR data was further combined with the GPS tracking of the UAV using a preprocess Python code, which was written by Claire Brenner and only adapted by me for this thesis. An additional Python script calculated the TIR image, which was nearest to the reference point in each subplot. Figure 17 shows the reference points on the left image (red and green points) and the chosen TIR images on the right image (yellow points). The rectangles also show the SUS subplots, where a straw mulch layer was placed as a substitution for the white clover underseed. The corners of the rectangles were measured with a high precision GPS device. Additionally, metal plates were placed on each corner as this material can be seen clearly on the TIR images as the emitted temperature is a lot higher than the nearby vegetation or soil parts. The green points on the left image show the centroids of the rectangles and were used as reference points.

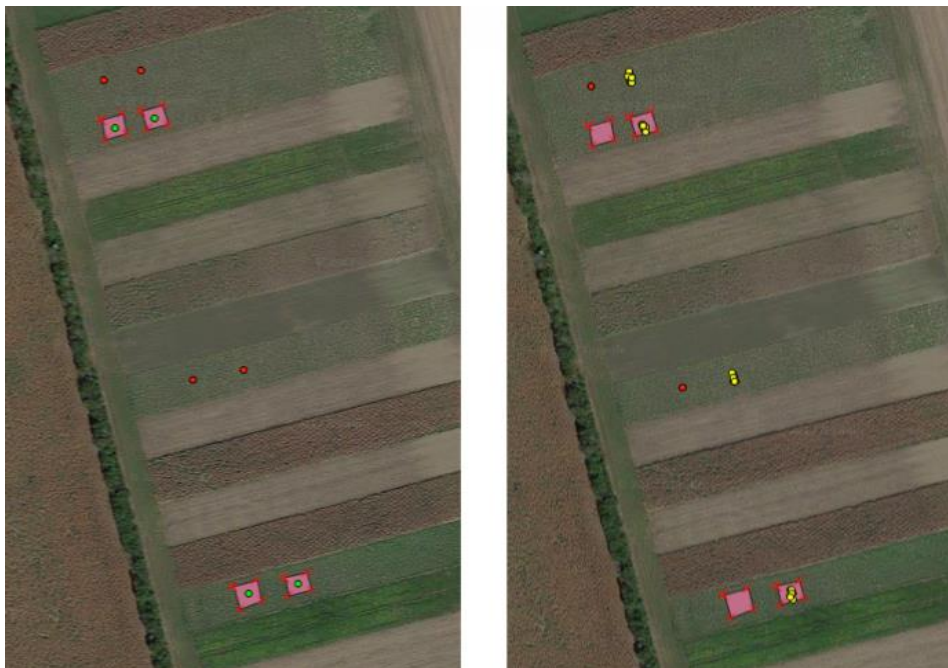


Figure 17 GPS reference points (left image), chosen images from flights (right image) (source: Valentin Löcker)

As the UAV was not able to follow the given GPS flight paths, many images of the 35m altitude flights contained of the maize plot and also sometimes the plot nearby. To erase errors in especially pixel separation, the images were cropped on the left and right ends. As seen in Figure 18, the red lines mark the borders where the image was cropped. Only the area in between the red lines were used for further calculations.

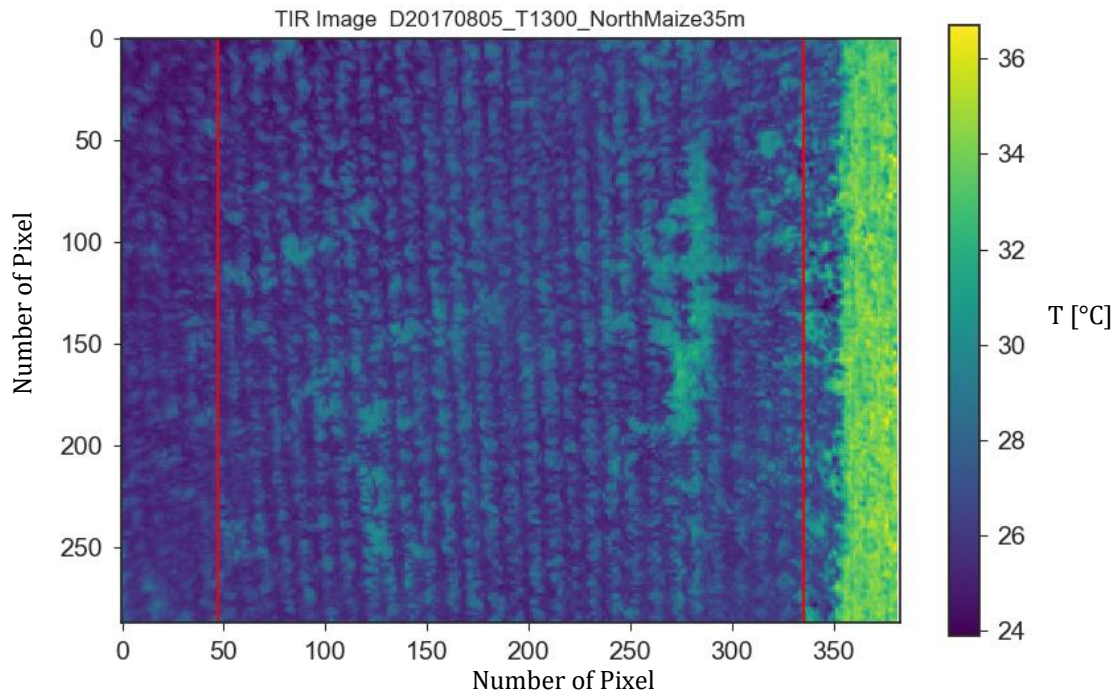


Figure 18 TIR image of a 35m altitude flight. Red lines mark the cropping line (source: Valentin Löcker)

For the comparison between IRT and TIR data, the values of the TIR images were gathered via the Optris PiConnect software. Images showing the calibration pads (see Figure 16) were taken and three values of each pad were chosen randomly by hand. The mean of the values gathered by this method was used in further calculations.

### 3.6.2 Flir data

The values of the IRT images were obtained via the Flir Tools software. This software contains functions to display temperature values from every pixel or mean temperature values from all pixels within certain drawn objects.

The collected Flir data was used to counter check the values collected by the Optris PiConnect camera.

In latter explanations, images taken by the Flir camera are referred as IRT images. Images taken by the UAV carried TIR camera are referred as TIR images.

### 3.7 Separation of soil and canopy pixels

A key element in small-scale remote sensing studies is the extraction of pure canopy pixels or in other words the separation of canopy pixels and non-canopy pixels. Many studies only used RGB images and carried out methods where they use different filters on the RGB camera or calculated different factors from the incoming wavelengths (Zarco-Tejada et al. 2013; Berni et al. 2009; Suárez et al. 2008). In this study methods to separate canopy pixels from soil pixels using only TIR images were tested.

#### 3.7.1 Statistical method

A simple method to derive canopy pixels from soil pixels in field crops was proposed by Meron et. al (2010). It is based on two empirical assumptions, which can be fully automated. In Assumption (A) (see Equation 9) the pixels of one image are separated into soil and other objects and canopy related pixels using air temperature to define upper and lower thresholds (Meron et al. 2010).

Equation 9

$$(T_{air} - 10) < T_{cr} < (T_{air} + 7)$$

where  $T_{air}$  is air temperature in °C and  $T_{cr}$  are the canopy related pixels.

Assumption (B) estimates canopy pixels using the coldest 33% of the canopy related pixels.  $T_{canopy}$  can be calculated using Equation 10

Equation 10

$$T_{canopy} = \frac{\sum_{i=1}^{0.33n} T_{cr} * f_i}{\sum_{i=1}^{0.33n} f_i}$$

where  $T_{canopy}$  (°C) is the canopy temperature,  $f$  is the number of pixels in each class  $c_r$  of the histogram, and  $n$  is the number of pixels retained after the non-crop related pixels.

#### 3.7.2 Method derived from Otsu (1979)

Another method to separate pixels is the Otsu method. Named after the scientist who first used it, the Otsu method is categorized as a clustering method. The aim is to build two clusters of values while minimizing their variances (Morse 2000; Otsu 1979). The Otsu method was originally used to separate background from foreground in black and white images (Otsu 1979). In this study the TIR images were converted into 8-bit black and

white images<sup>10</sup> and the Otsu threshold was calculated. All pixels colder than the threshold were treated as canopy pixels. All pixels warmer than the threshold were considered non-canopy related pixels.

The goal of the Otsu method is to minimize the within-class variances of two distributions, in our case the canopy and non-canopy distributions. One basic assumption of the Otsu method is that the data in the dataset are distributed bimodal. The presumed two distributions are not changeable so in order to achieve the given goal one needs to adjust where to separate the dataset (set the threshold). So, as one adjusts the threshold in one way to decrease the spread of one distribution, we simultaneously increase the spread of the other distribution. The goal then is to find the threshold that minimizes overlap between the distributions and minimizes the combined spread (Morse 2000; Otsu 1979).

The within class (intra-class) variance is defined as the weighted sum of variances of the two classes shown in Equation 11.

Equation 11

$$\sigma_{\omega}^2(t) = \omega_0(t)\sigma_0^2(t) + \omega_1(t)\sigma_1^2(t)$$

where  $\sigma_{\omega}^2$  is within class variance, weights  $\omega_0$  and  $\omega_1$  define the probabilities of the two classes separated by a threshold  $t$  and  $\sigma_0^2$  and  $\sigma_1^2$  are the variances of the two respective classes.

The class probabilities are estimated as

Equation 12

$$\omega_0(t) = \sum_{i=0}^{t-1} P(i)$$

Equation 13

$$\omega_1(t) = \sum_{i=t}^{L-1} P(i)$$

where  $L$  is the number of gray levels in a picture (or in general, the  $L$  bins of the histogram),  $i$  is the number of pixels and  $P$  is the probability.

The class means  $\mu$  are given by Equation 14 and Equation 15.

Equation 14

$$\mu_0(t) = \sum_{i=0}^{t-1} \frac{P(i)}{\omega_0}$$

---

<sup>10</sup> 8-bit black and white or grayscale images allow 256 shades of gray. The scale goes from 0 (total absence of light – black) to 1 (total presence – white) with values in between.

Equation 15

$$\mu_0(t) = \sum_{i=t}^{L-1} \frac{P(i)}{\omega_1}$$

Now the individual class variances can be calculated solving Equation 16 and Equation 17.

Equation 16

$$\sigma_0^2(t) = \sum_{i=0}^{t-1} [i - \mu_0(t)]^2 \frac{P(i)}{\omega_0(t)}$$

Equation 17

$$\sigma_1^2(t) = \sum_{i=1}^{L-1} [i - \mu_0(t)]^2 \frac{P(i)}{\omega_0(t)}$$

The next step is to analyze the full range of t values [1,256] and identify the value that minimizes  $\sigma_\omega^2(t)$ .

For any given threshold, the total variance is the sum of the within-class variances and the between class variance, which is the sum of weighted squared distances between the class means and the grand mean. (Otsu 1979) The Otsu threshold was calculated running the Otsu threshold algorithm of the Python code package 'skimage'. Therefore, the TIR images had to be transformed into a scale 8-bit scale ranging from 0 to 256 (grayscale) in order to run the script and calculate the threshold. The values were transformed to the original scale afterwards.

### 3.7.3 Sensitivity of thresholding

The major problem with thresholding is that one can never be certain if the threshold separates the right pixels. For instance, there is no proof that one pixel that is considered a canopy pixel in calculations is a canopy pixel in nature. One can include "false" pixels with ease and can easily miss "right" pixels on the other hand. These effects get worse with the quality and resolution of the image. The bigger the noise in the considered image is the less the image represents the circumstances found in nature. Therefore one has to use thresholds carefully (Morse 2000).

Particularly in this study there is no proof of the right separation because even the temperature changes within the vertical profile of the plants were severe. The height of the maize crops, mixed pixels<sup>11</sup>, wind, radiation and shadows are a few examples of factors, which come into play when canopy and soil need to be separated in dense vegetation (Jones and Sirault 2014).

---

<sup>11</sup> Mixed pixels are pixels where one pixel contains of canopy and soil. (Jones and Sirault 2014)

### 3.8 Estimating crop water stress using the CWSI

There exist various approaches to calculate the CWSI (Cohen et al. 2017; Zargar et al. 2011), a list of selected methods is displayed in Table 3. As shown in Equation 3 the CWSI accounts for the relationship between leaf and air temperature and uses wet and dry baselines. The lower (or wet) baseline should display a well-watered crop as a reference where the principle is that a fully watered crop is also fully transpiring and therefore has a lower surface temperature. The opposite is the upper (or dry) baseline, which represents a fully stressed crop. These two references in combination with the actual leaf-air temperature form the CWSI (Jackson and Idso 1981). Baselines are required to calculate the CWSI because lower and upper baselines are area and crop specific (Idso 1982). Payero and Irmak (2006) added that upper and lower baselines are also dependent on the crop's growth stage. Once the respective baselines for an area and crop species are established, the CWSI can be calculated straightforward just using the parameters plant surface temperature, atmospheric temperature and relative humidity. This makes the CWSI a relatively easy applicable water stress index (Cohen et al. 2017).

Table 3 shows different approaches to calculate the respective baselines. The approaches which were not applied in this thesis are not further explained.

Table 3 Methods to determine wet and dry baselines for the CWSI (Cohen et al. 2017)

<b>Methods to determine wet and dry baselines for the CWSI</b>		
<b>Baseline</b>	<b>Type</b>	<b>Measurement and respective calculation</b>
<b>Wet</b>	Empirical	Air temperature + X °C where X is an empirical estimate dependent on VPD
	Theoretical	Temperature calculation using the energy balance equations
	Measured bio-indicator	Temperature measurement of a real wet leaf
	Measured artificial surface	Temperature measurement of an artificial reference surface
	Statistical	Average temperature of the 5-10% of the coolest pixels
<b>Dry</b>	Empirical	Air temperature + X °C where X is an empirical estimate
	Theoretical	Temperature calculation using the energy balance equations
	Measured bio-indicator	Temperature measurements of a real leaf covered in petroleum jelly

In this thesis CWSI was calculated using the statistical and the empirical approach, respectively.

3.8.1.1 Empirical approach

The lower baseline of the empirical approach is established by several measurements on either reference days or irrigated reference plots. The values of these measurements form a “lower baseline”. The lower baseline is dependent on the relationship between leaf/air temperature and VPD (Idso 1982).

The upper baseline is not dependent on VPD and can be established using two different empirical approaches. One method is to measure canopy temperature of a non-irrigated, dry reference plot. The other method is to calculate the 95% percentile of the canopy temperature of the whole plot. Furthermore both methods are combined with the actual air temperature to calculate the ratio between air and canopy temperature (Rud et al. 2014). Most of the studies focus on the lower baseline and some published articles just determine a value for the upper baseline and comment the assumed value with (sometimes) just one sentence.

Studies have also shown that the upper and lower baselines are characteristic for a specific crop and region, respectively (Cohen et al. 2017). The big advantage of this method is that if an upper and lower baseline for a particular crop and region is established, the calculation of the CWSI can be achieved with very low technical input. In this case canopy temperature, air temperature and relative humidity have to be recorded additionally, and thereby allowing the calculation of the CWSI to be relatively straightforward. This makes the CWSI interesting for other applications than scientific purposes, such as PA (Cohen et al. 2017).

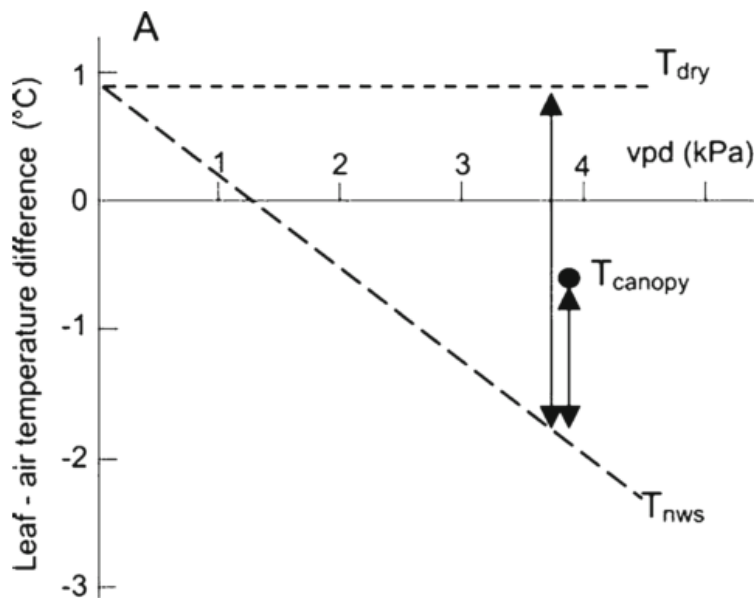


Figure 19 Example for an empirical CWSI calculation with lower and upper baselines (Lola Suárez and Berni 2012)

Figure 19 shows an example for a CWSI calculation using a lower and upper baseline. The lower baseline ( $T_{nws}$ )<sup>12</sup> shows a significant negative correlation between Leaf-Air temperature difference and VPD. The upper baseline ( $T_{dry}$ ) stays constant. The actual surface temperature (also dependent on VPD) is displayed as  $T_{canopy}$ . Using Equation 3, the CWSI can be calculated and usually produces a value between 0-1, where 0 is non water stressed and 1 is totally water stressed. However, under certain circumstances values that extend this range are possible (Idso 1982).

Payero and Irmak (2006) noted that baselines are not constant over a whole vegetation period. Basing on the research from Idso (1982) they tried to find relationships between the slope and intercept of the lower baseline and soil water depletion of the crop root zone. Idso (1982) also pointed out that there are many factors to influence the slope and intercept of the lower baselines. He concluded that scientists should take parameters such as plant height, what resumes in higher atmospheric resistance, into account when establishing lower baselines.

The upper baseline in this thesis was calculated as the difference between the mean of the hottest 5% of canopy pixels of each flight and the atmospheric temperature of every given flight. The value with the largest gap between canopy and air temperature was further on used as an upper boundary for all flights and to calculate the CWSI. This approach was used by Cohen et. al. (2017) who also worked with aerial imagery to estimate the CWSI.

Other studies (Sagarika and Ophori 2014; Payero and Irmak 2006) use the maximum value of all measurements for upper baseline calculations. However, these studies base on direct measurements of leaf (or canopy) temperature using handheld infrared thermometers. Therefore, these approaches have no uncertainty regarding any canopy separations and thresholds. Taking to account these differences, this approach was not applied for upper baseline calculations.

### **3.8.1.2 Statistical approach**

The lack of transferability of the empirical established baselines present a major disadvantage for the empirical approach (Payero and Irmak 2006). To avoid this circumstance, Alchanitis et. al. (2010) established a statistical approach for the lower (or wet) baseline. It assumes that different parts of the image are well or over irrigated. Therefore the average temperature of the coolest 5-10% of the pixels is utilized as a wet reference (Cohen et al. 2017; Rud et al. 2014; Alchanitis et al. 2010). The statistical approach poses the advantages that it can be calculated using solely the canopy temperature and does not require any static baselines (Cohen et al. 2017).

---

<sup>12</sup> non water stressed (nws)

This statistical approach proposes a solution for the wet reference. To estimate the upper (or dry) reference it is combined with the empirical approach as the upper reference from the empirical approach is constant (Cohen et al. 2017).

Having established the theoretical background of the measurements and the materials, methods and ways of calculations, the results of this thesis are displayed in the following section. The discussion of the results achieved is done as well in the next section.

## 4 Results and discussion

The results are structured according to the working steps that are needed in order to calculate the CWSI. First of all, the TRI camera calibration (drift) and comparison to IRT values is presented. In the subsequent part, the outcome of the two different methods to separate the soil and canopy pixels is depicted. Then, the two approaches to estimate the CWSI are compared and afterwards the CWSI between the SUS and CON plots is analyzed. In the final part of this section, a coincidentally discovered phenomenon, which does not directly correspond to the given research questions is presented as it could be interesting for further research.

### 4.1 TIR Camera validation

#### 4.1.1 TIR data acquisition

Data acquisition using a UAV carrier system was achieved relatively straightforward. The combination of RGB and TIR sensors fulfilled the given tasks. One concern in using UAV with such a relatively heavy pay load is the capacity of the batteries used, which do not allow relatively long flight times. Another challenge is the stability of the UAV under windier conditions. In days with more wind, the UAV had trouble to maintain the given flight track while stabilizing the carried sensors. Many images on windier days were blurred especially on the turning points of the UAV. In the first flights, the UAV did not reach the given flight height of 20 or 35 meters, respectively. The cause for this problem could be in the sensor unit of the UAV. The UAV controls flight height using sensible air pressure sensors. When the UAV started, there was mostly no wind as it was placed near the hedge. When flying upwards, the wind increased as the protection by the hedge was not given anymore. This leads to a small change of air pressure, resulting in the UAV miscalculating the flight height. Therefore, in later flights during this examination, the UAV was started in the middle of the field, further away from the hedge. After this measure taken, the flight heights were a lot more constant.

#### 4.1.2 Temperature Drift of TIR camera

As mentioned in 3.1, the UAV based TIR images were counterchecked with ground measurements of black and white pads. The black and white pads were also used to check if the TIR camera was drifting. Atmospheric corrections for the TIR measurements were not made because the correct flight height could not be determined accurately enough. Figure 20 shows a scatter plot from all flights, where the black and white pads were covered. The x and y – axis show the surface temperature of the pads when flying over at the start (x-axis) and in the end (y-axis) of the flight. The plot shows that there is a slight drift of the TIR camera to higher temperatures at the end of the flight. The two outliers from the black\_20m column can be explained as they both belong to the first flight of the

day and the pads were not placed on-site long enough before the flight, so they were still in the process of heating up and did not show a stable surface temperature. In these two occasions, the temperature of the white pads does not drift in the same extent as the black pads because the white pads reach stable conditions much faster. Generally, when analyzing the raw data, it can be observed that the temperature drift of the first flight (black pads) is always a little higher. For future applications, an earlier installment of the black and white pads before executing flights is recommended. Generally, the correlation between the observations is high. However, the correlation coefficients for the 35m flights ( $r=0.995$ , black and  $r=0.987$ , white) are higher than for 20m flights ( $r=0.836$ , black and  $r=0.971$ , white). Corresponding to that the root mean square error (RMSE) for the 35m flights (RMSE black = 1.625 and RMSE white = 1.383) is lower than for the 20m flights (RMSE black = 5.649 and RMSE white = 1.852). With a RMSE of 5.649 the black 20m flights performed particularly poor. The poorer result of the 20m flights can be explained, as outlined previously, with the matter that the 20m flights were operated first and so a stable surface temperature of the reference pads was not prevalent.

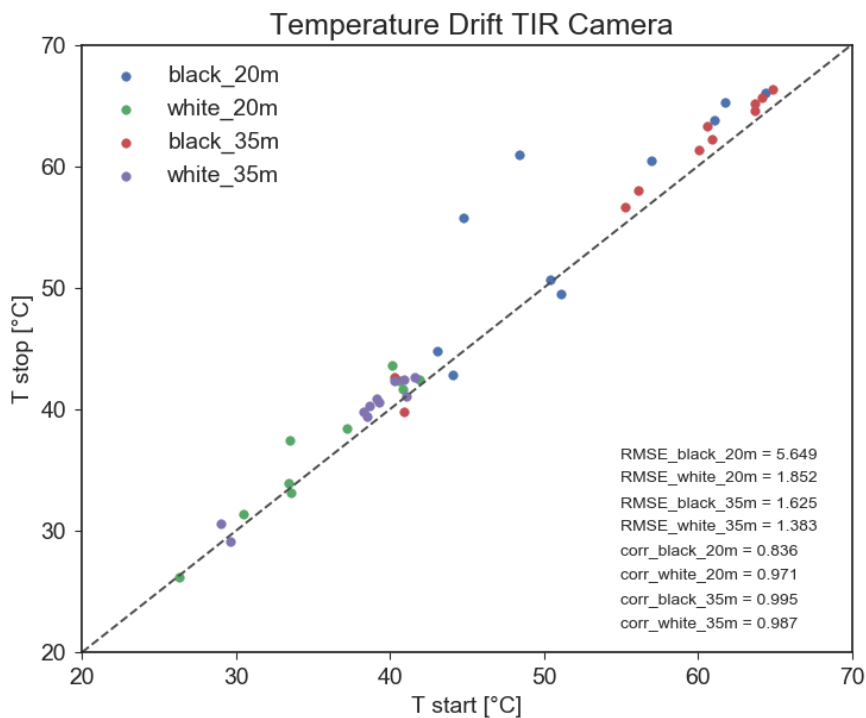


Figure 20 Temperature Drift TIR Camera (source: Valentin Löcker)

### 4.1.3 Temperature Drift of IRT camera

The same procedure as described in the subchapter 4.1.2 was applied to the measurements with the Flir IRT camera. As displayed in Figure 16, the correlation coefficient of the white panels ( $r=0.954$ ) is higher than the coefficient of the black panels ( $r=0.889$ ). Corresponding to that the root mean square error for the white panels is lower

(RMSE=2.623) than the black panels (RMSE=4.728). The RMSE Two measurements of black panels distinguish by more than 10°C between start and stop, which most likely is the result of a measurement error by the device itself. However, as displayed in Figure 21, the IRT trends in the opposite direction. For most flights, the temperature after the flight is colder than it was at the starting time. As the pads should get warmer the longer they are lit by the sun, a trend to colder temperatures in later measurements cannot represent the ground truth. So, the two measurement systems (although they are using the exact same measuring principle) drift in different directions. As the measurements were taken by hand, the flight altitude of the related flight is not issued in Figure 21.

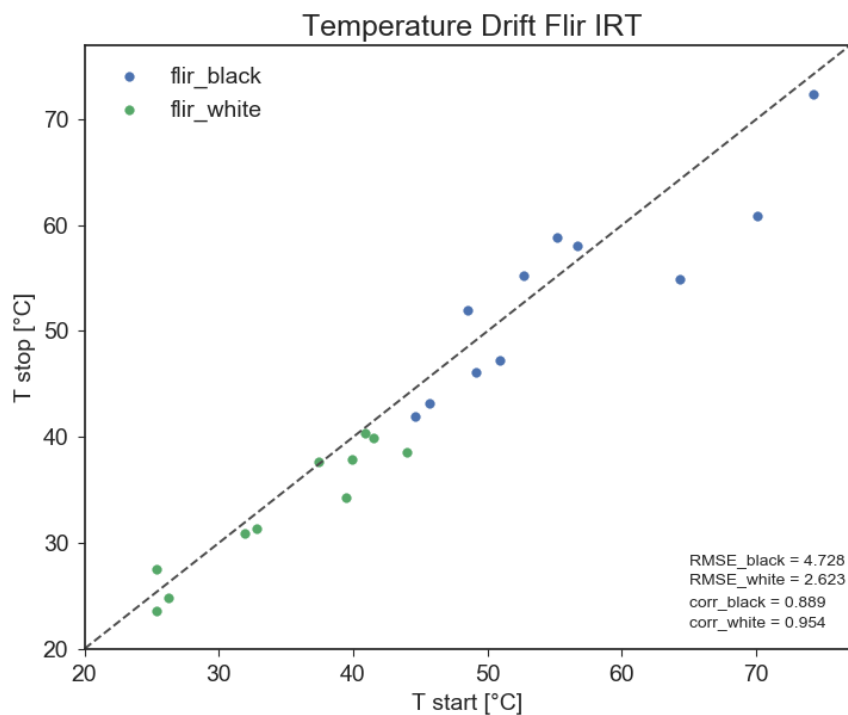


Figure 21 Temperature Drift Flir IRT. (source: Valentin Löcker)

### 4.1.4 Comparison of TIR and IRT

The TIR black and white pad measurements were counterchecked with Flir IRT measurements. Figure 22 shows the scatter plot of the compared methods to measure LST. The plot shows that the TIR measurements are trending to overestimate the temperature in comparison to the Flir measurements. Again, as can be seen in in Figure 20, the results of the white pads show a higher correlation ( $r=0.934$ ) in comparison to black pads ( $r=0.750$ ) Corresponding to that the RMSE for the white pads is lower (RMSE=2.368) than for the black pads (RMSE=4.169). The observations received by black pads, however, are a lot more inconsistent and have two significant outliers. As a consequence of the rare availability of the Flir IRT and technical difficulties with the TIR camera, there are only four flights with data of both devices available. With this small sample-size it seems impossible to formulate any reliable conclusions about this topic.

For future research, availability of Flir IRT has to be ensured in order to achieve sound sample size.

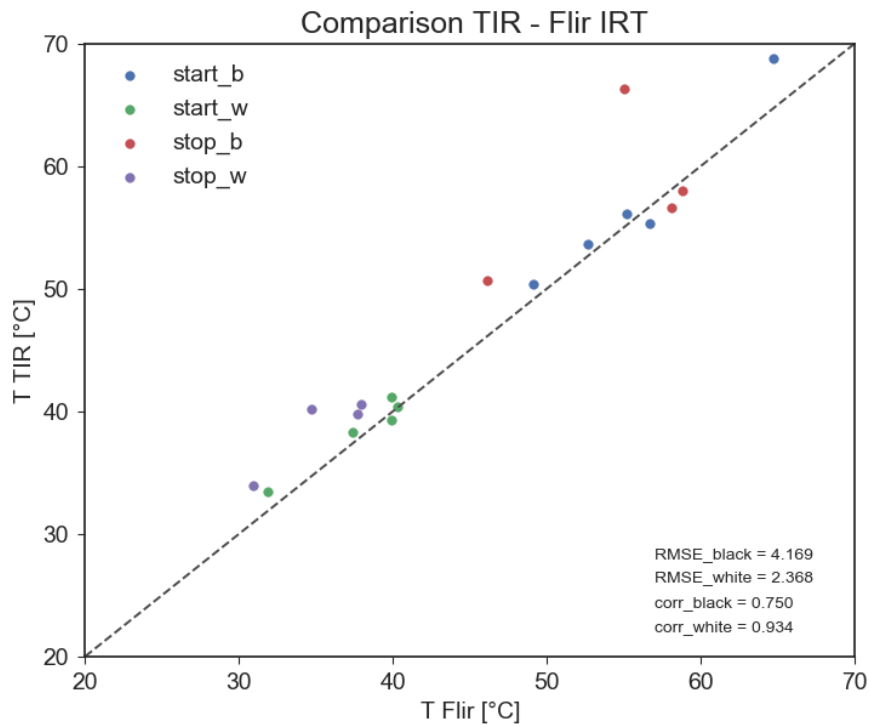


Figure 22 Comparison TIR Camera and Flir IRT camera. Start\_b=temperature of the black pad at the beginning of the flight ; start\_w = temperature of the white pad at the beginning of the flight ; stop\_b= temperature of the black pad at the end of the flight ; stop\_w= temperature of the white pad at the end of the flight (source: Valentin Löcker)

Looking at these results, it cannot be said with certainty that either one of these two measurement devices present the ground truth. Although the RMSE reveals that the TIR camera performed much better than the Flir IRT. The approach to validate the TIR camera values did not give satisfactory results. One detrimental factor was the material used for the pads. The pads were chipboards and stored at the field site during the campaign. As a result, the pads were soaked with water and therefore the chipboards were deformed and showed no homogenous surface temperature as the soaked spots could be seen on the thermal images. For further application and investigations, it is suggested to choose a more water-resistant material as well as a storage facility providing adequate shelter from weather conditions. Also, the pads were painted with spray paint, this painting technique did not provide a perfectly smooth and homogenous painted surface. So, an alternative painting technique for the pads resulting in smooth surfaces of homogeneous color is advised. Another improvement for the validation process would be to choose an alternative validation measurement method. In this study, the TIR camera and the handheld IRT camera used both the same principle of emitted infrared radiation. Both devices, however, do not provide a sufficient accuracy of  $\pm 1^{\circ}\text{C}$  (IRT) or  $\pm 2^{\circ}\text{C}$  (TIR), respectively.

## 4.2 Separation of Canopy pixels

Figure 23 shows a raw TIR image plotted from the NorthMaize20m flight, taken on 3<sup>rd</sup> of August 2017. In this plot, the maize crops represented by the coldest pixels, are clearly visible. Also, the spots with no vegetation are visible, as they show an up to almost 20°C hotter temperature compared to the canopy pixels. The challenge, however, as described in subsection 3.7.3 is to find a threshold that can separate the soil pixels from the canopy pixels. Applying combined methods using both RGB and TIR images is a very difficult task. The reasons for this are due to technical conditions of the compared cameras, e.g. different field of view, not matching camera resolutions, different mounting on the UAV, and also due to conditions in the process as the trigger to initiate the image capture applications had to be set manually. Figure 23 & Figure 24 show how distinguished two images, taken at the same time and place may be. This indicates the complex task to overlay and/or combine these two methods to separate canopy pixels from the surroundings. Therefore, statistical methods using only the single band of TIR images were used for further analysis in this study.

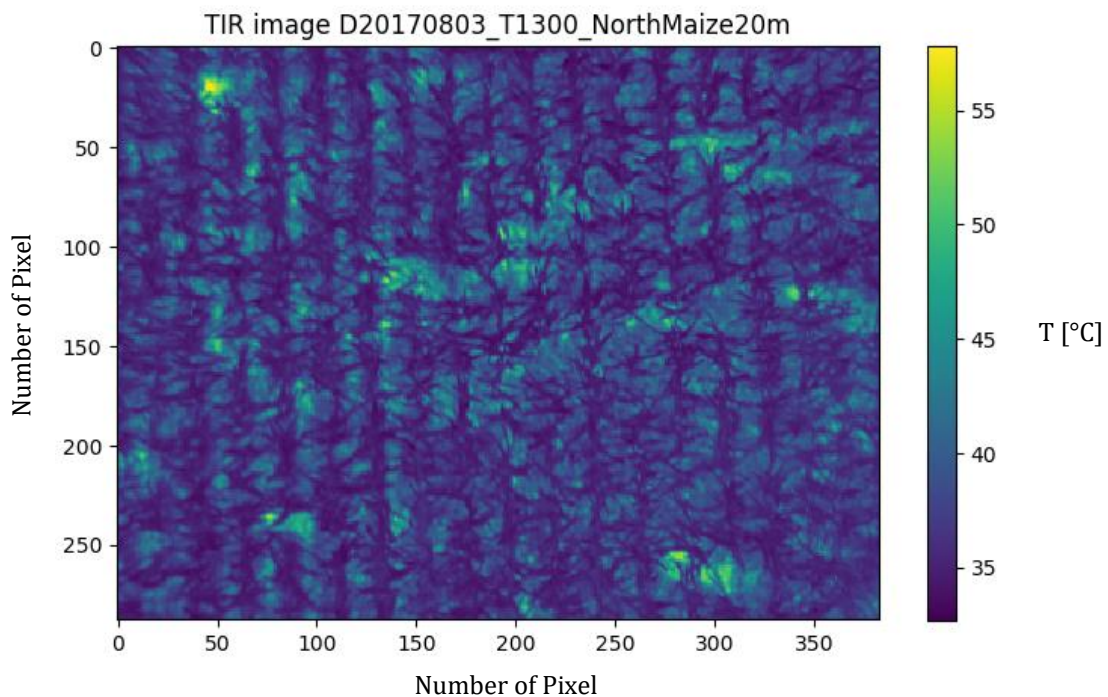


Figure 23 Sample TIR image plotted of the NorthMaize20m-flight 03.08.2017 (source: Valentin Löcker)



Figure 24 Matching RGB image (corresponding Figure 23) of the NorthMaize20m-flight 03.08.2017 (source: Valentin Löcker)

### 4.2.1 Statistical Method of pixel separation

The first assumption, outlined in subsection 3.7.1, separates the pixels, which can be clearly stated as ‘non canopy pixels’. As displayed in Figure 25, sparsely vegetated spots are already ruled out. Compared to the original image (Figure 23) the temperature range is less than half of the original image.

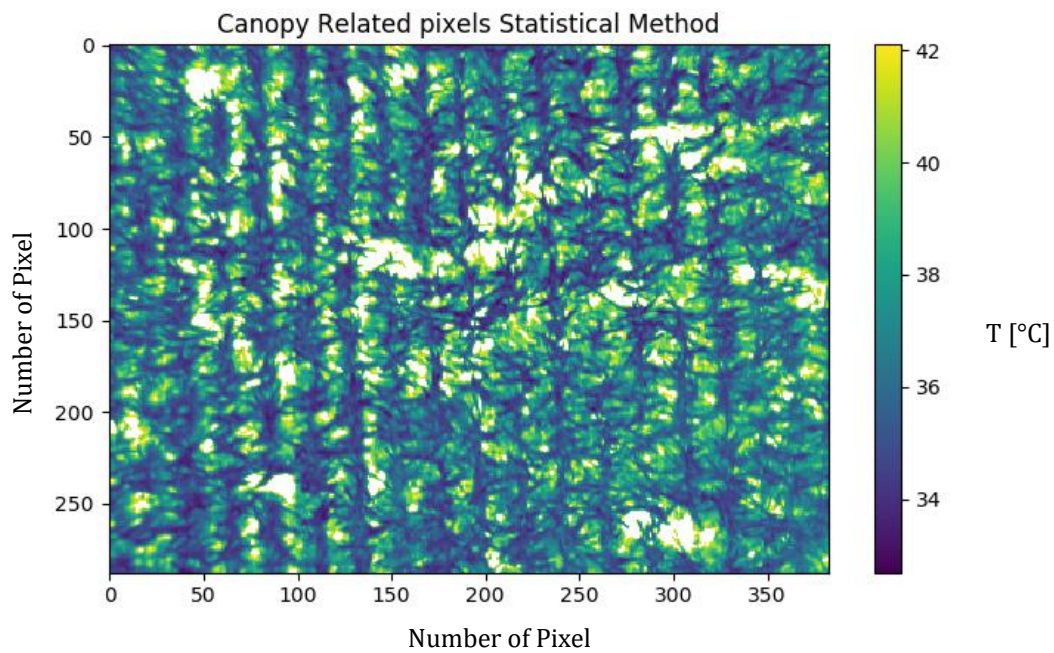


Figure 25 Canopy Related pixels (Assumption A) Statistical Method, NorthMaize20m 03.08.2017 (source: Valentin Löcker)

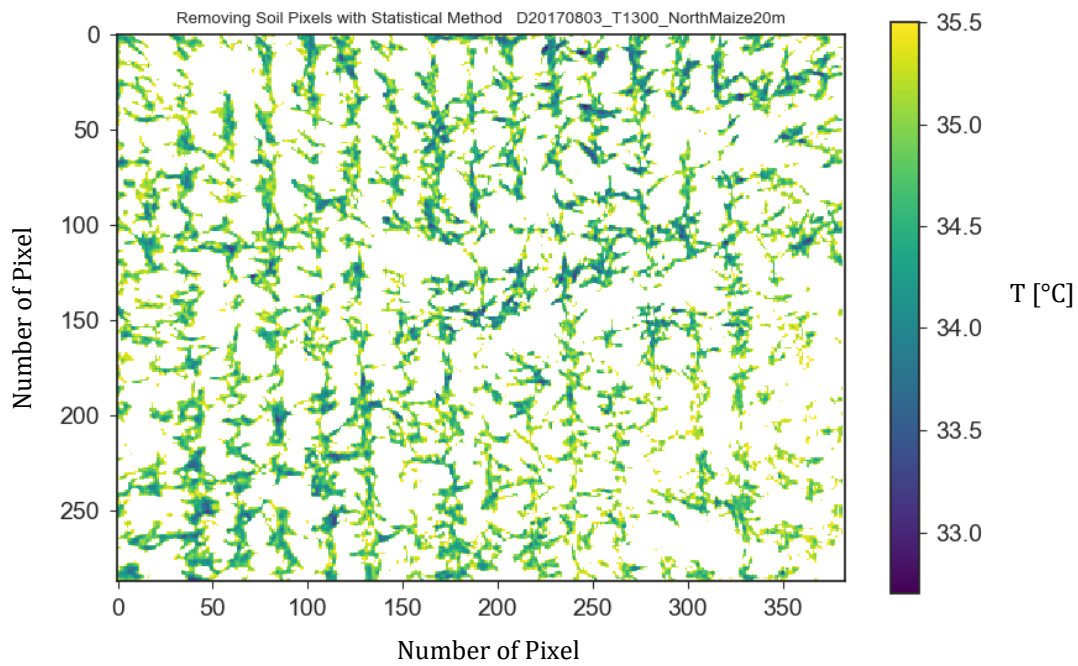


Figure 26 Canopy Pixels Statistical Method 20m, NorthMaize20m 03.08.2017 (source: Valentin Löcker)

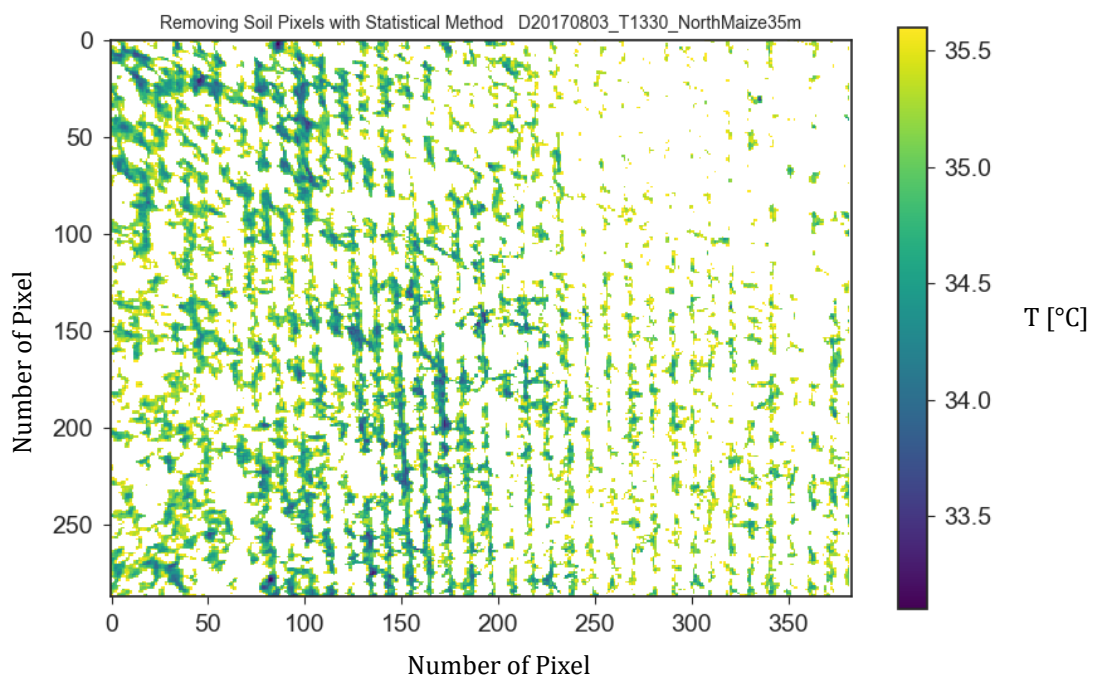


Figure 27 Separation of canopy pixels statistical method 35m, NorthMaize35m 03.08.2017 (source: Valentin Löcker)

Figure 26 & Figure 27 display the next step taken (Assumption B, see section 3.7.1) in the statistical method. This assumption specifies the true canopy pixels. The image calculated from 20m-flight altitude, at first sight, looks promising. Figure 27 shows an image from 35m-flight altitude. Although the maize rows are clearly visible in both images, it appears that a lot of pixels, which in nature are canopy pixels, are simply left out. The reason for this is that the statistical method applied takes 33% of the total canopy related pixels into account to keep them. This, in turn, leads to the cancelling of 67% percent of the canopy related pixels, without distinguishing if they should be considered canopy pixels or not. After further synchronization with RGB images, it can be said that the statistical method is underestimating the canopy density by far.

### 4.2.2 OTSU method

The same image that has been presented before (Figure 25), was manipulated using the OTSU method (see Figure 28, 20m flight altitude and Figure 29, 35m flight altitude).

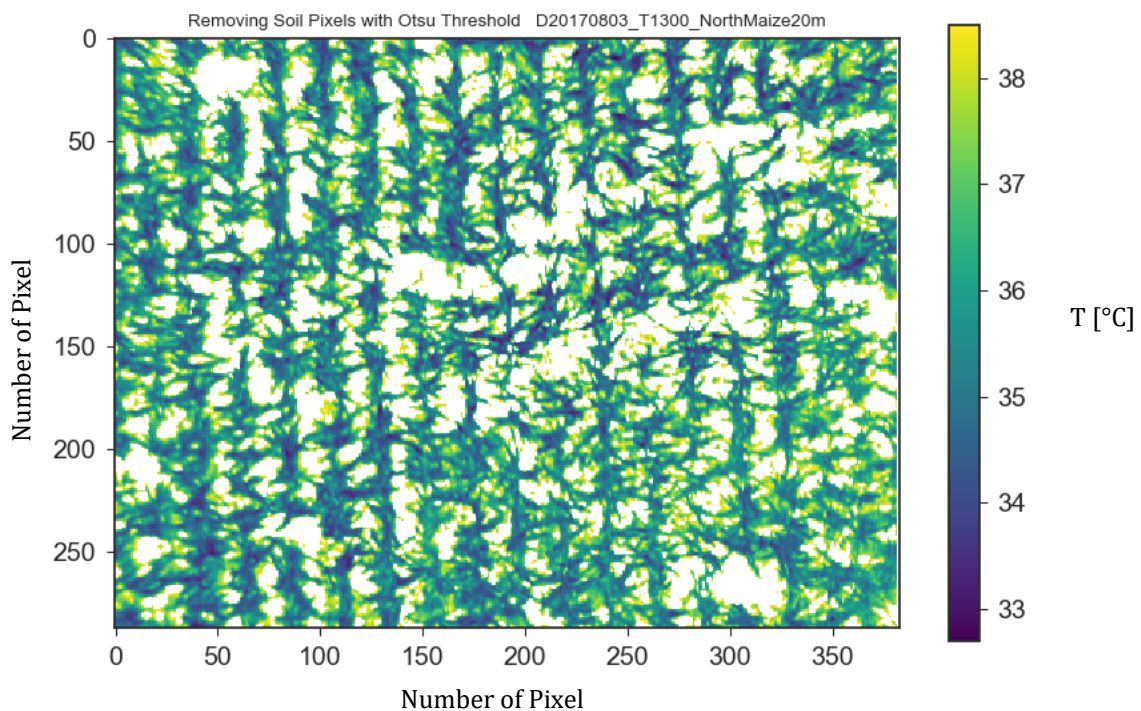


Figure 28 Separation of canopy pixels OTSU method 20m, NorthMaize20m 03.08.2017 (source: Valentin Löcker)

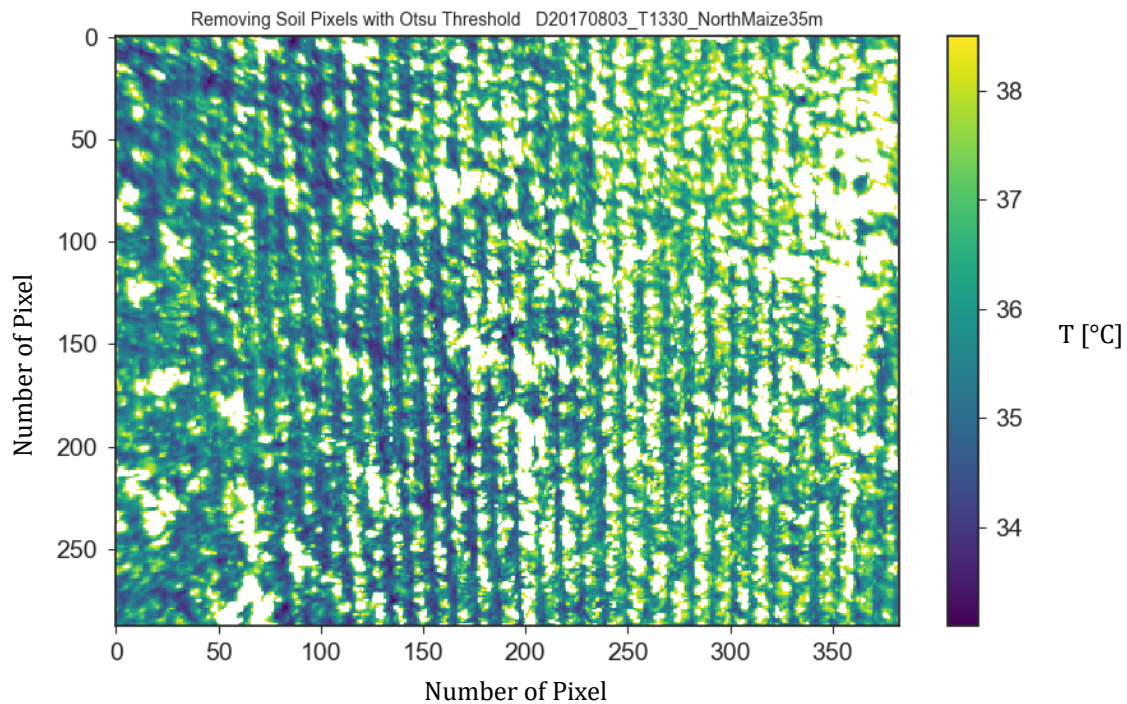


Figure 29 Separation of canopy pixels OTSU method 35m, NorthMaize35m 03.08.2017 (source: Valentin Löcker)

At first sight the OTSU method provides satisfactory results. Looking at Figure 28 and Figure 29 the results of the OTSU method looks plausible. These two images were taken on a very hot, clear sky day with high solar radiation. Figure 30 however shows the weaknesses of the OTSU method. The image belongs to a cloudy day with mediocre incoming solar radiation. The image is separated into two main parts. On the left side the larger, vegetated part and on the right side the smaller crop or non-vegetated part. The OTSU method now sets the threshold at a comparable high temperature (see histogram Figure 33). This leads to the fact that all clear non-vegetated pixels are separated due to generally hotter temperatures outside the vegetated area, but the pixels in-between the maize plots are nearly all considered canopy pixels. In the vegetated part obvious hotter parts, where the vegetation is scarcer and soil pixels shine through, can be seen. However, the OTSU threshold is set too high to capture these pixels and separate them from true canopy pixels. So, the conclusion of this image is that the OTSU threshold does not provide satisfactory results when the evaluated area does contain two different vegetation statuses.

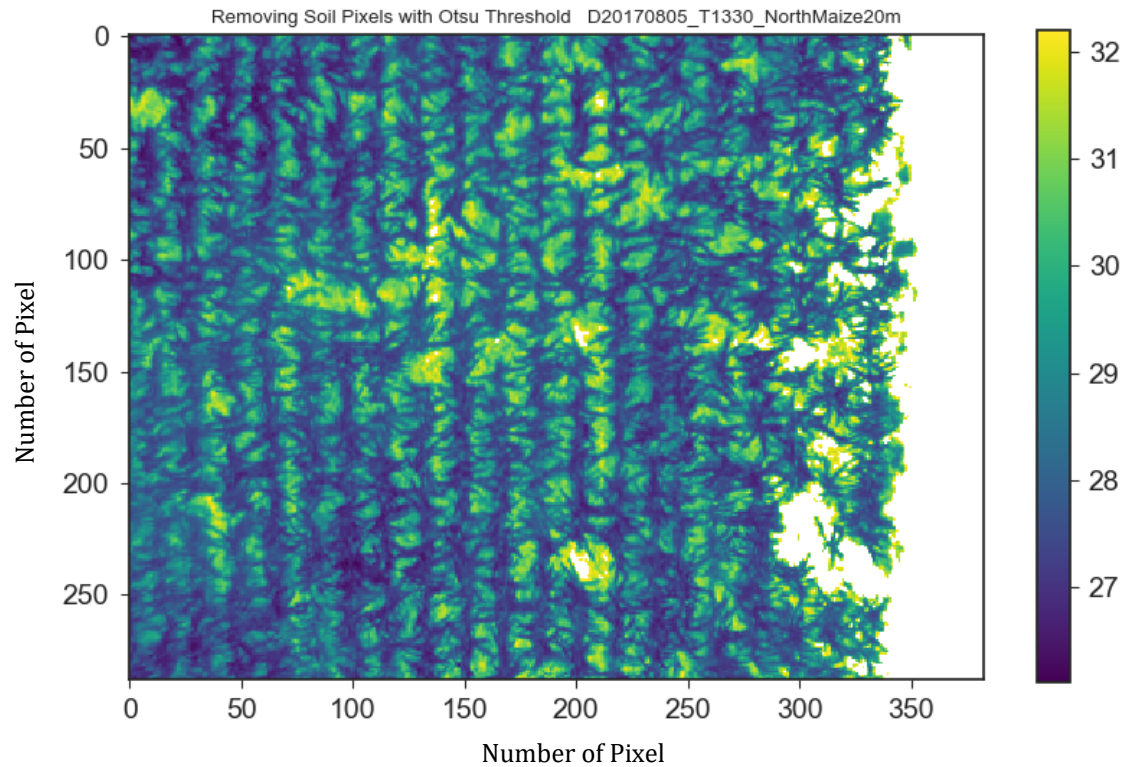


Figure 30 OTSU performance on a day with lower incoming radiation, 20m NorthMaize 05.08.2017 (source: Valentin Löcker)

### 4.2.3 Comparison of the two approaches

In the following section, the statistical method and the OTSU method are compared. For this purpose, temperature distribution histograms are used. Within these histograms, the respective thresholds for separation are displayed to demonstrate the resulting differences.

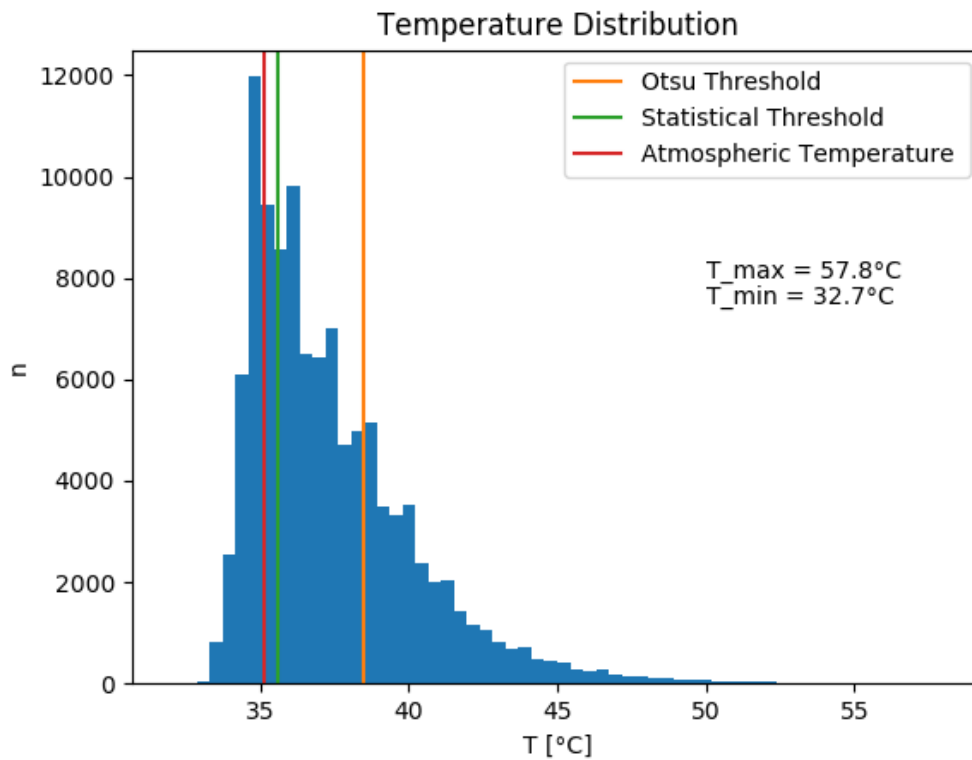


Figure 31 Temperature Distribution histogram of the NorthMaize20m-flight 03.08.2017 (source: Valentin Löcker)

The histogram displayed in Figure 31 shows that the surface temperature ranges from 32°C to more than 52°C. This broad range of surface temperature points out that radiation has had to be very high at the measured time. Most pixels have values close to the atmospheric temperature, which indicates that the maize crops are transpiring. This forms a very good basis to separate pixels because the heated soil pixels can be clearly separated from the canopy pixels.

The statistical threshold is just above the atmospheric temperature, which does not reflect the conditions in the maize plots, as sunlit leaves usually exhibit higher surface temperatures compared to atmospheric temperature, even when the plant is moderately transpiring.

The OTSU threshold, however, is set a lot higher than the statistical threshold, which reflects the canopy temperature better. Nevertheless, there is no certainty that the OTSU captured all canopy pixels or was set too low or too high.

The distribution of temperature, taken from the two flights on August, 3<sup>rd</sup> 2017 (displayed in Figure 31 & Figure 32, North 20m and 35m) appears very similar, but as the atmospheric temperature rises for about 1°C and the solar radiation goes down, the shift of the thresholds becomes prominent (see figure 27). The statistical threshold is now almost a degree below the atmospheric temperature, whereas the OTSU threshold temperature and the atmospheric temperature are almost the same, causing the lines in the histogram to overlay.

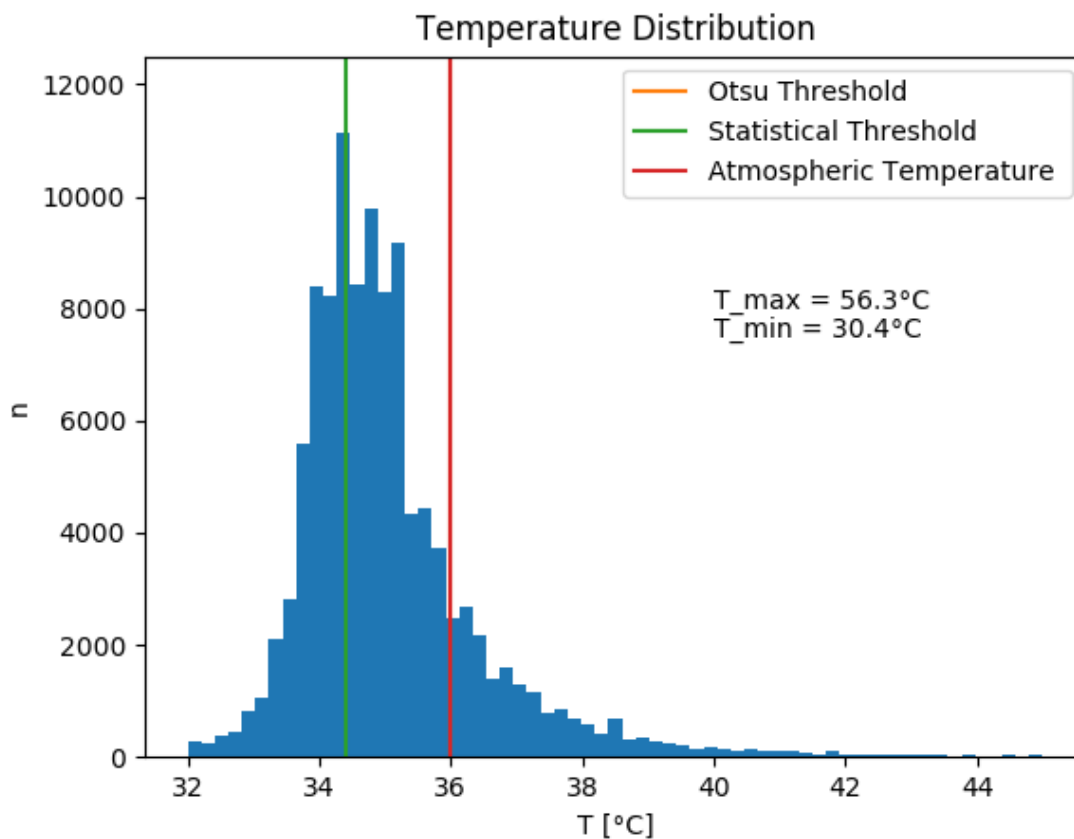


Figure 32 Temperature Distribution histogram of the NorthMaize35m-flight 03.08.2017 (source: Valentin Löcker)

To compare the performances of the two thresholds on colder days, two sample histograms (Figure 33, Figure 34) from flights on the 05.08.2017 were calculated. As stated before, this was a rather cloudy day, leading to expect a rather low radiation. Figure 33 shows the 20m flight from day. In comparison to hotter days, e.g. August 3<sup>rd</sup> 2017 (Figure 31, Figure 32), the temperature range is a lot narrower and the coldest surface temperature measured in this flight is hotter than the atmospheric temperature. Therefore, the two thresholds are hotter than the atmospheric temperature. The OTSU threshold does perform very poorly in this example because it overestimates the threshold temperature by far. This finding is supported by results displayed in Figure 30.

In conclusion, it can be said that analyzing the TIR data separately, using either the statistical approach or Otsu method to separate the soil pixels from the canopy pixels, did not provide a satisfying outcome. The two methods are both using just numerical information of the TIR pixels, which in this case, was not sufficient to achieve satisfying separation of canopy and soil. Therefore, a combined approach with RGB and TIR, or even RGB with near infrared, could yield better results. In situations with standalone trees with no vegetation around, especially the Otsu method is expected to provide better results. In dense vegetation like a maize field, the difference between a sunlit canopy pixel and a shaded soil pixel cannot be distinguished solely by LST values. Another suggestion would be a combined approach using the TIR data in combination with a given vegetation index, e.g. the NDVI or a using a new algorithm basing on the standard deviation of the TIR data

distribution (Han et al. 2016). Another basic idea to assess the plausibility of the thresholds would be to compare CWSI calculations with and without pixel separation methods.

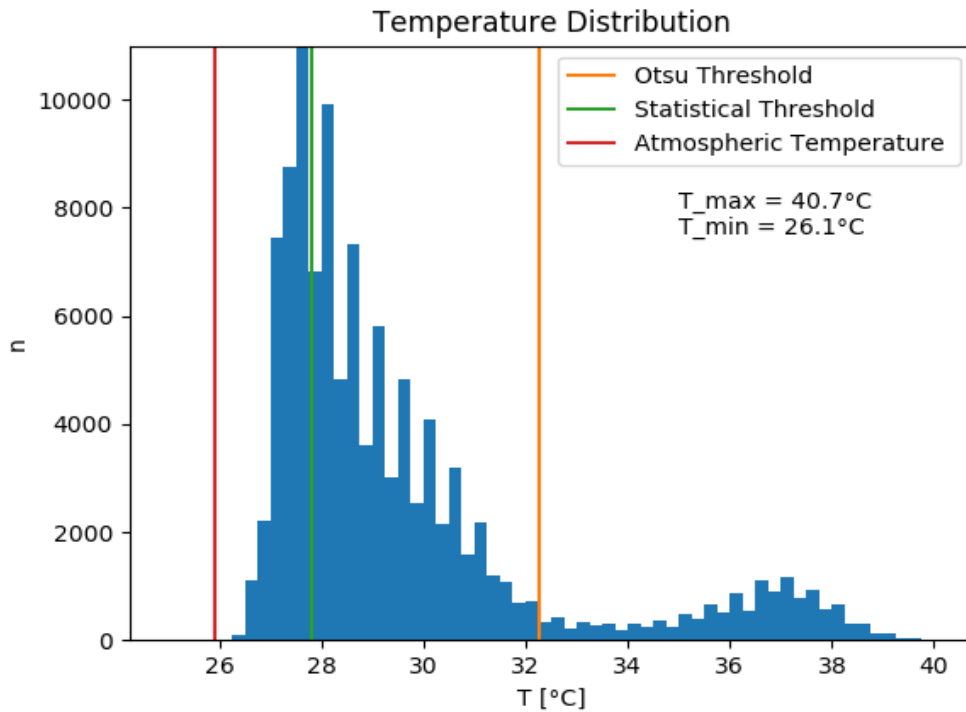


Figure 33 Temperature Distribution histogram of the NorthMaize20m-flight 05.08.2017 (source: Valentin Löcker)

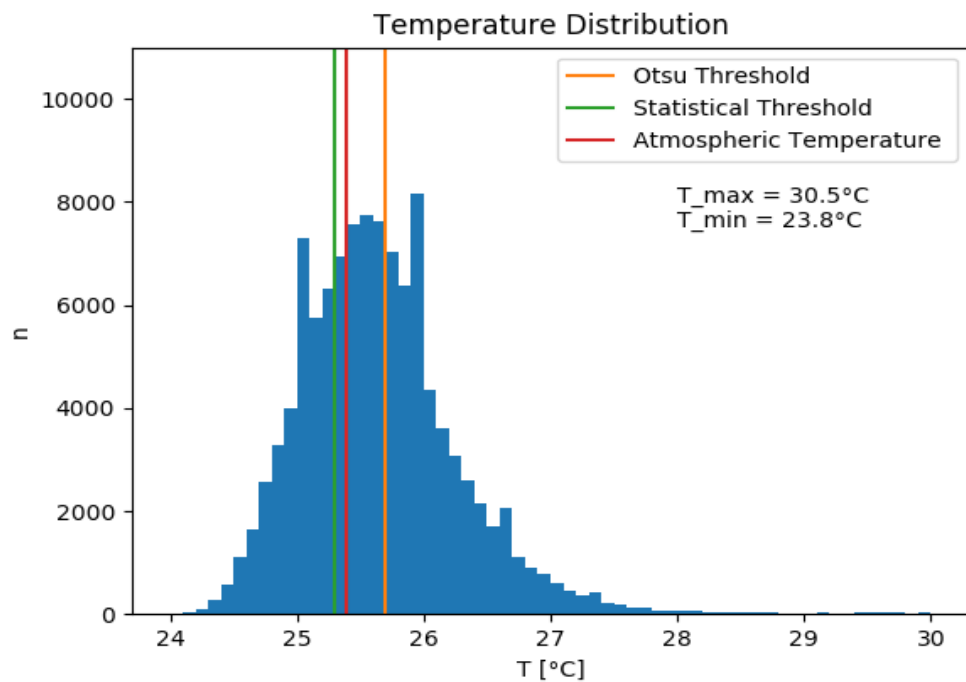


Figure 34 Temperature Distribution histogram of the NorthMaize35m-flight 05.08.2017 (source: Valentin Löcker)

### 4.3 Temperature difference as the foundation of CWSI

The temperature difference between atmospheric temperature and canopy temperature builds the foundation for further calculations of the CWSI. Therefore, this delta value already can indicate if plants are stressed or not.

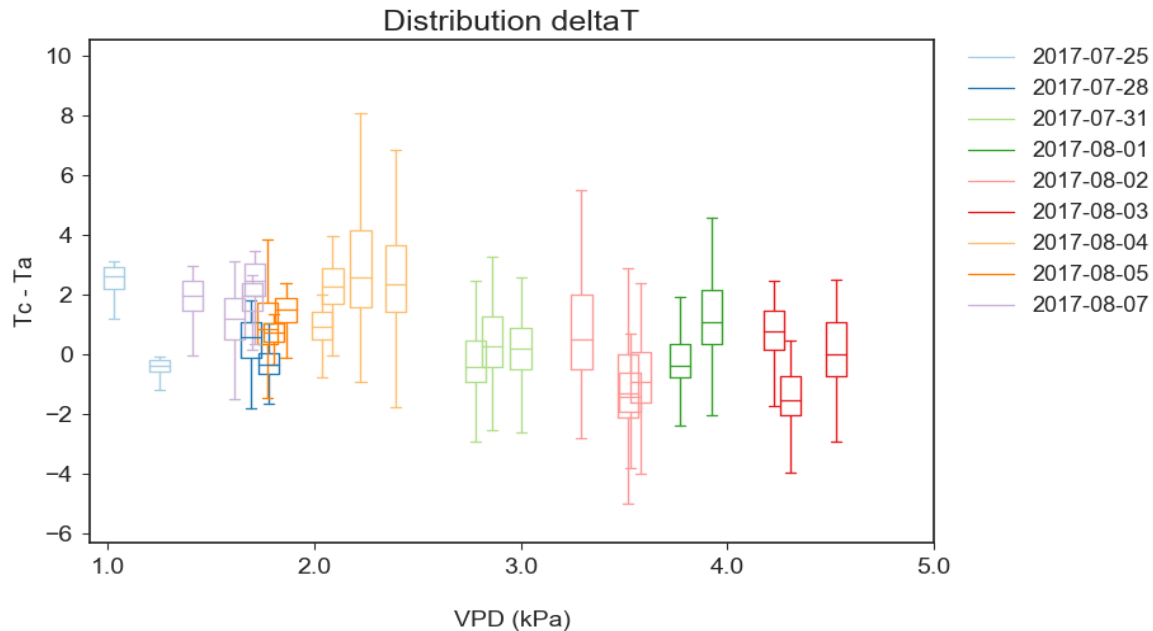


Figure 35 Boxplot of all delta T values from all flights; Tc= canopy temperature ; Ta= atmospheric temperature, VPD= vapour pressure deficit(source: Valentin Löcker)

The boxplot in Figure 35 displays the range of all operated flights. Each boxplot displays one flight. A correlation between higher VPD and broader range can be seen as the flights from 25.7.,28.7.,05.08.,07.08 each have a relatively small range of delta T values compared to the other flights. These said flights all were operated at cloudy conditions. It can be stated, that the flights carried out at conditions <2kPa of VPD display a smaller range than flights carried out at > 2 kPa VPD. During the field campaign all flights with <2kPa were carried out at cloudy weather conditions. Therefore, the gradient between canopy and air temperature was smaller. This reinforces the statement that distribution of the canopy temperature during flights in cloudy conditions is more homogenous than during flights in clear sky conditions.

One of the biggest advantages of remote sensed data is that they provide spatial data. Figure 36 shows the spatial distribution of the delta T differential. Here can be seen that the temperature gradient drops below zero where the vegetation is denser. On the edges of the vegetation pixels, the gradient tends to be higher. For this given flight the maize crops transpired because the canopy temperature is mostly lower or the same than the outside temperature. If the crops would not transpire, the delta T value will be a lot higher.

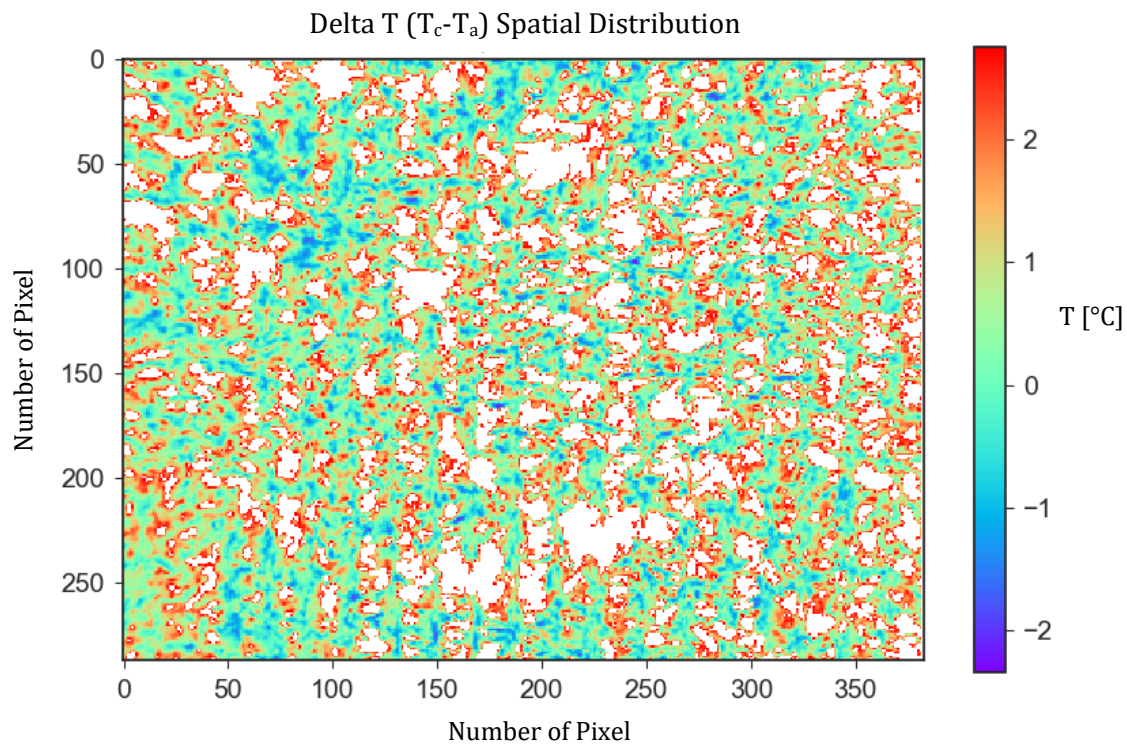


Figure 36 Delta T spatial distribution of the 03.08.2019 North 20m flight (source: Valentin Löcker)

Although the delta T distributions can indicate water stress, further calculations need to be made as delta T values are not comparable with each other because of the always changing conditions. Therefore, lower and upper baselines are needed for establishing a reliable water stress index.

#### 4.4 Applying the CWSI

In the following subsection the CWSI is applied using two different approaches. The statistical method and the empirical method.

##### 4.4.1 Statistical Method

As mentioned before the Statistical Method proposed by (Alchanitis et. al. (2010)) does not use a fixed upper or lower baseline. Therefore, the baselines are calculated separately for each event and there is no possibility of values outside the stated range from 0 to 1. Figure 37 shows calculation of all operated flights using the statistical threshold for separating soil and canopy pixels. The y-Axis displays the calculated CWSI value and the x-Axis displays the outside temperature during the given flight. Here the shortcomings of the statistical threshold can be seen as there is no difference in CWSI between heat stress days and colder reference days. All flights lead to similar CWSI values which is highly unlikely.

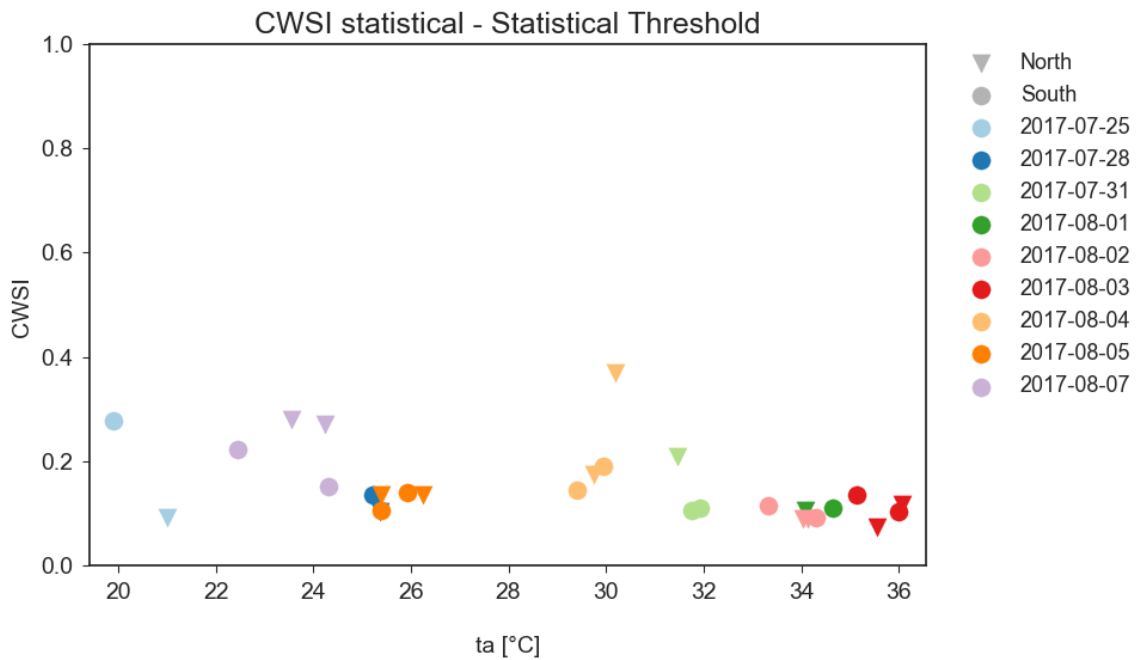


Figure 37 CWSI CWSI estimated according to the statistical method and statistical threshold proposed by (Alchanitis et. al. (2010)). Ta= atmospheric temperature . (source: Valentin Löcker)

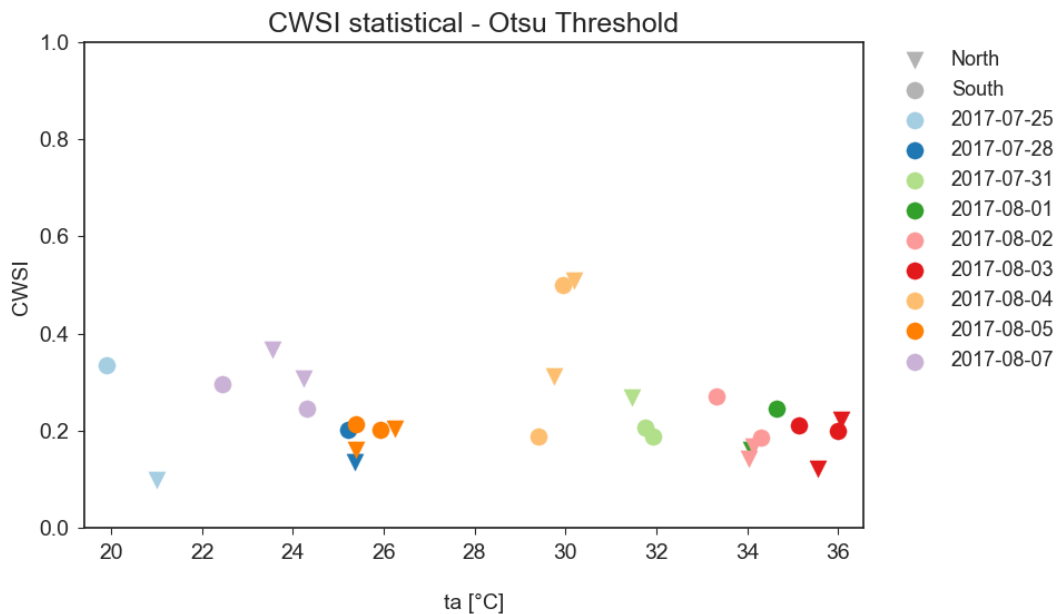


Figure 38 CWSI calculated according to the statistical method proposed by (Alchanitis et. al. (2010)) in comparison with the CWSI computed with OTSU threshold (Otsu 1979). Ta= atmospheric temperature (source: Valentin Löcker)

CWSI values in Figure 38 were calculated with the same method than in Figure 37, but instead the OTSU threshold was used for canopy separation. The CWSI values drop as the outside temperature is rising, which cannot represent the water stress conditions in the field because the hotter it gets the more water stressed the plants are (although this

assumption is not always correct as the relative atmospheric humidity strongly influences the process).

### 4.4.2 Empirical Method

In order to apply the empirical method of the CWSI, the establishment of a lower baseline as well as an upper baseline is necessary. In the following subsections, the attempts made to establish a lower baseline and an upper baseline are described and the results are discussed.

#### 4.4.2.1 Attempt to establish a lower baseline

One part of the thesis was to establish a lower baseline for the CWSI, maize crops and the Tulln region. However, the setup of the SUSI plots did not contain an irrigation system. Accordingly, the lower baseline data acquisition was done on days following precipitation events and on cloudy reference days. In total, 8 reference flights were taken into account for the calculation of a lower Baseline. Figure 39 shows the scatter plot of the 8 flights and the linear regression line to determine the lower baseline. It has to be stated that although the linear regression was calculated, a clear linear relationship of the different reference flights was not given. Due to better overall results, indicated by the histogram analyses in subsection 4.2.3, the lower baseline was calculated using the OTSU threshold of the given flights. The calculated baseline for Tulln is  $y = -0.94x + 2.63$ . This lower baseline is taken into further calculation for the empirical method of the CWSI in subsection 4.4.2.

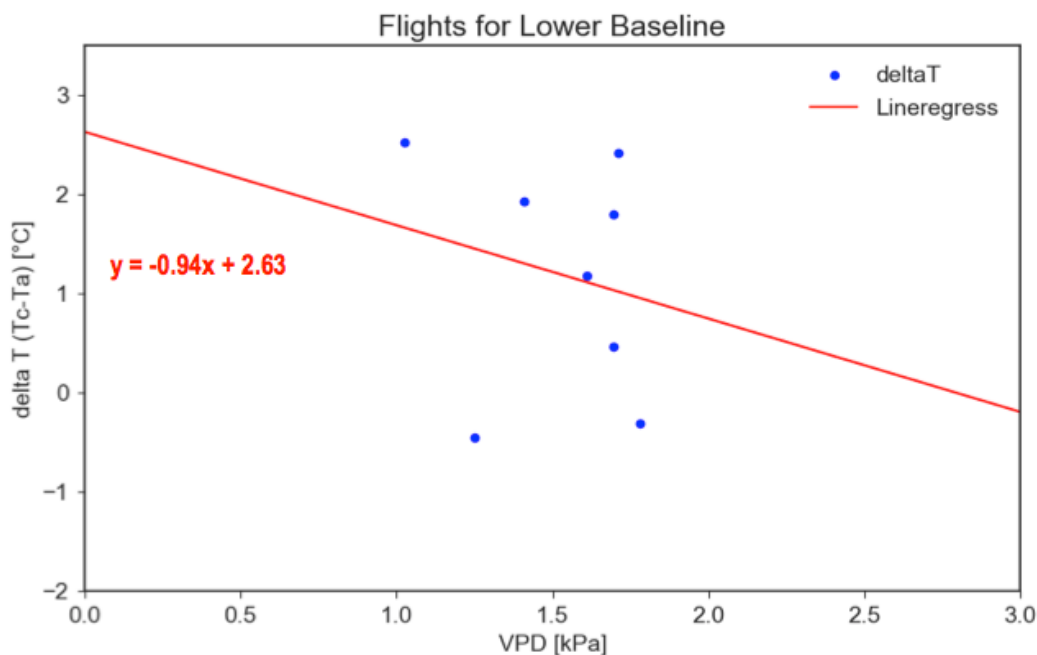


Figure 39 Lower Baseline Tulln VPD= vapor pressure deficit (source: Valentin Löcker)

Due to the lack of irrigation and the relatively small sample size, it remains questionable if the plots were actually non-water stressed during the lower baseline flights. Additionally, many flights were taken during cloudy conditions, whereas according to Jackson and Idso (1981), the CWSI should only be estimated in clear sky conditions. Therefore, the validity of the established lower baseline for Tulln needs further investigation/confirmation from further research. Taking into account that lower baselines are specific to climate and crop species, a similar lower baseline was researched in the literature (Dagdelen et al. 2008).

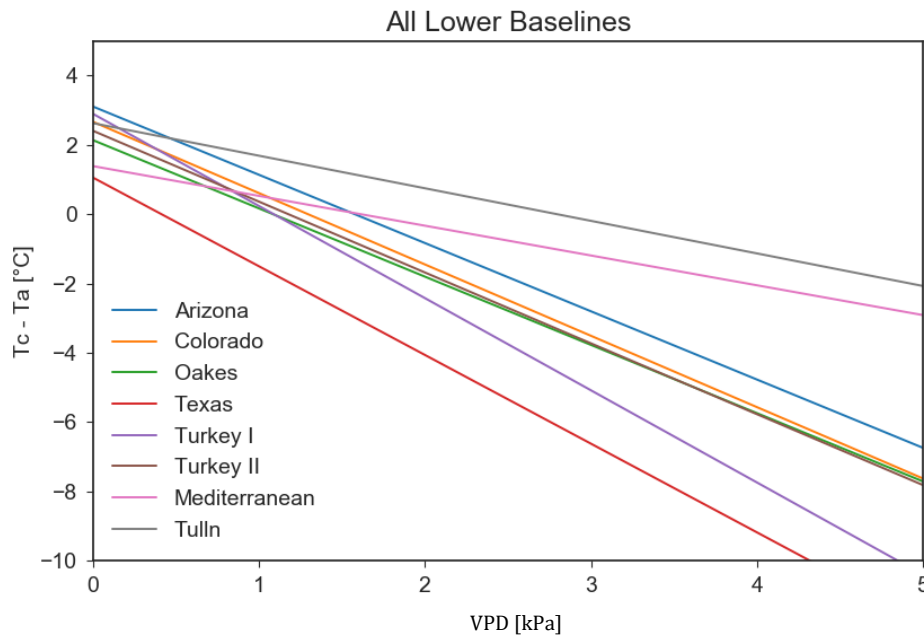


Figure 40 Lower Baselines found in literature (source: Valentin Löcker)

Most established lower baselines refer to regions, which are not comparable to the area under research in this thesis (Tulln), because heat stress studies are usually done in hot and arid regions. The climate data from Oakes, North Dakota (ND), USA, however, seems comparable to the inspected region (see Figure 41 and Figure 42, respectively).

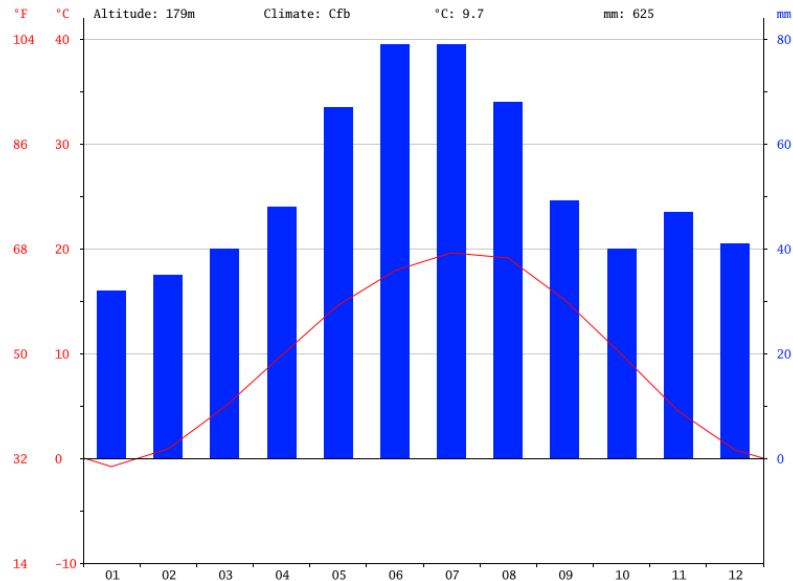


Figure 41 Climate diagram from Tulln, Austria (time range of data: 1982-2012) (source: de.climate-data.org)

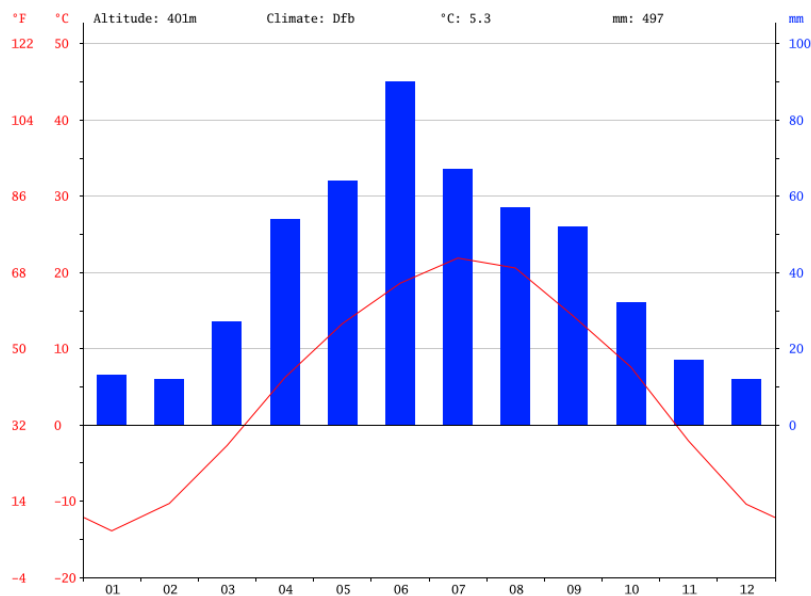


Figure 42 Climate diagram from Oakes, North Dakota, USA (time range of data: 1982-2012) (source: de.climate-data.org)

In order to investigate a possible comparability between the baselines of Oakes, ND, USA and Tulln, Lower Austria, the climate diagrams are analysed. The annual precipitation is about 130mm higher in Tulln (625mm) than in Oakes (497mm). Additionally, the average temperature is higher in Tulln (9,7°C) compared to Oakes (5,2°C) due to very cold winters in ND. The summer temperature in both regions is at an average of approximately 20°C. The precipitation sums in the spring and summer months (from April to September) are also similar to another (Tulln: 390 mm, Oakes: 384 mm). Therefore, for further CWSI calculations, the lower baseline from Oakes and Tulln were compared. However, it has to

be noted that the scale of the precipitation axis of Figure 41 and Figure 42 are differing (!).

### **4.4.2.2 Attempt to establish an upper baseline**

The biggest gap between measured air temperature and 95 percentile of canopy temperature occurred at the North 20m flight on August 4<sup>th</sup>. The Upper Baseline for further calculations was set at 7,56°C. The upper baselines found in literature range from 3°C to > 10°C (Payero and Irmak 2006).

### **4.4.2.3 CWSI calculations**

With the results from the subsections 4.4.2.1 & 4.4.2.2, the empirical CWSI was calculated. The CWSI was calculated using two different lower baselines, lower baseline Tulln and lower baseline from Oakes, ND, USA. These two approaches were compared. Attempting to answer the central research question, the CWSI values of the SUS and CON plots were compared. The pixel separation for these calculations were always done using the Otsu threshold.

According to the CWSI calculations (see Figure 43) using the lower baseline Tulln, the maize plots were not stressed during the field campaign. The highest CWSI value occurred on August 4<sup>th</sup>. However, no trends or correlations can be seen as flights of reference days have more or less the same CWSI values than flights of heat stress days. At some reference days a negative CWSI value occurs.

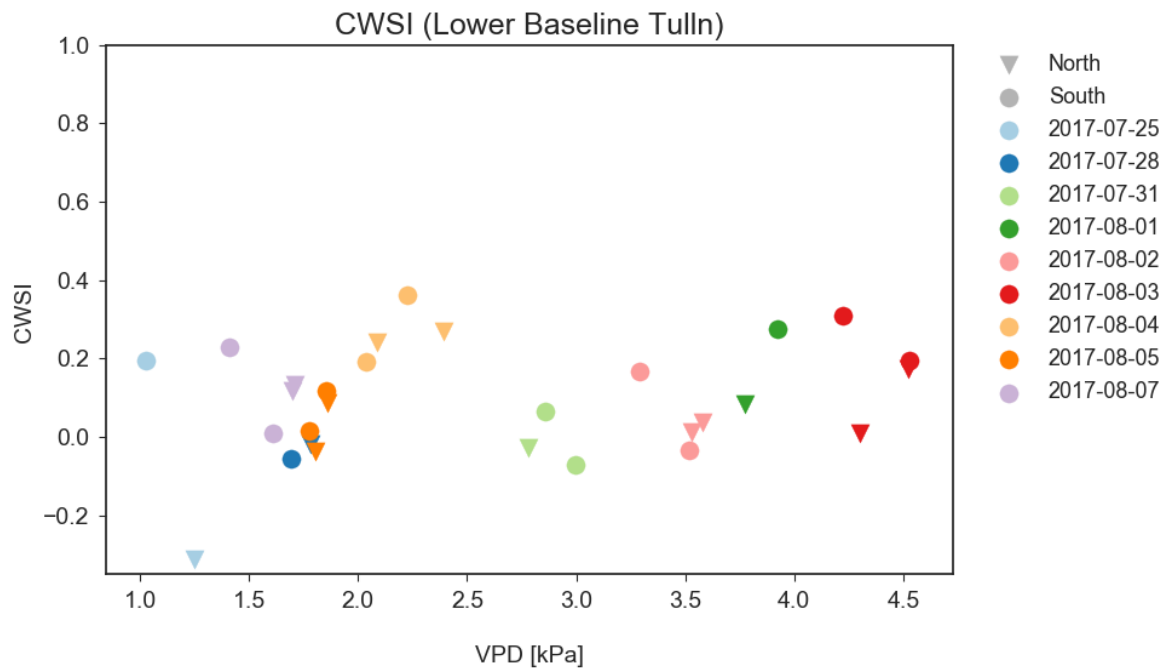


Figure 43 Calculated CWSI with Lower Baseline Tulln (source: Valentin Löcker)

Figure 44 displays the CWSI values using the lower baseline from Oakes. Except for generally higher CWSI values the results do not differ much from the calculations using the lower baseline from Tulln. The calculations show a slight trend to higher CWSI values with higher VPD.

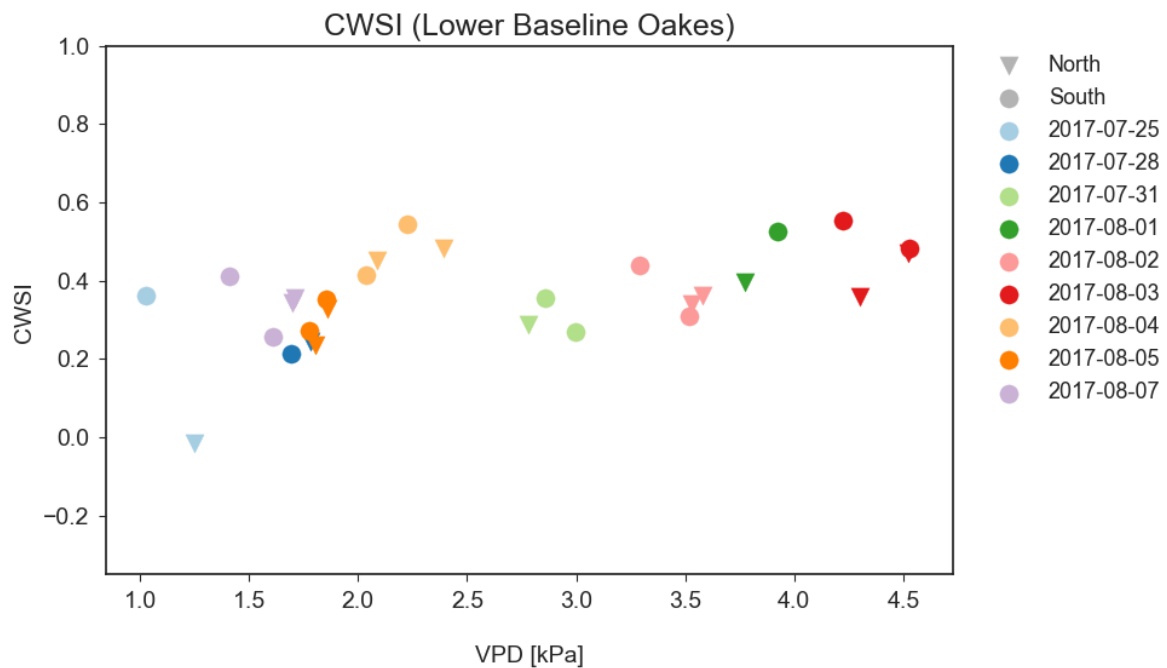


Figure 44 Calculated CWSI with Lower Baseline Oakes (source: Valentin Löcker)

Spatial distribution CWSI data of one flight is displayed in Figure 45. According to the CWSI calculations the maize crops do not suffer from water stress as the max CWSI values do not even reach 0.5. However the certain pixels even show values below zero, which is plausible because the lower baseline is a mean value for not water stressed crops which according to (Idso 1982) can be undercut punctually. When values fall below the lower baseline on a regular basis, the lower baseline should be refined.

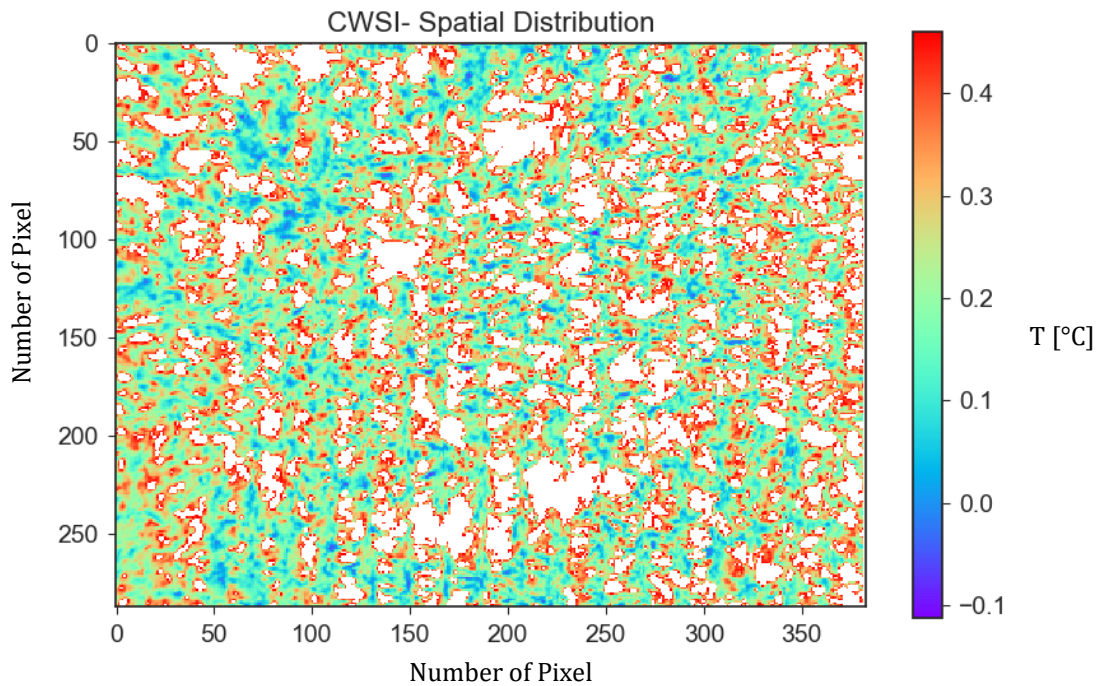


Figure 45 Spatial distribution of the CWSI values from the 03.08.2017 North 20m flight (source: Valentin Löcker)

There is no validation or countercheck for these two different methods. One possible approach would be, comparing these results to the simultaneously measured LC\_Pro<sup>13</sup> measurements.

### 4.4.3 Comparison SUS vs CON

The central question of the thesis was the comparison of the sustainable and the conventional managed maize plots. Using the empirical method of the CWSI as instrument, comparisons were made in the following.

---

<sup>13</sup> LC\_Pro is a portable photosynthesis measurement device, which measures conductance, photosynthesis rate and transpiration. This device was used during the SUSI project from other participants.

For the comparison between SUS and CON plots, only 20m altitude flight were chosen because the 35m altitude flights cover the whole width of the maize plots. The images chosen from the 20m altitude flights cover the examined subplots.

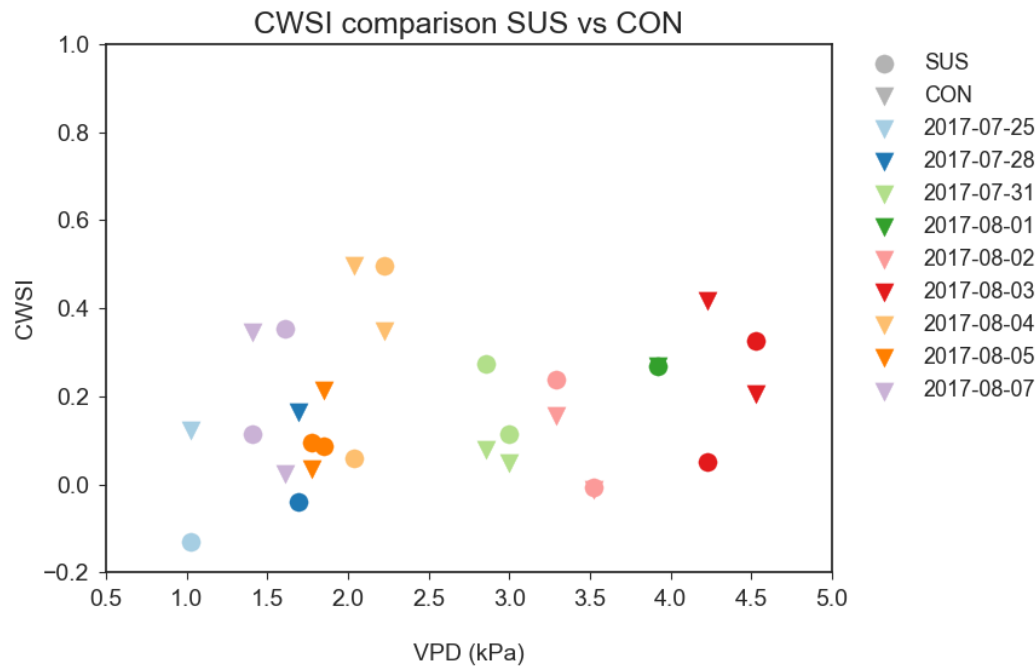


Figure 46 CWSI comparison of all flights. For each flight two pictures were compared. SUS = sustainable ; CON = conventional ; (source: Valentin Löcker)

Figure 46 shows all CWSI comparisons between SUS and CON plots. The lower baseline Tulln was used for these calculations. For each flight two images were compared. The plot shows that no clear statement can be made whether SUS or CON plots tend to be less or more water stressed. In fact, in 7 out of 15 flights the one of each cultivation scheme was less water stressed and one flight shows the exact results for both schemes.

In conclusion can be said that the SUS and CON plots are not substantial different in terms of water stress. This assumption is backed by the thesis of Vivian Sethmacher (Sethmacher 2018). One factor, which did not prove to make a difference, was the outlaid straw mulch. The higher the crops grow and the denser the vegetation is, the less important the mulch cover becomes (Zamir et al. 2013). In this investigation, the maize crops were fully grown, and therefore the vegetation cover was fully developed. Another factor was that maize in general is relatively well accommodated to heat and water stress (Crafts-Brandner and Salvucci 2002).

However, it has to be stated that the methods used for the calculation of the comparison contain too many uncertainties. So, it is not possible to make a valid statement whether the SUS or CON plots suffering different levels of water stress. Furthermore, no statement can be made which of the different influencing parameters causes the most inaccuracies in the results.

#### 4.5 Mean Temperature Distribution

During plausibility analyses of the 35m altitude flights (only on heat stress days (heat stress days were defined as days with an atmospheric temperature of 30°C or more)), abnormal temperature distributions were observed. The analyses contained the mean temperature distribution from every picture taken from the maize field. The goal of this analysis was to confirm that the mean temperature in all pictures was comparable and that the images taken are representative for the whole maize plot.

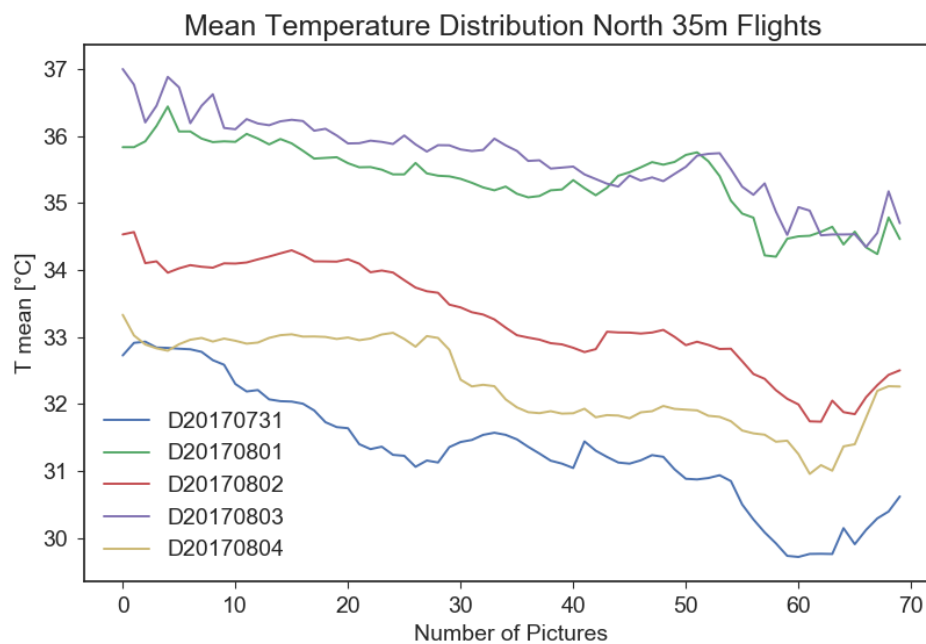


Figure 47 Mean temperature distribution of all north route 35m altitude flights on heat stress days. Graphs show the variation of mean temperature during the flight from west to east on every flight (source: Valentin Löcker)

This assumption, however, was confirmed for most of the plot, but not in total. The last images of the eastern end of the maize plot all showed a substantially lower mean temperature when compared to the images on the western end of the plot. In fact, a severe drop in mean temperature of up to two degrees Celsius could be found at the exact same area of each examined flight. Figure 47 shows the distribution of the mean temperature for each 35m altitude flight operated during the field campaign. The x-Axis displays the picture number where number one is the first picture taken over the western part of the maize plot. The higher the number the more to the east moved the UAV. The analyses stop when the UAV takes on to turn back to fly over the second plot (see Figure 49). Other comparisons with flights from the south route produced more or less the same results, which can be seen in Figure 48. The light blue shading in Figure 48 displays the standard deviation of the mean temperature.

The first aim of the analysis was to evaluate if the TIR camera is drifting in one direction. This was primary seen as a supporting analysis for subsection 4.1.2. But the results of the

analysis in subsection 4.1.2 trend in the exact opposite direction as the temperatures in the end of the flight tend to be higher than in the beginning. So, this leaves out the possibility of a technical error of the TIR camera. One assumption is that the moderate downward trend of the mean temperature can be caused by the hedge located in the west end of the field site. As the UAV is moving further away from the hedge, the wind intensity is getting higher, which could be observed during the field measurements. This causes a downward trend in mean temperature. It has to be stated that there is no measured proof of this assumption.

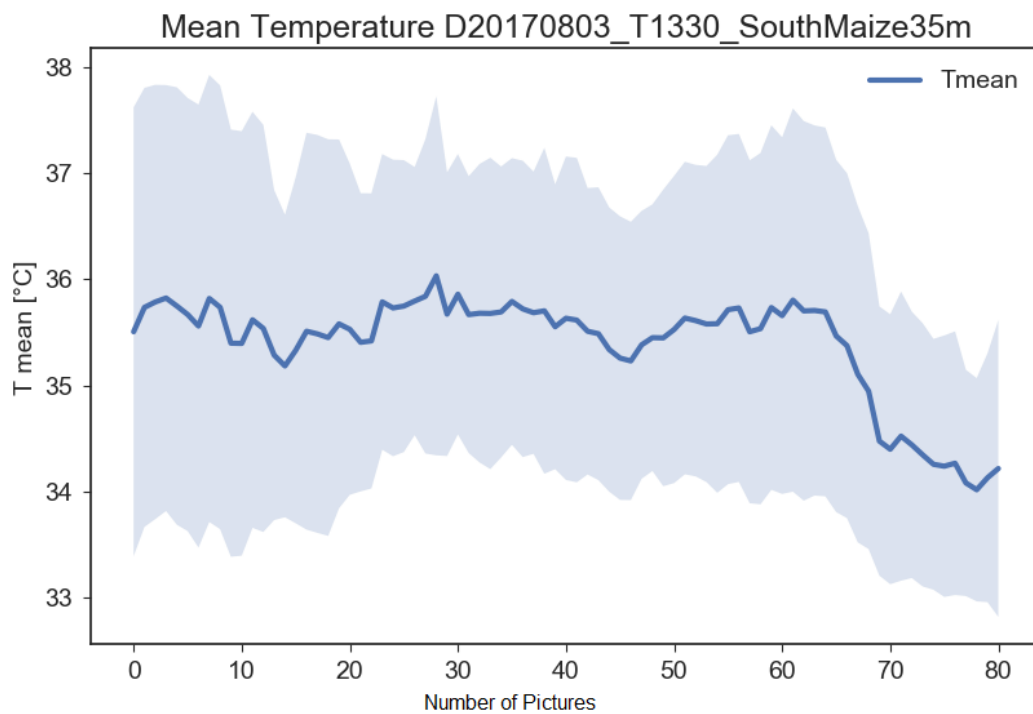


Figure 48 Mean temperature distribution of south 35m altitude flight on August 3<sup>rd</sup> at 13:30 (source: Valentin Löcker)

As marked with the red line in Figure 49, the temperature drop appears always at the same point in the field. The soil in the part east (or seen as right in Figure 49) of the red line consists of backfilled material. This can be seen with aerial images as the colors of the soil are lighter and the vegetation is scarcer than in the western part of the plots. However, the backfilled material and the scarcer vegetation should lead to higher surface temperatures as lighter ground material cannot fix as much water as the clay rich soil of the western part. Also, the scarcer the vegetation is the higher the surface temperatures are. These results need further research in order to make a dependable statement.

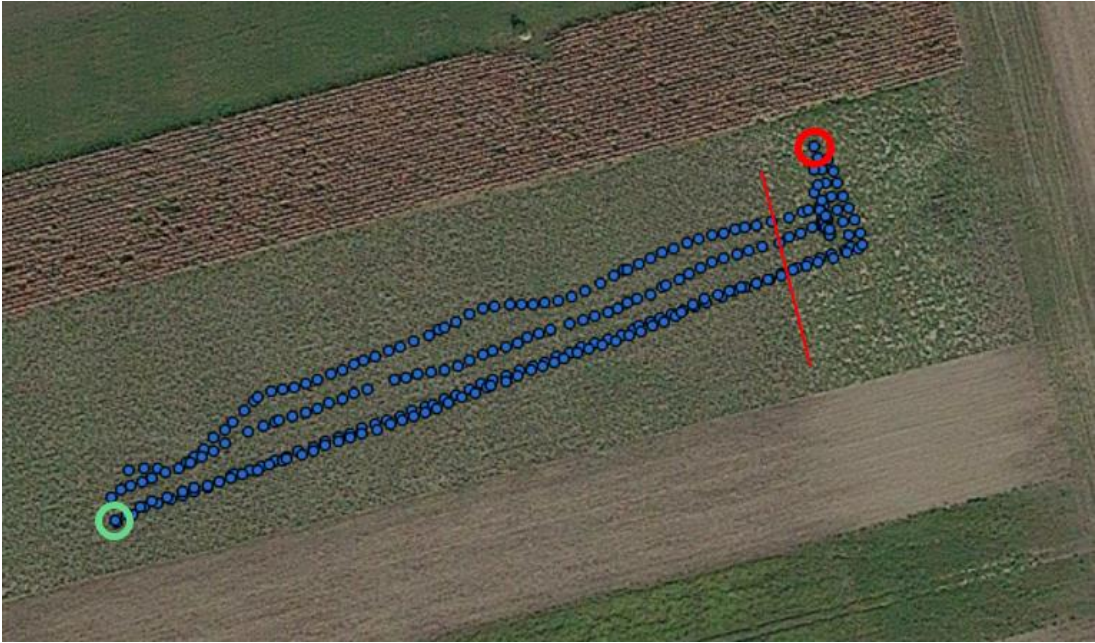


Figure 49 Flight tracks from Figure 36. green circle= start / picture 1 ; red circle = stop / last picture ; red line = temperature drop (source: Valentin Löcker)

### 5 Conclusion and outlook

Decreasing precipitation and higher atmospheric temperatures during the summer months will present challenges for the agricultural industry in central Europe (Gobiet and Truhetz 2008), e.g. due to increase in water stress in crops. Given these challenges, the existing agricultural system needs to be prepared for water scarcity. Land surface temperature (LST) serves as an indicator for water stress in arable crops. This thesis performed measurements of LST using an (unmanned aerial vehicle) UAV and ground based measurements using a mobile multi-sensor application called Ecobot. For this matter, the long-term sustainable intensification (SUSI) project, where sustainable (SUS) and conventional (CON) crop management systems are compared to each other, can present viable information in how to proceed with agricultural management in the future.

Data acquisition using an UAV carrier system was achieved relatively straightforward. The thermal infrared (TIR) sensors fulfilled the given tasks. However technical shortcomings in terms of battery capacity, stability of the whole carrier unit in windier conditions and flight height settings still contain potential for improvement.

It was not possible to validate the measured LST sufficiently. The use of black and white pads to generate a homogenous surface did not work as planned. Many technical challenges from the material of the pads themselves, the painting technique, the storage of the pads during the campaign and the insufficient accuracy of the measurement devices lead to not satisfactory results.

The preprocessing of the data using python scripts, which were originally written by Claire Brenner and just adapted by me for this thesis, worked very smooth and can be applied with a few small changes for any given UAV measurement campaign. The possibilities for UAV campaigns seem to be endless. And with technology in this field evolving rapidly every year, the change from a carrier-based approach to a sensor-based approach could bring a big leap in terms of broad use of these systems.

The combination of UAV data, Ecobot data and data from the ground survey bears the possibility of a holistic analysis of the whole SUSI project. In this thesis, the focus was on the procession and analysis of data gathered from the UAV, temperature and relative humidity data from the Ecobot. The Ecobot presents a possibility of data collection in a high spatial and temporal resolution. However, the application of the Ecobot in a study with more than head high maize crops was not optimal. In this particular thesis, this was not an issue as the data received from Ecobot was sufficient for the purposes of this investigation. However, when the application or trial makes it necessary to use the whole potential from the Ecobot, either smaller crops should be chosen or a system to elevate the person carrying the Ecobot needs to be installed.

Separating canopy pixels from all surface pixels was not achieved sufficiently. The two considered approaches could not provide certain information of the status of the pixels as both methods used just the TIR information. The statistical method did perform very poor in all conditions. The Otsu method did perform subjectively good in clear cloudy conditions. However, there is no validation if the threshold represents the true canopy pixels or not. For better pixel separation it would be interesting to combine TIR images

with RGB images. Here it makes sense to compare the given threshold with results of other indices such as the NDVI.

Using canopy temperature and combining its data with information on atmospheric temperature is a common approach for water stress research and provides the foundation for many different water stress indices. Excluding a few outliers, the gradient was mostly at about 0 – 2 degrees, which means that the maize crops did not suffer severe water stress and were transpiring also at the hottest days. The temperature gradient however does not consider other factors such as humidity or crop or area specific information. Therefore, water stress indices are being applied to account for these shortcomings.

The application of the crop water stress index (CWSI) needs a more sophisticated setup. The statistical approach did perform very poor, as one major part of this approach was missing. This was due to the fact that the statistical approach needs a part of the plot which is fully or even over irrigated. Without any irrigation, the statistical approach does not provide good results. The attempt to establish a lower baseline for the empirical approach also missed irrigation. The executed alternative using reference days did not provide satisfactory results due to a relatively small sample size.

In this thesis, no significant differences were found between SUS and CON subplots. The effect of the straw mulch, which was laid out in the SUS subplots, could be neglected because the maize crops were almost fully grown. There was no detected water stress because the maize crops did not suffer severe water stress. However, the methods used each contained so many uncertainties that no valid statement can be made.

As discussed above one idea to identify the biggest errors would be to first compare CWSI calculations with and without pixel separation. To assess the errors of the TIR camera the CWSI should be calculated using the measured temperature  $\pm 2^\circ\text{C}$ . After these two measures a valid statement about the accuracy and the errors of the measurement campaign can be made.

Because the SUSI field site cannot be changed easily, it is suggested to focus on different arable crops. Given the crops in the four-year conventional crop rotation (winter wheat (2x), maize and sugar beet) the best suggestion in terms of visibility and measurability of water stress would be sugar beet because of the relatively big leaves and the low resistance to higher temperatures compared to the other options available. Another improvement would be to measure the crops during different growing stages. At last the biggest improvement would be to combine the remote sensed TIR data with the ground measured SMC, LAI and transpiration rate data of the SUSI project.

## 6 References

- Al-Kaisi, M.M., and I. Broner. 2014. "Crop Water Use and Growth Stages." *Colorado State University*. Colorado State University.
- Alchanatis, V., Y. Cohen, S. Cohen, M. Moller, M. Sprinstin, M. Meron, J. Tsipris, Y. Saranga, and E. Sela. 2010. "Evaluation of Different Approaches for Estimating and Mapping Crop Water Status in Cotton with Thermal Imaging." *Precision Agriculture* 11 (1): 27–41. <https://doi.org/10.1007/s11119-009-9111-7>.
- Allen, Richard G., Luis S. Pereira, Dirk Raes, and Martin Smith. 1998. *Crop Evapotranspiration - Guidelines for Computing Crop Water Requirements - FAO Irrigation and Drainage Paper 56*. Rome: FAO - Food and Agriculture Organization of the United Nations. <http://www.fao.org/docrep/X0490E/X0490E00.htm>.
- Anderson, M. C., Richard G. Allen, Anthony Morse, and William P. Kustas. 2012. "Use of Landsat Thermal Imagery in Monitoring Evapotranspiration and Managing Water Resources." *Remote Sensing of Environment* 122: 50–65. <https://doi.org/10.1016/j.rse.2011.08.025>.
- Bai, Jian-jun, Yuan Yu, and Liping Di. 2016. "Comparison between TVDI and CWSI for Drought Monitoring in the Guanzhong Plain, China." *Journal of Integrative Agriculture* 15 (0): 389–97. [https://doi.org/10.1016/S2095-3119\(15\)61302-8](https://doi.org/10.1016/S2095-3119(15)61302-8).
- Bai, Jian-Jun, Yuan Yu, and Liping Di. 2016. "Comparison between TVDI and CWSI for Drought Monitoring in the Guanzhong Plain, China." *Journal of Integrative Agriculture* 15 (0): 389–97. [https://doi.org/10.1016/S2095-3119\(15\)61302-8](https://doi.org/10.1016/S2095-3119(15)61302-8).
- Berni, Jose A. J., Pablo J. Zarco-Tejada, Lola Suárez, and Elias Fereres. 2009. "Thermal and Narrowband Multispectral Remote Sensing for Vegetation Monitoring From an Unmanned Aerial Vehicle." *IEEE Transactions on Geoscience and Remote Sensing* 47 (3): 1–17. <https://doi.org/10.1109/TGRS.2008.2010457>.
- Bonan, Gordon. 2008. *Ecological Climatology, Concepts and Applications*. 2nd ed. Cambridge University Press.
- Brouwer, C, and M Heibloem. 1986. "Irrigation Water Management." *FAO Land and Water Development Division*, 3–6.
- Cammalleri, Carmelo, and Jürgen Vogt. 2015. "On the Role of Land Surface Temperature as Proxy of Soil Moisture Status for Drought Monitoring in Europe." *Remote Sensing* 7 (12): 16849–64. <https://doi.org/10.3390/rs71215857>.
- Cohen, Y., V. Alchanatis, Y. Saranga, O. Rosenberg, E. Sela, and A. Bosak. 2017. "Mapping Water Status Based on Aerial Thermal Imagery: Comparison of Methodologies for Upscaling from a Single Leaf to Commercial Fields." *Precision Agriculture* 18 (5): 801–22. <https://doi.org/10.1007/s11119-016-9484-3>.
- Coll, César, Vicente Caselles, Enric Valor, and Raquel Nicolòs. 2012. "Remote Sensing of

## References

---

- Environment Comparison between Different Sources of Atmospheric Profiles for Land Surface Temperature Retrieval from Single Channel Thermal Infrared Data.” *Remote Sensing of Environment* 117: 199–210.  
<https://doi.org/10.1016/j.rse.2011.09.018>.
- Crafts-Brandner, Steven J, and Michael E Salvucci. 2002. “Sensitivity of Photosynthesis in a C4 Plant , Maize , to Heat Stress” 129 (August): 1773–80.  
<https://doi.org/10.1104/pp.002170.or>.
- Crausbay, Shelley D., Aaron R. Ramirez, Shawn L. Carter, Molly S. Cross, Kimberly R. Hall, Deborah J. Bathke, Julio L. Betancourt, et al. 2017. “Defining Ecological Drought for the Twenty-First Century.” *Bulletin of the American Meteorological Society* 98 (12): 2543–50. <https://doi.org/10.1175/BAMS-D-16-0292.1>.
- Dagdelen, N, T Gurbuz, Y Erdem, F Sezgin, E Yilmaz, S Akcay, and E Yesilirmak. 2008. “Determination of Crop Water Stress Index (CWSI) of Second Crop Corn in a Semiarid Climate.” *International Meeting on Soil Fertility Land Management and Agroclimatology*, 805–14.
- Dash, P., F.-M. Göttsche, F.-S. Olesen, and H. Fischer. 2002. “Land Surface Temperature and Emissivity Estimation from Passive Sensor Data: Theory and Practice-Current Trends.” *International Journal of Remote Sensing* 23 (13): 2563–94.  
<https://doi.org/10.1080/01431160110115041>.
- Eitzinger, Josef. 2007. “Einfluss Des Klimawandels Auf Die Produktionsrisiken in Der Österreichischen Landwirtschaft Und Mögliche Anpassungsstrategien.” *Ländlicher Raum* 2007: 1–8.
- Elsässer, Florian. 2015. “CONCEPT ELABORATION AND IMPLEMENTATION OF A UAV-BASED RECORDING SYSTEM FOR LAND SURFACE TEMPERATURES FOR ( EVAPOTRANSPIRATION AND SOIL MOISTURE ).” University of Life Sciences Vienna.
- European Commission Joint Research Centre. 2017. “Copernicus Global Land Service.” 2017. <https://land.copernicus.eu/global/products/lst>.
- Feng, Yu, Daozhi Gong, Xurong Mei, Weiping Hao, Dahua Tang, and Ningbo Cui. 2017. “Energy Balance and Partitioning in Partial Plastic Mulched and Non-Mulched Maize Fields on the Loess Plateau of China” 191: 193–206.
- Gerhards, Max, Martin Schlerf, Kaniska Mallick, and Thomas Udelhoven. 2019. “Challenges and Future Perspectives of Multi-/Hyperspectral Thermal Infrared Remote Sensing for Crop Water-Stress Detection: A Review.” *Remote Sensing* 11 (10): 2018–21. <https://doi.org/10.3390/rs11101240>.
- Gobiet, A., and H. Truhetz. 2008. “Auswirkungen Des Klimawandels Auf Die Österreichische Wasserwirtschaft.” In *Klimamodelle, Klimaszenarien Und Ihre Bedeutung Für Österreich*, 71–82. [http://www.uni-graz.at/print/igam7www\\_gobiet\\_truhetz-2008-oewavbrochure.pdf](http://www.uni-graz.at/print/igam7www_gobiet_truhetz-2008-oewavbrochure.pdf).

## References

---

- Gowik, U., and P. Westhoff. 2011. "The Path from C3 to C4 Photosynthesis." *Plant Physiology* 155 (1): 56–63. <https://doi.org/10.1104/pp.110.165308>.
- Graham, Steve. 2000. "Drought: The Creeping Disaster." *NASA Earth Observatory*, August 2000. <https://earthobservatory.nasa.gov/features/DroughtFacts>.
- Han, Ming, Huihui Zhang, Kendall C. DeJonge, Louise H. Comas, and Thomas J. Trout. 2016. "Estimating Maize Water Stress by Standard Deviation of Canopy Temperature in Thermal Imagery." *Agricultural Water Management* 177: 400–409. <https://doi.org/10.1016/j.agwat.2016.08.031>.
- Idso, Sherwood B. 1982. "Non-Water-Stressed Baselines: A Key to Measuring and Interpreting Plant Water Stress." *Agricultural Meteorology* 27 (1–2): 59–70. [https://doi.org/10.1016/0002-1571\(82\)90020-6](https://doi.org/10.1016/0002-1571(82)90020-6).
- Ihuoma, Samuel O., and Chandra A. Madramootoo. 2017. "Recent Advances in Crop Water Stress Detection." *Computers and Electronics in Agriculture* 141: 267–75. <https://doi.org/10.1016/j.compag.2017.07.026>.
- Jackson, Ray, and Sherwood Idso. 1981. "Canopy Temperature as a Crop Water Stress Indicator." *WATER RESOURCES RESEARCH* 17 (4): 1133–38.
- Jaleel, C.A., P. Manivannan, A. Wahid, M. Farooq, R. Somasundaram, and R. Panneerselvam. 2009. "Drought Stress in Plants : A Review on Morphological Characteristics and Pigments Composition." *International Journal of Agriculture & Biology* 11: 100–105. <http://www.fao.org/docrep/X0490E/X0490E00.htm>.
- Jones, H.G., and Xavier Sirault. 2014. "Scaling of Thermal Images at Different Spatial Resolution: The Mixed Pixel Problem." *Agronomy* 4 (3): 380–96. <https://doi.org/10.3390/agronomy4030380>.
- Jones, H.G., and R.A. Vaughan. 2010. "Jones\_2010\_RemoteSensingOfVegetation\_Ch9.PDF." In *Remote Sensing of Vegetation: Principles, Techniques, and Applications*, 353. Oxford University Press.
- Kalma, Jetse D., Tim R. McVicar, and Matthew F. McCabe. 2008. "Estimating Land Surface Evaporation: A Review of Methods Using Remotely Sensed Surface Temperature Data." *Surveys in Geophysics* 29 (4–5): 421–69. <https://doi.org/10.1007/s10712-008-9037-z>.
- Laliberte, Andrea S., Mark A. Goforth, Caitriana M. Steele, and Albert Rango. 2011. "Multispectral Remote Sensing from Unmanned Aircraft: Image Processing Workflows and Applications for Rangeland Environments." *Remote Sensing* 3 (11): 2529–51. <https://doi.org/10.3390/rs3112529>.
- Li, Nana, Fuqiang Tian, Hongchang Hu, Hui Lu, and Guanghui Ming. 2016. "Effects of Plastic Mulch on Soil Heat Flux and Energy Balance in a Cotton Field in Northwest China." *Atmosphere*. <https://doi.org/10.3390/atmos7080107>.
- Li, Z.I., and S.B. Duan. 2018. "Land Surface Temperature." In *Comprehensive Remote Sensing*, 264–83. Elsevier. <https://doi.org/10.1016/B978-0-12-409548-9.10375-6>.

## References

---

- Lisar, Seyed Y.S., Rouhollah Motafakkerazad, Mosharraf M. Hossain, and Ismail M.M. Rahman. 2012. *Water Stress in Plants: Causes, Effects and Responses*. Water Stress. InTech. <http://www.intechopen.com/books/water-stress/water-stress-in-plants-causes-effects-and-responses%0AInTech>.
- Martinez, J., G. Egea, J. Aguera, and M. Perez-Ruiz. 2016. "A Cost-Effective Canopy Temperature Measurement System for Precision Agriculture: A Case Study on Sugar Beet." *Precision Agriculture*, 1–16. <https://doi.org/10.1007/s11119-016-9470-9>.
- Martínez, J, @bullet G Egea, M Pérez-Ruiz, and Manuelperez@us Es. n.d. "A Cost-Effective Canopy Temperature Measurement System for Precision Agriculture: A Case Study on Sugar Beet." *Precision Agriculture*. <https://doi.org/10.1007/s11119-016-9470-9>.
- Meron, M., J. Tsipris, Valerie Orlov, V. Alchanatis, and Yafit Cohen. 2010. "Crop Water Stress Mapping for Site-Specific Irrigation by Thermal Imagery and Artificial Reference Surfaces." *Precision Agriculture* 11 (2): 148–62. <https://doi.org/10.1007/s11119-009-9153-x>.
- Monteith, John, and Mike Unsworth. 2013. *Principles of Environmental Physics: Plants, Animals, and the Atmosphere: Fourth Edition*. *Principles of Environmental Physics: Plants, Animals, and the Atmosphere: Fourth Edition*. <https://doi.org/10.1016/C2010-0-66393-0>.
- Morse, Bryan S. 2000. "Lecture 4 : Thresholding." Provo, Utah, USA: Brigham Young University.
- NDMC. 2019. "Types of Drought." National Drought Mitigation Center. 2019. <https://drought.unl.edu/Education/DroughtIn-depth/TypesofDrought.aspx>.
- Otsu, Nobuyuki. 1979. "A Treshold Selection Method from Gray-Level Histograms." *IEEE Transactions on Systems, Man and Cybernetics* 9 (1): 62–66. <https://doi.org/10.1109/TSMC.1979.4310076>.
- Payero, J. O., and S. Irmak. 2006. "Variable Upper and Lower Crop Water Stress Index Baselines for Corn and Soybean." *Irrigation Science* 25 (1): 21–32. <https://doi.org/10.1007/s00271-006-0031-2>.
- Pirson, A, and M H Zimmermann. 1982. *Encyclopedia of Plant Physiology Plant Ecology II Water Relations and Carbon Assimilation*. 12 B. Vol. 12. Springer.
- Raven, J a, and D Edwards. 2001. "Roots: Evolutionary Origins and Biogeochemical Significance." *Journal of Experimental Botany* 52 (Spec Issue): 381–401. [https://doi.org/10.1093/jexbot/52.suppl\\_1.381](https://doi.org/10.1093/jexbot/52.suppl_1.381).
- Rouse, J.W., R.H. Haas, J.A. Schell, and D.W. Deering. 1974. "Monitoring Vegetation Systems in the Great Plains with ERTS." *Third Earth Resources Technology Satellite - 1 Symposium 1 (Technical Presentations)*: 309–17.
- Rud, Ronit, Y. Cohen, V. Alchanatis, A. Levi, R. Brikman, C. Shenderey, B. Heuer, et al. 2014. "Crop Water Stress Index Derived from Multi-Year Ground and Aerial Thermal Images as an Indicator of Potato Water Status." *Precision Agriculture* 15

## References

---

- (3): 273–89. <https://doi.org/10.1007/s11119-014-9351-z>.
- Sagarika, Roy, and Duke Ophori. 2014. "Estimation of Crop Water Stress Index in Almond Orchards Using Thermal Aerial Imagery Sagarika Roy 1 \*, and Duke Ophori 1 ." *Journal of Spatial Hydrology* 12 (1).
- Sandholt, Inge, Kjeld Rasmussen, and Jens Andersen. 2002. "A Simple Interpretation of the Surface Temperature/Vegetation Index Space for Assessment of Surface Moisture Status." *Remote Sensing of Environment* 79 (2–3): 213–24. [https://doi.org/10.1016/S0034-4257\(01\)00274-7](https://doi.org/10.1016/S0034-4257(01)00274-7).
- Sethmacher, Vivian. 2018. "Vergleich Der Bodenfeuchte Und Saugspannung Sowie Der Transpirationsleistung in Maisparzellen Mit Verschiedenen Behandlungen Während Hitze- Und Trockenperioden."
- Shao, Hong Bo, Li Ye Chu, C.A. Jaleel, and Chang Xing Zhao. 2008. "Water-Deficit Stress-Induced Anatomical Changes in Higher Plants." *Comptes Rendus - Biologies* 331 (3): 215–25. <https://doi.org/10.1016/j.crvi.2008.01.002>.
- Suárez, L., P. J. Zarco-Tejada, G. Sepulcre-Cantó, O. Pérez-Priego, J. R. Miller, J. C. Jiménez-Muñoz, and J. Sobrino. 2008. "Assessing Canopy PRI for Water Stress Detection with Diurnal Airborne Imagery." *Remote Sensing of Environment* 112 (2): 560–75. <https://doi.org/10.1016/j.rse.2007.05.009>.
- Suárez, Lola, and Jose A. J. Berni. 2012. "Spectral Response of Citrus and Their Application to Nutrient and Water Constraints Diagnosis." In *Advances in Citrus Nutrition*, 9789400741:1–477. <https://doi.org/10.1007/978-94-007-4171-3>.
- Taghvaeian, Saleh, Louise Comas, Kendall C. DeJonge, and Thomas J. Trout. 2014. "Conventional and Simplified Canopy Temperature Indices Predict Water Stress in Sunflower." *Agricultural Water Management* 144: 69–80. <https://doi.org/10.1016/j.agwat.2014.06.003>.
- Trnka, Miroslav, Jan Balek, Petr Štěpánek, Pavel Zahradníček, Martin Možný, Josef Eitzinger, Zdenek Žalud, et al. 2016. "Drought Trends over Part of Central Europe between 1961 and 2014." *Climate Research* 70 (2–3): 143–60. <https://doi.org/10.3354/cr01420>.
- Walker, Tom, Tom Hash, Fred Rattunde, and Eva Weltzien. 2016. *Improved Crop Productivity for Africa's Drylands*. World Bank. Washington DC: World Bank.
- Wall, Patrick C. 2007. "Tailoring Conservation Agriculture to the Needs of Small Farmers in Developing Countries: An Analysis of Issues." *Journal of Crop Improvement* 19 (August 2014): 137–55. [https://doi.org/10.1300/J411v19n01\\_07](https://doi.org/10.1300/J411v19n01_07).
- Ward, Christopher, Raphael Torquebiau, and Hua Xie. 2016. *Improved Agricultural Water Management for Africa's Drylands*. World Bank. Wash: World Bank. <https://doi.org/10.1596/978-1-4648-0832-6>.
- Wilhite, Donald A., and Michael H. Glantz. 1985. "Understanding the Drought Phenomenon: The Role of Definitions." *Drought Mitigation Center Faculty*

## References

---

- Publications* 20: 11–27. <http://digitalcommons.unl.ed/droughtfacpub/20>.
- Wohlfahrt, Georg, and Erich Tasser. 2014. "A Mobile System for Quantifying the Spatial Variability of the Surface Energy Balance: Design and Application." *International Journal of Biometeorology*, 617–27. <https://doi.org/10.1007/s00484-014-0875-8>.
- Zamir, M.S.I., H.M.R. Javeed, W Ahmed, N Sarwar, M Shehzad, M A Sarwar, and S Iqbal. 2013. "EFFECT OF TILLAGE AND MULCHES ON YIELD COMPONENTS OF MAIZE AND SOIL PHYSICAL PROPERTIES EFFECT OF TILLAGE AND ORGANIC MULCHES ON GROWTH , YIELD AND QUALITY OF AUTUMN PLANTED MAIZE ( ZEA MAYS L .) AND SOIL PHYSICAL PROPERTIES." *Cercetări Agronomice În Moldova XLVI* (2). <https://doi.org/10.2478/v10298-012-0080-z>.
- Zarco-Tejada, P. J., V. González-Dugo, L. E. Williams, L. Suárez, J. A J Berni, D. Goldhamer, and E. Fereres. 2013. "A PRI-Based Water Stress Index Combining Structural and Chlorophyll Effects: Assessment Using Diurnal Narrow-Band Airborne Imagery and the CWSI Thermal Index." *Remote Sensing of Environment* 138 (November): 38–50. <https://doi.org/10.1016/j.rse.2013.07.024>.
- Zargar, Amin, Rehan Sadiq, Bahman Naser, and Faisal I. Khan. 2011. "A Review of Drought Indices." *Environmental Reviews* 19 (NA): 333–49. <https://doi.org/10.1139/a11-013>.
- Zhang, Chunhua, and John M. Kovacs. 2012. "The Application of Small Unmanned Aerial Systems for Precision Agriculture: A Review." *Precision Agriculture* 13 (6): 693–712. <https://doi.org/10.1007/s11119-012-9274-5>.

# 7 Appendix

## 7.1 Checklist UAV Flight

- ½h vor Abflug: TIR Kamera einschwingen
- Fokus der beiden Kameras kontrollieren
- Fahrgestell überprüfen  
→ ev. Festziehen
- Propellerschrauben überprüfen und Position zueinander überprüfen  
→ ev. Festschrauben
- Checken ob beide SD Karten in den Kameras sind
- „Reserveakku“ in Drohne → Starten
- Gimbal überprüfen  
→ ev. mit Wasserwaage horizontieren
- Netbox mit PC verbinden  
→ Zeit synchronisieren (SyncView)
  - Ravi mit 1 Hz (Skipped Mode)
  - Speicherort des Ravi Files checken (/E:)
- Kameras auf Gimbal montieren
- Wegpunkte an Drohne/Fernbedienung senden
- Auf Flugakku wechseln
- Drohne auf ihren Startplatz aufstellen  
→ auf Vegetation achten – keine langen Grashalme, Äste etc.  
→ Ausrichtung des Fahrgestells beachten  
→ Haube der Drohne überprüfen
- Drohne Kalibrieren
- Flir Messungen von Referenzplatten
- Messungen Ecobot

### Unmittelbar vor dem Start

- Flugakku prüfen
- Fernbedienung prüfen
  - Satelliten
  - Wegpunkte übertragen
  - Akku

## Appendix

---

- Höhe AUS

### 7.2 Flight Log book

---

Logbuch Flüge			
<b>Datum</b>	10.05.2017	<b>Flug Nr.</b>	1
<b>Uhrzeit</b>	15:30	<b>Kameras</b>	TIR&RGB
<b>Wetter</b>	leicht bewölkt	<b>Fotos TIR</b>	yes
<b>Wind</b>	aus O, leichte Brise	<b>Fotos RGB</b>	yes
<b>Flugroute</b>	Tulln, Susi	<b>Ort</b>	Tulln
<b>Anmerkungen:</b>	nur südlicher Teil der SUSI Plots befliegen		

---

Logbuch Flüge			
<b>Datum</b>	02.06.2017	<b>Flug Nr.</b>	2
<b>Uhrzeit</b>	11:00	<b>Kameras</b>	TIR&RGB
<b>Wetter</b>	diffus, heiter	<b>Fotos TIR</b>	yes
<b>Wind</b>	leichter Wind	<b>Fotos RGB</b>	yes
<b>Flugroute</b>	Tulln/Süd	<b>Ort</b>	Tulln
<b>Anmerkungen:</b>	Akkus 7+8 entleeren sehr schnell		

---

Logbuch Flüge			
<b>Datum</b>	02.06.2017	<b>Flug Nr.</b>	3
<b>Uhrzeit</b>	12:00	<b>Kameras</b>	TIR&RGB
<b>Wetter</b>	diffus, heiter	<b>Fotos TIR</b>	yes
<b>Wind</b>	mäßiger Wind	<b>Fotos RGB</b>	yes
<b>Flugroute</b>	Tulln/Nord	<b>Ort</b>	Tulln
<b>Anmerkungen:</b>	RGB Fotos unscharf, (1.Foto auf nahes Kabel fokussiert, Autofokus hat das nicht mehr korrigiert)		

---

Logbuch Flüge			
<b>Datum</b>	02.06.2017	<b>Flug Nr.</b>	4
<b>Uhrzeit</b>	12:30	<b>Kameras</b>	TIR&RGB
<b>Wetter</b>	diffus, heiter	<b>Fotos TIR</b>	no
<b>Wind</b>	mäßiger Wind	<b>Fotos RGB</b>	yes
<b>Flugroute</b>	Tulln/Panorama	<b>Ort</b>	Tulln
<b>Anmerkungen:</b>	TIR Fotos nicht verwertbar / Fehler im Format -- "There is unsafe format" -- 'date'.tmp file -- kann nicht wiederhergestellt werden		

---

Logbuch Flüge			
<b>Datum</b>	02.06.2017	<b>Flug Nr.</b>	5
<b>Uhrzeit</b>	13:00	<b>Kameras</b>	TIR&RGB
<b>Wetter</b>	diffus, heiter	<b>Fotos TIR</b>	yes
<b>Wind</b>	mäßiger Wind	<b>Fotos RGB</b>	yes

---

## Appendix

---

<b>Flugroute</b>	Tulln/Nord	<b>Ort</b>	Tulln
<b>Anmerkungen:</b>	RGB Fotos nicht optimal scharf		

### Logbuch Flüge

<b>Datum</b>	17.07.2017	<b>Flug Nr.</b>	6
<b>Uhrzeit</b>	13:15	<b>Kameras</b>	TIR&RGB
<b>Wetter</b>	bewölkt bis heiter	<b>Fotos TIR</b>	yes
<b>Wind</b>	leichte Brise	<b>Fotos RGB</b>	yes
<b>Flugroute</b>	Tulln / Süd 4 lines	<b>Ort</b>	Tulln
<b>Anmerkungen:</b>	Drohne beim Start verdreht, alle Bilder im Hochformat, Flughöhe von 30m nicht eingehalten		

### Logbuch Flüge

<b>Datum</b>	17.07.2017	<b>Flug Nr.</b>	7
<b>Uhrzeit</b>	13:30	<b>Kameras</b>	TIR&RGB
<b>Wetter</b>	heiter	<b>Fotos TIR</b>	no
<b>Wind</b>	leichte Brise	<b>Fotos RGB</b>	no
<b>Flugroute</b>	Tulln / Süd 6 lines	<b>Ort</b>	Tulln
<b>Anmerkungen:</b>	RGB nur wenige Fotos (Probleme mit Serienbild App), TIR wieder .tmp file (wie bei Flug Nr. 4		

### Logbuch Flüge

<b>Datum</b>	17.07.2017	<b>Flug Nr.</b>	8
<b>Uhrzeit</b>	14:30	<b>Kameras</b>	TIR&RGB
<b>Wetter</b>	heiter	<b>Fotos TIR</b>	yes
<b>Wind</b>	leichte Brise	<b>Fotos RGB</b>	yes
<b>Flugroute</b>	Tulln/ nord	<b>Ort</b>	Tulln
<b>Anmerkungen:</b>	-		

### Logbuch Flüge

<b>Datum</b>	18.07.2017	<b>Flug Nr.</b>	9
<b>Uhrzeit</b>	13:15	<b>Kameras</b>	TIR&RGB
<b>Wetter</b>	heiter	<b>Fotos TIR</b>	yes
<b>Wind</b>	ca. 20km/h - böig	<b>Fotos RGB</b>	yes
<b>Flugroute</b>	Tulln - Mais - Nord	<b>Ort</b>	Tulln
<b>Anmerkungen:</b>	-		

### Logbuch Flüge

<b>Datum</b>	18.07.2017	<b>Flug Nr.</b>	10
<b>Uhrzeit</b>	14:00	<b>Kameras</b>	TIR&RGB
<b>Wetter</b>	leicht bewölkt	<b>Fotos TIR</b>	yes
<b>Wind</b>	ca. 20km/h - böig	<b>Fotos RGB</b>	yes
<b>Flugroute</b>	Tulln - Mais - Süd	<b>Ort</b>	Tulln
<b>Anmerkungen:</b>	Richtung Kameras / Drohne war falsch (Nord-Ausrichtung Drohne)		

## Appendix

---

<b>Logbuch Flüge</b>			
<b>Datum</b>	18.07.2017	<b>Flug Nr.</b>	11
<b>Uhrzeit</b>	14:30	<b>Kameras</b>	TIR&RGB
<b>Wetter</b>	leicht bewölkt	<b>Fotos TIR</b>	yes
<b>Wind</b>	ca. 20km/h - böig	<b>Fotos RGB</b>	yes
<b>Flugroute</b>	Tulln - Mais - Süd	<b>Ort</b>	Tulln
<b>Anmerkungen:</b>	Carefree Richtung ca. 65° , Generator WP: 65° bzw. 155°		

---

<b>Logbuch Flüge</b>			
<b>Datum</b>	18.07.2017	<b>Flug Nr.</b>	12
<b>Uhrzeit</b>	15:00	<b>Kameras</b>	TIR&RGB
<b>Wetter</b>	leicht bewölkt	<b>Fotos TIR</b>	yes
<b>Wind</b>	ca. 20km/h - böig	<b>Fotos RGB</b>	yes
<b>Flugroute</b>	Tulln - Mais - Süd	<b>Ort</b>	Tulln
<b>Anmerkungen:</b>	Akkus entladen sehr schnell		

---

<b>Logbuch Flüge</b>			
<b>Datum</b>	19.07.2017	<b>Flug Nr.</b>	13
<b>Uhrzeit</b>	14:00	<b>Kameras</b>	TIR&RGB
<b>Wetter</b>	leicht bewölkt	<b>Fotos TIR</b>	unscharf
<b>Wind</b>	still - böig (wechselnd)	<b>Fotos RGB</b>	yes
<b>Flugroute</b>	Nord - Mais - (60m)	<b>Ort</b>	Tulln
<b>Anmerkungen:</b>	erster Flug mit neuen Akkus; Höhe 30m / v=3m/s		

---

<b>Logbuch Flüge</b>			
<b>Datum</b>	19.07.2017	<b>Flug Nr.</b>	14
<b>Uhrzeit</b>	14:15	<b>Kameras</b>	TIR&RGB
<b>Wetter</b>	leicht bewölkt	<b>Fotos TIR</b>	unscharf
<b>Wind</b>	still - böig (wechselnd)	<b>Fotos RGB</b>	yes
<b>Flugroute</b>	Süd - Mais - (60m)	<b>Ort</b>	Tulln
<b>Anmerkungen:</b>	neue Akkus 2.Paar, 1. Flug , TIR unscharf, Carefree 75° (etwas zu viel), Höhe 30m / v= 3m/s		

---

<b>Logbuch Flüge</b>			
<b>Datum</b>	19.07.2017	<b>Flug Nr.</b>	15
<b>Uhrzeit</b>	14:45	<b>Kameras</b>	TIR&RGB
<b>Wetter</b>	Gewitter im Entstehen	<b>Fotos TIR</b>	yes
<b>Wind</b>	still - böig (wechselnd)	<b>Fotos RGB</b>	yes
<b>Flugroute</b>	Süd - Mais --1Feld	<b>Ort</b>	Tulln
<b>Anmerkungen:</b>	Höhe 30m / v=2m/s		

---

### Logbuch Flüge

## Appendix

---

<b>Datum</b>	20.07.2017	<b>Flug Nr.</b>	16
<b>Uhrzeit</b>	13:00	<b>Kameras</b>	TIR&RGB
<b>Wetter</b>	sonnig	<b>Fotos TIR</b>	yes
<b>Wind</b>	leichte Brise am Boden - deutlich stärker über der Hecke	<b>Fotos RGB</b>	yes
<b>Flugroute</b>	S- Mais - 20m	<b>Ort</b>	Tulln
<b>Anmerkungen:</b>	UAV wieder deutlich zu niedrig, Flugroute zu weit nördlich, Servomotor (Gimbal) Hälfte kaputt -- Fotos im 0° Winkel anstatt Nadir (90°)		

---

### Logbuch Flüge

<b>Datum</b>	20.07.2017	<b>Flug Nr.</b>	17
<b>Uhrzeit</b>	13:15	<b>Kameras</b>	TIR&RGB
<b>Wetter</b>	sonnig	<b>Fotos TIR</b>	yes
<b>Wind</b>	leichte Brise am Boden - deutlich stärker über der Hecke	<b>Fotos RGB</b>	yes
<b>Flugroute</b>	N- Mais - 20m	<b>Ort</b>	Tulln
<b>Anmerkungen:</b>	Servo Motor kaputt (noch nicht behoben, weil nicht bemerkt (Servo stellt auf 0° bei Landung u Start), Fotos mit 0° Winkel statt 90°		

---

### Logbuch Flüge

<b>Datum</b>	20.07.2017	<b>Flug Nr.</b>	18
<b>Uhrzeit</b>	13:45	<b>Kameras</b>	TIR&RGB
<b>Wetter</b>	sonnig	<b>Fotos TIR</b>	no
<b>Wind</b>	wie zuvor	<b>Fotos RGB</b>	yes
<b>Flugroute</b>	S- Mais -35m	<b>Ort</b>	Tulln
<b>Anmerkungen:</b>	Gimbal mit Kabelbinder auf 90° repariert, keine Speicherkarte in Mini (onboard) PC, SW Platte 65/40		

---

### Logbuch Flüge

<b>Datum</b>	20.07.2017	<b>Flug Nr.</b>	19
<b>Uhrzeit</b>	14:00	<b>Kameras</b>	TIR&RGB
<b>Wetter</b>	sonnig	<b>Fotos TIR</b>	no
<b>Wind</b>	wie zuvor	<b>Fotos RGB</b>	yes
<b>Flugroute</b>	N- Mais -35m	<b>Ort</b>	Tulln
<b>Anmerkungen:</b>	Speicherkarte vergessen -- SW Platte 24/34		

---

### Logbuch Flüge

<b>Datum</b>	20.07.2017	<b>Flug Nr.</b>	20
<b>Uhrzeit</b>	14:15	<b>Kameras</b>	TIR&RGB
<b>Wetter</b>	sonnig	<b>Fotos TIR</b>	yes
<b>Wind</b>	wie zuvor	<b>Fotos RGB</b>	yes
<b>Flugroute</b>	S - Test	<b>Ort</b>	Tulln
<b>Anmerkungen:</b>	Testflug für neue Flugrouten, 20m Flughöhe viel zu niedrig		

---

## Appendix

---

---

<b>Logbuch Flüge</b>			
<b>Datum</b>	25.07.2017	<b>Flug Nr.</b>	21
<b>Uhrzeit</b>	13:15	<b>Kameras</b>	TIR&RGB
<b>Wetter</b>	bewölkt	<b>Fotos TIR</b>	yes
<b>Wind</b>	sehr stark (ca.30km/h)	<b>Fotos RGB</b>	yes
<b>Flugroute</b>	N_Maize_20m	<b>Ort</b>	Tulln
<b>Anmerkungen:</b>	große Schwierigkeiten für UAV Punkte zu treffen und zu halten (wegen Wind)		

---

<b>Logbuch Flüge</b>			
<b>Datum</b>	25.07.2017	<b>Flug Nr.</b>	22
<b>Uhrzeit</b>	13:45	<b>Kameras</b>	TIR&RGB
<b>Wetter</b>	bewölkt	<b>Fotos TIR</b>	yes
<b>Wind</b>	sehr stark (ca.30km/h)	<b>Fotos RGB</b>	yes
<b>Flugroute</b>	S_Maize_20m	<b>Ort</b>	Tulln
<b>Anmerkungen:</b>	TIR Bilder haben vereinzelt Streifen (nur einzelne Bilder)		

---

<b>Logbuch Flüge</b>			
<b>Datum</b>	28.07.2017	<b>Flug Nr.</b>	23
<b>Uhrzeit</b>	13:00	<b>Kameras</b>	TIR&RGB
<b>Wetter</b>	leicht bewölkt	<b>Fotos TIR</b>	yes
<b>Wind</b>	sehr stark (ca.25km/h)	<b>Fotos RGB</b>	yes
<b>Flugroute</b>	N_Maize_20m	<b>Ort</b>	Tulln
<b>Anmerkungen:</b>	Drohne viel zu tief geflogen		

---

<b>Logbuch Flüge</b>			
<b>Datum</b>	28.07.2017	<b>Flug Nr.</b>	24
<b>Uhrzeit</b>	13:15	<b>Kameras</b>	TIR&RGB
<b>Wetter</b>	leicht bewölkt	<b>Fotos TIR</b>	yes
<b>Wind</b>	sehr stark (ca.25km/h)	<b>Fotos RGB</b>	yes
<b>Flugroute</b>	S_Maize_20m	<b>Ort</b>	Tulln
<b>Anmerkungen:</b>	Drohen im Feld gestartet (im Wind) um besser die Höhe zu treffen, -1. Flir Messung Falsch (weiße platte)		

---

<b>Logbuch Flüge</b>			
<b>Datum</b>	31.07.2017	<b>Flug Nr.</b>	25
<b>Uhrzeit</b>	13:00	<b>Kameras</b>	TIR&RGB
<b>Wetter</b>	sonnig	<b>Fotos TIR</b>	yes
<b>Wind</b>	windstill	<b>Fotos RGB</b>	yes
<b>Flugroute</b>	N_Maize_20m	<b>Ort</b>	Tulln
<b>Anmerkungen:</b>	-		

---

### Logbuch Flüge

## Appendix

---

<b>Datum</b>	31.07.2017	<b>Flug Nr.</b>	26
<b>Uhrzeit</b>	13:15	<b>Kameras</b>	TIR&RGB
<b>Wetter</b>	sonnig	<b>Fotos TIR</b>	yes
<b>Wind</b>	windstill	<b>Fotos RGB</b>	yes
<b>Flugroute</b>	S_Maize_20m	<b>Ort</b>	Tulln
<b>Anmerkungen:</b>	-		

---

### Logbuch Flüge

<b>Datum</b>	31.07.2017	<b>Flug Nr.</b>	27
<b>Uhrzeit</b>	13:30	<b>Kameras</b>	TIR&RGB
<b>Wetter</b>	sonnig	<b>Fotos TIR</b>	yes
<b>Wind</b>	windstill	<b>Fotos RGB</b>	yes
<b>Flugroute</b>	Panorama	<b>Ort</b>	Tulln
<b>Anmerkungen:</b>	RGB u TIR nicht an Entfernung (Flughöhe 100m) angepasst		

---

### Logbuch Flüge

<b>Datum</b>	31.07.2017	<b>Flug Nr.</b>	28
<b>Uhrzeit</b>	14:00	<b>Kameras</b>	TIR&RGB
<b>Wetter</b>	sonnig	<b>Fotos TIR</b>	yes
<b>Wind</b>	windstill	<b>Fotos RGB</b>	yes
<b>Flugroute</b>	N_Maize_35m	<b>Ort</b>	Tulln
<b>Anmerkungen:</b>	-		

---

### Logbuch Flüge

<b>Datum</b>	31.07.2017	<b>Flug Nr.</b>	29
<b>Uhrzeit</b>	14:00	<b>Kameras</b>	TIR&RGB
<b>Wetter</b>	sonnig	<b>Fotos TIR</b>	yes
<b>Wind</b>	windstill	<b>Fotos RGB</b>	yes
<b>Flugroute</b>	S_Maize_35m	<b>Ort</b>	Tulln
<b>Anmerkungen:</b>	-		

---

### Logbuch Flüge

<b>Datum</b>	01.08.2017	<b>Flug Nr.</b>	30
<b>Uhrzeit</b>	13:00	<b>Kameras</b>	TIR&RGB
<b>Wetter</b>	sonnig	<b>Fotos TIR</b>	yes
<b>Wind</b>	stark aus SO	<b>Fotos RGB</b>	yes
<b>Flugroute</b>	N_Maize_20m	<b>Ort</b>	Tulln
<b>Anmerkungen:</b>	-		

---

### Logbuch Flüge

<b>Datum</b>	01.08.2017	<b>Flug Nr.</b>	31
<b>Uhrzeit</b>	13:15	<b>Kameras</b>	TIR&RGB
<b>Wetter</b>	sonnig	<b>Fotos TIR</b>	yes
<b>Wind</b>	stark aus SO	<b>Fotos RGB</b>	yes
<b>Flugroute</b>	S_Maize_20m	<b>Ort</b>	Tulln
<b>Anmerkungen:</b>	-		

---

### Logbuch Flüge

<b>Datum</b>	01.08.2017	<b>Flug Nr.</b>	32
--------------	------------	-----------------	----

## Appendix

---

<b>Uhrzeit</b>		13:45	<b>Kameras</b>	TIR&RGB
<b>Wetter</b>	sonnig		<b>Fotos TIR</b>	yes
<b>Wind</b>	stark aus SO		<b>Fotos RGB</b>	yes
<b>Flugroute</b>	N_Maize_35m		<b>Ort</b>	Tulln
<b>Anmerkungen:</b>	-			

---

### Logbuch Flüge

<b>Datum</b>		02.08.2017	<b>Flug Nr.</b>	33
<b>Uhrzeit</b>		13:30	<b>Kameras</b>	TIR&RGB
<b>Wetter</b>	sonnig		<b>Fotos TIR</b>	yes
<b>Wind</b>	leichte Brise		<b>Fotos RGB</b>	yes
<b>Flugroute</b>	N_Maize_20m		<b>Ort</b>	Tulln
<b>Anmerkungen:</b>	späterer Start weil Festplatte vergessen, Flug wieder zu niedrig			

---

### Logbuch Flüge

<b>Datum</b>		02.08.2017	<b>Flug Nr.</b>	34
<b>Uhrzeit</b>		13:45	<b>Kameras</b>	TIR&RGB
<b>Wetter</b>	sonnig		<b>Fotos TIR</b>	yes
<b>Wind</b>	leichte Brise		<b>Fotos RGB</b>	yes
<b>Flugroute</b>	S_Maize_20m		<b>Ort</b>	Tulln
<b>Anmerkungen:</b>	-			

---

### Logbuch Flüge

<b>Datum</b>		02.08.2017	<b>Flug Nr.</b>	35
<b>Uhrzeit</b>		14:00	<b>Kameras</b>	TIR&RGB
<b>Wetter</b>	sonnig		<b>Fotos TIR</b>	yes
<b>Wind</b>	leichte Brise		<b>Fotos RGB</b>	yes
<b>Flugroute</b>	N_Maize_35m		<b>Ort</b>	Tulln
<b>Anmerkungen:</b>	-			

---

### Logbuch Flüge

<b>Datum</b>		02.08.2017	<b>Flug Nr.</b>	36
<b>Uhrzeit</b>		14:00	<b>Kameras</b>	TIR&RGB
<b>Wetter</b>	sonnig		<b>Fotos TIR</b>	yes
<b>Wind</b>	leichte Brise		<b>Fotos RGB</b>	yes
<b>Flugroute</b>	S_Maize_35m		<b>Ort</b>	Tulln
<b>Anmerkungen:</b>	-			

---

### Logbuch Flüge

<b>Datum</b>		02.08.2017	<b>Flug Nr.</b>	37
<b>Uhrzeit</b>		14:15	<b>Kameras</b>	TIR&RGB
<b>Wetter</b>	sonnig		<b>Fotos TIR</b>	yes
<b>Wind</b>	leichte Brise		<b>Fotos RGB</b>	yes
<b>Flugroute</b>	Panorama		<b>Ort</b>	Tulln
<b>Anmerkungen:</b>	-			

---

### Logbuch Flüge

<b>Datum</b>		03.08.2017	<b>Flug Nr.</b>	38
<b>Uhrzeit</b>		13:00	<b>Kameras</b>	TIR&RGB

## Appendix

---

<b>Wetter</b>	sonnig/ zeitweise bewölkt	<b>Fotos TIR</b>	yes
<b>Wind</b>	10km/h SO	<b>Fotos RGB</b>	yes
<b>Flugroute</b>	N_Maize_20m	<b>Ort</b>	Tulln
<b>Anmerkungen:</b>	-		

---

### Logbuch Flüge

<b>Datum</b>	03.08.2017	<b>Flug Nr.</b>	39
<b>Uhrzeit</b>	13:15	<b>Kameras</b>	TIR&RGB
<b>Wetter</b>	sonnig/ zeitweise bewölkt	<b>Fotos TIR</b>	yes
<b>Wind</b>	10km/h SO	<b>Fotos RGB</b>	yes
<b>Flugroute</b>	S_Maize_20m	<b>Ort</b>	Tulln
<b>Anmerkungen:</b>	-		

---

### Logbuch Flüge

<b>Datum</b>	03.08.2017	<b>Flug Nr.</b>	40
<b>Uhrzeit</b>	13:30	<b>Kameras</b>	TIR&RGB
<b>Wetter</b>	sonnig/ zeitweise bewölkt	<b>Fotos TIR</b>	yes
<b>Wind</b>	10km/h SO	<b>Fotos RGB</b>	yes
<b>Flugroute</b>	N_Maize_35m	<b>Ort</b>	Tulln
<b>Anmerkungen:</b>	-		

---

### Logbuch Flüge

<b>Datum</b>	03.08.2017	<b>Flug Nr.</b>	41
<b>Uhrzeit</b>	13:30	<b>Kameras</b>	TIR&RGB
<b>Wetter</b>	sonnig/ zeitweise bewölkt	<b>Fotos TIR</b>	yes
<b>Wind</b>	10km/h SO	<b>Fotos RGB</b>	yes
<b>Flugroute</b>	S_Maize_35m	<b>Ort</b>	Tulln
<b>Anmerkungen:</b>	-		

---

### Logbuch Flüge

<b>Datum</b>	03.08.2017	<b>Flug Nr.</b>	42
<b>Uhrzeit</b>	13:45	<b>Kameras</b>	TIR&RGB
<b>Wetter</b>	sonnig/ zeitweise bewölkt	<b>Fotos TIR</b>	yes
<b>Wind</b>	10km/h SO	<b>Fotos RGB</b>	yes
<b>Flugroute</b>	Panorama	<b>Ort</b>	Tulln
<b>Anmerkungen:</b>	-		

---

### Logbuch Flüge

<b>Datum</b>	04.08.2017	<b>Flug Nr.</b>	43
<b>Uhrzeit</b>	09:45	<b>Kameras</b>	TIR&RGB
<b>Wetter</b>	bewölkt	<b>Fotos TIR</b>	yes
<b>Wind</b>	windstill	<b>Fotos RGB</b>	yes
<b>Flugroute</b>	N_Maize_20m	<b>Ort</b>	Tulln
<b>Anmerkungen:</b>	-		

---

### Logbuch Flüge

<b>Datum</b>	04.08.2017	<b>Flug Nr.</b>	44
<b>Uhrzeit</b>	10:00	<b>Kameras</b>	TIR&RGB
<b>Wetter</b>	bewölkt	<b>Fotos TIR</b>	yes
<b>Wind</b>	windstill	<b>Fotos RGB</b>	yes

## Appendix

---

<b>Flugroute</b>	S_Maize_20m	<b>Ort</b>	Tulln
<b>Anmerkungen:</b>	-		
<b>Logbuch Flüge</b>			
<b>Datum</b>	04.08.2017	<b>Flug Nr.</b>	45
<b>Uhrzeit</b>	13:00	<b>Kameras</b>	TIR&RGB
<b>Wetter</b>	bewölkt	<b>Fotos TIR</b>	yes
<b>Wind</b>	windstill	<b>Fotos RGB</b>	yes
<b>Flugroute</b>	N_Maize_20m	<b>Ort</b>	Tulln
<b>Anmerkungen:</b>	-		
<b>Logbuch Flüge</b>			
<b>Datum</b>	04.08.2017	<b>Flug Nr.</b>	46
<b>Uhrzeit</b>	13:15	<b>Kameras</b>	TIR&RGB
<b>Wetter</b>	leicht bewölkt	<b>Fotos TIR</b>	yes
<b>Wind</b>	leichte Brise	<b>Fotos RGB</b>	yes
<b>Flugroute</b>	S_Maize_20m	<b>Ort</b>	Tulln
<b>Anmerkungen:</b>	-		
<b>Logbuch Flüge</b>			
<b>Datum</b>	04.08.2017	<b>Flug Nr.</b>	47
<b>Uhrzeit</b>	13:30	<b>Kameras</b>	TIR&RGB
<b>Wetter</b>	sonnig	<b>Fotos TIR</b>	yes
<b>Wind</b>	windstill	<b>Fotos RGB</b>	yes
<b>Flugroute</b>	Panorama	<b>Ort</b>	Tulln
<b>Anmerkungen:</b>	-		
<b>Logbuch Flüge</b>			
<b>Datum</b>	04.08.2017	<b>Flug Nr.</b>	48
<b>Uhrzeit</b>	13:30	<b>Kameras</b>	TIR&RGB
<b>Wetter</b>	sonnig	<b>Fotos TIR</b>	yes
<b>Wind</b>	windstill	<b>Fotos RGB</b>	yes
<b>Flugroute</b>	N_Maize_35m	<b>Ort</b>	Tulln
<b>Anmerkungen:</b>	-		
<b>Logbuch Flüge</b>			
<b>Datum</b>	04.08.2017	<b>Flug Nr.</b>	49
<b>Uhrzeit</b>	13:30	<b>Kameras</b>	TIR&RGB
<b>Wetter</b>	sonnig	<b>Fotos TIR</b>	yes
<b>Wind</b>	windstill	<b>Fotos RGB</b>	yes
<b>Flugroute</b>	S_Maize_35m	<b>Ort</b>	Tulln
<b>Anmerkungen:</b>	-		
<b>Logbuch Flüge</b>			
<b>Datum</b>	04.08.2017	<b>Flug Nr.</b>	50
<b>Uhrzeit</b>	15:45	<b>Kameras</b>	TIR&RGB
<b>Wetter</b>	sonnig	<b>Fotos TIR</b>	yes
<b>Wind</b>	windstill	<b>Fotos RGB</b>	yes
<b>Flugroute</b>	N_Maize_20m	<b>Ort</b>	Tulln

## Appendix

---

Anmerkungen: -

---

Logbuch Flüge			
Datum	04.08.2017	Flug Nr.	51
Uhrzeit	16:00	Kameras	TIR&RGB
Wetter	sonnig	Fotos TIR	yes
Wind	windstill	Fotos RGB	yes
Flugroute	S_Maize_20m	Ort	Tulln
Anmerkungen:	-		

---

Logbuch Flüge			
Datum	05.08.2017	Flug Nr.	52
Uhrzeit	12:50	Kameras	TIR&RGB
Wetter	bewölkt	Fotos TIR	yes
Wind	kaum wind aus N	Fotos RGB	yes
Flugroute	N_Maize_35m	Ort	Tulln
Anmerkungen:	Drohne etwas höher als 35m		

---

Logbuch Flüge			
Datum	05.08.2017	Flug Nr.	53
Uhrzeit	13:10	Kameras	TIR&RGB
Wetter	bewölkt	Fotos TIR	yes
Wind	kaum wind	Fotos RGB	yes
Flugroute	S_Maize_35m	Ort	Tulln
Anmerkungen:	-		

---

Logbuch Flüge			
Datum	05.08.2017	Flug Nr.	54
Uhrzeit	13:25	Kameras	TIR&RGB
Wetter	Sonne kommt wieder raus	Fotos TIR	yes
Wind	windstill	Fotos RGB	yes
Flugroute	N_Maize_20m	Ort	Tulln
Anmerkungen:	-		

---

Logbuch Flüge			
Datum	05.08.2017	Flug Nr.	55
Uhrzeit	13:25	Kameras	TIR&RGB
Wetter	etwas Sonne	Fotos TIR	yes
Wind	windstill	Fotos RGB	yes
Flugroute	S_Maize_20m	Ort	Tulln
Anmerkungen:	Vergessen die Einstellungen in PiConnetct zu ändern --> mit 27Hz gefilmt --> alles da		

---

Logbuch Flüge			
Datum	07.08.2017	Flug Nr.	56
Uhrzeit	13:15	Kameras	TIR&RGB
Wetter	leicht bewölkt	Fotos TIR	yes
Wind	leichte Brise v SO	Fotos RGB	yes

---

## Appendix

---

<b>Flugroute</b>	N_Maize_20m	<b>Ort</b>	Tulln
<b>Anmerkungen:</b>	Batterie Flir aus		
<b>Logbuch Flüge</b>			
<b>Datum</b>	07.08.2017	<b>Flug Nr.</b>	57
<b>Uhrzeit</b>	13:15	<b>Kameras</b>	TIR&RGB
<b>Wetter</b>	leicht bewölkt	<b>Fotos TIR</b>	yes
<b>Wind</b>	leichte Brise v SO	<b>Fotos RGB</b>	yes
<b>Flugroute</b>	S_Maize_20m	<b>Ort</b>	Tulln
<b>Anmerkungen:</b>	Christina Messung mit IKT weiß: 24°C schwarz 40°C		
<b>Logbuch Flüge</b>			
<b>Datum</b>	07.08.2017	<b>Flug Nr.</b>	58
<b>Uhrzeit</b>	13:45	<b>Kameras</b>	TIR&RGB
<b>Wetter</b>	leicht bewölkt	<b>Fotos TIR</b>	yes
<b>Wind</b>	leichte Brise v SO	<b>Fotos RGB</b>	yes
<b>Flugroute</b>	N_Maize_35m	<b>Ort</b>	Tulln
<b>Anmerkungen:</b>	-		
<b>Logbuch Flüge</b>			
<b>Datum</b>	07.08.2017	<b>Flug Nr.</b>	59
<b>Uhrzeit</b>	13:45	<b>Kameras</b>	TIR&RGB
<b>Wetter</b>	leicht bewölkt	<b>Fotos TIR</b>	yes
<b>Wind</b>	leichte Brise v SO	<b>Fotos RGB</b>	yes
<b>Flugroute</b>	S_Maize_35m	<b>Ort</b>	Tulln
<b>Anmerkungen:</b>	Wolke bei EcoBot Messungen		
<b>Logbuch Flüge</b>			
<b>Datum</b>	07.08.2017	<b>Flug Nr.</b>	60
<b>Uhrzeit</b>	14:00	<b>Kameras</b>	TIR&RGB
<b>Wetter</b>	leicht bewölkt	<b>Fotos TIR</b>	yes
<b>Wind</b>	leichte Brise v SO	<b>Fotos RGB</b>	yes
<b>Flugroute</b>	Panorama	<b>Ort</b>	Tulln
<b>Anmerkungen:</b>	-		

**7.3 SUSI Layout 2016 / 2017**

